

## FAKULTÄT MASCHINENBAU

Master of Science in Manufacturing Technology

Institut für Umformtechnik und Leichtbau

Prof. Dr.-Ing. Dr. h.c. Matthias Kleiner

Prof. Dr.-Ing. Dr.-Ing. E.h. A. Erman Tekkaya

M a s t e r ' s   T h e s i s

# **“Formability analysis of 3105 aluminium composite panels by means of the multi-point forming process”**

by

Sadam Hamis Wapande

Matriculation no.: 198557

Supervisors:

Dr.-Ing. Cagatay Elibol

Prof. Dr.-Ing. Dr.-Ing. E.h. A. Erman Tekkaya

M.Sc. Hamed Dardaei Joghhan

Submitted on: 17<sup>th</sup> September 2019

**TURKISH-GERMAN UNIVERSITY**  
**INSTITUTE FOR GRADUATE STUDIES IN SCIENCE AND ENGINEERING**  
**MASTER'S PROGRAM IN MECHANICAL ENGINEERING**  
**(MANUFACTURING TECHNOLOGY)**  
**THESIS PRESENTATION PROTOCOL**

27.09.2019

The result of the thesis presentation of Sadam Hamis WAPANDE, who is registered in the joint graduate program Manufacturing Technology between Turkish-German University and Technical University Dortmund with the registration number 1661011102, titled "Formability analysis of 3105 aluminium composite panels by means of the multi-point forming process" held on 27.09.2019 at 14:00 is presented below.

Successful

Extension (3 months)

Unsuccessful

Thesis Presentation Committee:


Dr.-Ing. Çağatay ELİBOL  
(Advisor)



Prof. Dr.-Ing. A. Erman TEKKAYA  
(Co-advisor)




Prof. Dr. Hüseyin ÇİMENOĞLU  
(Member)



Prof. Dr. Mehmet Ali GÜLGÜN  
(Member)



Prof. Dr. Emel TABAN  
(Member)



# Eidesstattliche Versicherung (Affidavit)

Name, Vorname  
(Last name, first name)

Matrikelnr.  
(Enrollment number)

Ich versichere hiermit an Eides statt, dass ich die vorliegende Bachelorarbeit/Masterarbeit\* mit dem folgenden Titel selbstständig und ohne unzulässige fremde Hilfe erbracht habe. Ich habe keine anderen als die angegebenen Quellen und Hilfsmittel benutzt sowie wörtliche und sinngemäße Zitate kenntlich gemacht. Die Arbeit hat in gleicher oder ähnlicher Form noch keiner Prüfungsbehörde vorgelegen.

I declare in lieu of oath that I have completed the present Bachelor's/Master's\* thesis with the following title independently and without any unauthorized assistance. I have not used any other sources or aids than the ones listed and have documented quotations and paraphrases as such. The thesis in its current or similar version has not been submitted to an auditing institution.

Titel der Bachelor-/Masterarbeit\*:  
(Title of the Bachelor's/ Master's\* thesis):

\*Nichtzutreffendes bitte streichen  
(Please choose the appropriate)

Ort, Datum  
(Place, date)

Unterschrift  
(Signature)

## Belehrung:

Wer vorsätzlich gegen eine die Täuschung über Prüfungsleistungen betreffende Regelung einer Hochschulprüfungsordnung verstößt, handelt ordnungswidrig. Die Ordnungswidrigkeit kann mit einer Geldbuße von bis zu 50.000,00 € geahndet werden. Zuständige Verwaltungsbehörde für die Verfolgung und Ahndung von Ordnungswidrigkeiten ist der Kanzler/die Kanzlerin der Technischen Universität Dortmund. Im Falle eines mehrfachen oder sonstigen schwerwiegenden Täuschungsversuches kann der Prüfling zudem exmatrikuliert werden. (§ 63 Abs. 5 Hochschulgesetz - HG - ).

Die Abgabe einer falschen Versicherung an Eides statt wird mit Freiheitsstrafe bis zu 3 Jahren oder mit Geldstrafe bestraft.

Die Technische Universität Dortmund wird gfls. elektronische Vergleichswerkzeuge (wie z.B. die Software „turnitin“) zur Überprüfung von Ordnungswidrigkeiten in Prüfungsverfahren nutzen.

Die oben stehende Belehrung habe ich zur Kenntnis genommen:

## Official notification:

Any person who intentionally breaches any regulation of university examination regulations relating to deception in examination performance is acting improperly. This offense can be punished with a fine of up to €50,000.00. The competent administrative authority for the pursuit and prosecution of offenses of this type is the chancellor of TU Dortmund University. In the case of multiple or other serious attempts at deception, the examinee can also be unenrolled, section 63, subsection 5 of the North Rhine-Westphalia Higher Education Act (*Hochschulgesetz*).

The submission of a false affidavit will be punished with a prison sentence of up to three years or a fine.

As may be necessary, TU Dortmund will make use of electronic plagiarism-prevention tools (e.g. the "turnitin" service) in order to monitor violations during the examination procedures.

I have taken note of the above official notification:\*\*

Ort, Datum  
(Place, date)

Unterschrift  
(Signature)

**\*\*Please be aware that solely the German version of the affidavit ("Eidesstattliche Versicherung") for the Bachelor's/ Master's thesis is the official and legally binding version.**



## **Abstract**

The use of composite materials especially aluminium-plastic composite as building materials has grown drastically in recent. This development has been accelerated by the suitability of mass production of the composite, high strength-to-weight ratios and good resistance to harsh environmental conditions.

In the frame of this thesis work, the formability of aluminium composite panel made from two 3105 aluminium alloy sheets and a layer of low-density polyethylene (LDPE) is analysed using multi-point forming (MPF) process. This type of aluminium composite panel is commonly used for building application such as making of the facade. The Multi-point forming process is an advanced manufacturing technology used to produce three-dimensional shaped sheet metal parts using a set of punches instead of traditional die.

Literature research is conducted to analyse the effect of forming parameters on the quality of the formed part by multi-point forming process. Then, material characterization of the aluminium composite panel is conducted using five different mechanical tests: T-peel stripping test, tensile test, In-plane torsion test, Nakajima test and friction test. The numerical analysis of the forming process is performed using a commercial Abaqus/Explicit software and a multi-point forming die is designed using SolidWorks® software.

Mechanical characterization results showed that the bond between AA3105 and LDPE has higher peel strength than the minimum limit defined by TS 13777 standard. Also, the aluminium composite material has higher formability than AA3105 and the effect of strain rate sensitivity on aluminium composite panel can be neglected. Finite element simulation results showed that dimples found on the surface of the aluminium composite panel can be suppressed by using an elastic cushion. The fluctuation of thickness variation along a defined path from the centre of the formed part decreases as the thickness of elastic cushion increases.

**Keywords:** Aluminium composite panel, multi-point forming (MPF), formability, material characterization, numerical analysis

## **Acknowledgment**

This Master thesis work was carried out according to the collaboration between TU Dortmund, Turkish – Germany university and ASAS aluminium company as a final condition for my graduation from the international joint master’s degree program called the Master of Science in Manufacturing Technology (MMT).

As the first Tanzanian to graduate from this program, I have been fortunated enough to study with students from all around the world and get high-quality education from the two beautiful countries I always wished to study.

First, I would like to thank my beloved mother, Mariam Wapande, my late father, Hamis M. Wapande, my sister Pendo Wapande and two brothers, Salim and Faraji Wapande for being there for me during every stage of my life. Words can’t express my sincere appreciation to you. Special thanks to my aunty Jackie J. Kibiki and uncle Prof. Gibson Kibiki for their support, motivation and being there as my mentors.

I would like to express my appreciation to Prof. A. Erman Tekkaya for the invaluable knowledge he shared with us during his courses and for the chance to conduct my work at his institute. My gratitude to Mr. Hamed Dardaei Jaghan who was also my supervisor from TU Dortmund for his support, guidance, patience and constructive criticism.

From the Turkish – German university; my special gratitude to Assist. Prof. Dr. Mehmet Ipekoglu who has been there for me since the day I was selected for this program. Also, to Dr.-Ing. Cagatay Elibol for supervising my thesis work.

From ASAS aluminium company in Sakarya/Turkey; I would like to thank the head of the R&D department, Mr. Gorkem Ozcelik for the chance to conduct this work at their factory. My sincere appreciation to Murat Konar, M. Bugra Guner, M. Serkan Ozcan and other workers at ASAS aluminium factory for their unconditional help to this work. To all my classmates, teachers and friends from TU Dortmund and Turkish – German university, thank you very much for the amazing three years full of good times, traveling all around Europe and lifetime experience. It has been my pleasure to know you all.

A special thanks to a very special person – Tania Gottwald. Lastly, I would like to end with a modern Swahili proverb, **“Yajayo yanafurahisha”**.

# Table of Contents

<b>Abstract</b>	<b>III</b>
<b>Acknowledgment</b>	<b>IV</b>
<b>Table of Contents</b>	<b>v</b>
<b>Formula Symbols and Abbreviation</b>	<b>viii</b>
<b>List of Figures</b>	<b>x</b>
<b>List of Tables</b>	<b>xv</b>
<b>1 Introduction</b>	<b>1</b>
<b>2 State of the Art</b>	<b>3</b>
2.1 Forming .....	3
2.2 Multi-Point Forming Process .....	6
2.2.1 Components of Multi-Point Forming System .....	7
2.2.2 Types of Multi-Point Forming Processes .....	7
2.2.3 Advantages of Multi-Point Forming .....	10
2.2.4 Mechanical Defects in MPF Processes .....	10
2.2.5 Studies on Multi-Point Forming Processes .....	11
2.3 Formability .....	20
2.4 Composite Materials .....	21
2.4.1 Classification of Composite Materials .....	22
2.4.2 Composites in Building Applications.....	22
<b>3 Goal of the Work</b>	<b>24</b>
<b>4 Material Characterization</b>	<b>25</b>
4.1 3105 Aluminium Composite Panel .....	25
4.1.1 Physical and Mechanical Properties of 3105 Aluminium Alloy.....	26
4.1.2 Production Process of the 3105 Aluminium Composite Panel .....	27

---

4.2	T-Peel Stripping Test .....	28
4.2.1	Specimen Preparation.....	28
4.2.2	Experimental Setup .....	29
4.2.3	Data Analysis.....	30
4.3	Tensile Test .....	30
4.3.1	Specimen Preparation.....	30
4.3.2	Experimental Setup .....	32
4.3.3	Data Analysis.....	34
4.3.4	Fracture Analysis with Scanning Electron Microscope .....	34
4.4	In-plane Torsion Test .....	35
4.4.1	Specimen Preparation.....	37
4.4.2	Experimental Setup .....	38
4.4.3	Data Analysis.....	39
4.5	Nakajima Test .....	40
4.5.1	Specimen Preparation.....	41
4.5.2	Experimental Setup .....	42
4.5.3	Data Analysis.....	44
4.6	Friction Test .....	45
4.6.1	Specimen Preparation.....	46
4.6.2	Experimental Setup .....	47
4.6.3	Data Analysis.....	49
4.7	Results .....	50
4.7.1	T-Peel Stripping Test Results.....	50
4.7.2	Tensile Test Results.....	51
4.7.3	In-Plane Torsion Test Results .....	62
4.7.4	Nakajima Test Results.....	64
4.7.5	Friction Test Results.....	66



---

<b>5</b>	<b>Numerical Analysis</b>	<b>68</b>
5.1	Punch Design .....	68
5.2	Targeted Part Geometry .....	70
5.3	Numerical Simulation .....	70
5.3.1	Element Model .....	71
5.3.2	Material Model .....	73
5.3.3	Contact Interfaces .....	74
5.3.4	Boundary Conditions .....	75
5.4	Numerical Analysis Results .....	76
5.4.1	Punch (Forming) Force .....	76
5.4.2	Stress Distribution .....	78
5.4.3	Equivalent Plastic Strain Distribution .....	79
5.4.4	Thickness Distribution .....	80
<b>6</b>	<b>Multi-Point Forming Die Design</b>	<b>85</b>
6.1	Lower and Upper Plates .....	85
6.2	Blank Holder .....	86
6.3	Punches .....	86
<b>7</b>	<b>Summary and Outlook</b>	<b>87</b>
<b>8</b>	<b>References</b>	<b>89</b>
	<b>Appendix A</b>	<b>93</b>
	<b>Appendix B</b>	<b>96</b>
	<b>Appendix C</b>	<b>98</b>

## Formula Symbols and Abbreviation

### Formula Symbols

<b>Variable</b>	<b>Unit</b>	<b>Description</b>
$E$	GPa	Young's modulus
$F$	N	Force
$F_{BH}$	N	Blank holder force
$\sigma$	MPa	Stress
$\tau$	MPa	Shear stress
$k_f$	MPa	Yield stress
$R_m$	MPa	Tensile strength
$R_{p0,2}$	MPa	Yield strength at 0.2%
$s$	mm	Sheet thickness
$t$	s	Time
$r$	-	Plane strain ratio
$\bar{r}$	-	Average plane strain ratio
$\overline{\Delta r}$	-	Plane anisotropy
$\varepsilon$	-	Strain
$\varphi$	-	True strain
$\gamma$	-	Shear strain
$\dot{\varphi}$	1/s	Strain rate
$m$	-	Strain rate sensitivity
$n$	-	Strain-hardening exponent
$K$	MPa	Strength coefficient
$\mu$	-	Coefficient of friction
$\rho$	kg·m <sup>-3</sup>	Density
$\nu$	-	Poisson ratio

*Indices*

<b>Index</b>	<b>Description</b>
<i>0</i>	Initial value
<i>max</i>	Maximum
<i>min</i>	Minimum

*Abbreviations*

<b>Abbreviation</b>	<b>Description</b>
IUL	Institut für Umformtechnik und Leichtbau
CAD	Computer Aided Design
CAM	Computer Aided Manufacturing
FEM	Finite Element Method
MPF	Multi-Point Forming
MPDF	Multi-Point Die Forming
MPHDF	Multi-Point Half Die Forming
MPPF	Multi-Point Press Forming
MPHPF	Multi-Point Half Press Forming
DIN	German Institute for Standardization
ISO	International Organization for Standardization
TSE	Turkish Standards Institution
FLD	Forming Limit Diagram
FLC	Forming Limit Curve
PVDF	Polyvinylidene fluoride
LDPE	Low Density Polyethylene
AA	Aluminium Alloy

## List of Figures

<b>Figure 2.1:</b> Classification of manufacturing processes according to DIN 8580 .....	3
<b>Figure 2.2 a)</b> Extrusion forming process, <b>b)</b> Forging forming process .....	4
<b>Figure 2.3:</b> Classification of production processes used in forming under DIN 8582.....	5
<b>Figure 2.4:</b> Schematic diagram of MPF with blank-holder .....	6
<b>Figure 2.5:</b> Methods of punch adjustment .....	8
<b>Figure 2.6 :</b> Classification of multi-point forming processes according to punch adjustments.....	9
<b>Figure 2.7 a)</b> Dimpling defect on part formed by MPF process, <b>b)</b> Wrinkling defect on a formed part.....	11
<b>Figure 2.8:</b> The $z$ coordinates distribution of the line OA on spherical and saddle-shaped parts with different forming pressures. <b>a)</b> Spherical part, <b>b)</b> Saddle-shaped part .....	12
<b>Figure 2.9:</b> The average shape error of formed parts with different forming pressures ...	12
<b>Figure 2.10:</b> Thickness stress variation when four different elastic cushions are used to form a spherical part using MPSD <b>a)</b> along OR <b>b)</b> along OC .....	13
<b>Figure 2.11:</b> Thickness strain variation when four different elastic cushions are used to form a spherical part using MPSD <b>a)</b> along OR <b>b)</b> along OC .....	14
<b>Figure 2.12:</b> Graph of forming force against the displacement of the punch .....	15
<b>Figure 2.13:</b> Graph of sectional node displacement against the width of the formed 3D curved part simulated with three different MPF modes.....	16
<b>Figure 2.14 a)</b> Effect of the radius of curvature and pin size on wrinkling, <b>b)</b> Pressure distribution on both sides of the sheet when radius of curvature is 400 mm.....	17
<b>Figure 2.15:</b> Effect of different punch dimensions on thickness strain of spherical part formed using MPSD <b>a)</b> along OR, <b>b)</b> Along OC .....	18
<b>Figure 2.16 a)</b> Effect of strain-hardening ( $n$ ) on FLC, <b>b)</b> Effect of strain rate sensitivity ( $m$ ) on FLC .....	21
<b>Figure 2.17:</b> Classification of composite materials.....	22

---

<b>Figure 4.1:</b> Layers of NATURALBOND® composite panel .....	25
<b>Figure 4.2:</b> Production process of aluminium composite panel.....	27
<b>Figure 4.3:</b> T-Peel stripping test specimen geometry according to ASTM D 903-98 .....	29
<b>Figure 4.4:</b> T-Peel test setup according to ASTM D 903-98 .....	29
<b>Figure 4.5 a)</b> Tensile test specimen geometry according to DIN EN ISO 6892-1, <b>b)</b> Type I tensile test specimen geometry according to ASTM D 638-14 .....	31
<b>Figure 4.6:</b> Tensile test setup using Zwick/Roell Z250 machine.....	33
<b>Figure 4.7:</b> AA3105 tensile test specimens <b>a)</b> before the test, <b>b)</b> after the test .....	33
<b>Figure 4.8 a)</b> grinding and polishing machines used for the preparation of Bakelite, <b>b)</b> Zeiss EVO MAT15 scanning electron microscope used for fracture analysis .....	35
<b>Figure 4.9:</b> SEM specimen preparation procedures <b>a)</b> preparation of the Bakelite <b>b)</b> condensed Bakelite 12 hours after preparation <b>c)</b> Bakelite after several grinding and polishing.....	35
<b>Figure 4.10 a)</b> Schematic design of the in-plane torsion test, <b>b)</b> Deformation of a radial line during testing.....	36
<b>Figure 4.11 a)</b> Design of the non-grooved in-plane torsion specimens, <b>b)</b> Details of the grooved specimen.....	37
<b>Figure 4.12:</b> Set up of in-plane torsion test integrated into a Zwick/Roell Z250 machine	39
<b>Figure 4.13:</b> Forming limit diagram.....	40
<b>Figure 4.14:</b> Nakajima test specimen geometry according to DIN ISO 12004-2.....	41
<b>Figure 4.15 a)</b> Schematic design of the Nakajima test, <b>b)</b> Test set up for the determination of the FLC .....	43
<b>Figure 4.16 a)</b> Nakajima test specimens before the test, <b>b)</b> after the test .....	43
<b>Figure 4.17 a)</b> Selection of the specimen deformed surface area before creating sections, <b>b)</b> creation of five sections on an image before the specimen formed a crack.....	44
<b>Figure 4.18:</b> Renault procedure.....	46
<b>Figure 4.19:</b> Geometry of the planar shaped friction pad .....	46

---

<b>Figure 4.20:</b> Devices used during friction test .....	47
<b>Figure 4.21:</b> LabView interface used to control the equipment during friction tests .....	48
<b>Figure 4.22:</b> The average graph of Force in N/25mm against path in mm.....	50
<b>Figure 4.23:</b> Engineering stress-strain graph of AA3105 sheet and aluminium composite panel.....	52
<b>Figure 4.24:</b> Engineering stress - strain graph of LDPE.....	53
<b>Figure 4.25:</b> Engineering stress - strain graphs of AA3105, LDPE and aluminium composite panel.....	53
<b>Figure 4.26:</b> Flow curve of AA3105 sheet and aluminium composite panel .....	55
<b>Figure 4.27:</b> Flow curve of LDPE.....	55
<b>Figure 4.28:</b> Flow curves of AA3105 sheet and aluminium composite panel at a different strain rate .....	57
<b>Figure 4.29:</b> Flow curves of LDPE at a different strain rate.....	57
<b>Figure 4.30:</b> SEM pictures from, <b>a and b</b> ) aluminium composite specimen with AA3105-0° tested at 0.001 /s, strain 11.5%; <b>c and d</b> ) aluminium composite specimen with AA3105-0° tested at 0.01 /s, strain 14.5% .....	61
<b>Figure 4.31:</b> Shear stress – shear strain graph of the three specimen geometries.....	62
<b>Figure 4.32:</b> Equivalent stress - strain graphs of in-plane torsion test specimens and tensile test specimen .....	63
<b>Figure 4.33:</b> Comparison of the AA3105 grooved (coated) specimen and AA3105 tensile test specimens results .....	63
<b>Figure 4.34 a)</b> 200 mm Nakajima specimen when hemispherical punch used, <b>b)</b> 200 mm Nakajima specimen when hydraulic pressure used.....	64
<b>Figure 4.35:</b> Multiple peaks on the strain-length curve of the 100 mm geometry section obtained from ARAMIS software.....	65
<b>Figure 4.36:</b> Forming limit diagram of aluminium composite panel.....	65
<b>Figure 4.37:</b> Friction test results of aluminium composite panel and MPF die material..	66

---

<b>Figure 4.38:</b> Friction test results of aluminium composite panel and a polyurethane layer .....	66
<b>Figure 4.39:</b> Interaction plot for COF between sliding velocity and normal force.....	67
<b>Figure 5.1 a)</b> Geometry of Multi-Point Die Forming (MPDF) punch, <b>b)</b> Schematic design of lower MPFD punch set .....	68
<b>Figure 5.2:</b> Location of the punch.....	69
<b>Figure 5.3:</b> Geometry of the targeted part to be formed .....	70
<b>Figure 5.4:</b> Schematic design of a quarter of the MPDF simulation in Abaqus/ Explicit software.....	71
<b>Figure 5.5:</b> Graph of von Mises stress and equivalent plastic strain at point O against the total number of blank elements .....	72
<b>Figure 5.6:</b> Total punch force-displacement graph for different elastic cushion.....	76
<b>Figure 5.7:</b> Total punch (forming) force - displacement graph for different COF values without cushion .....	77
<b>Figure 5.8:</b> Total punch (forming) force - displacement graph for different COF values with 2mm cushion .....	77
<b>Figure 5.9:</b> Stress (Mises) distribution on the surface of the sheet (without cushion) .....	78
<b>Figure 5.10:</b> Stress (Mises) distribution for <b>a)</b> 2 mm, <b>b)</b> for 4mm elastic cushion .....	79
<b>Figure 5.11:</b> Equivalent plastic strain distribution <b>a)</b> without elastic cushion, <b>b)</b> 2 mm elastic cushion <b>c)</b> 4 mm elastic cushion and <b>d)</b> 10 mm elastic cushion.....	80
<b>Figure 5.12:</b> Thickness variation on the surface of aluminium composite panel with 10 mm elastic cushion .....	81
<b>Figure 5.13:</b> Thickness variation of the formed part from the centre to the end of the blank holder <b>a)</b> along OA path, <b>b)</b> along OB path.....	82
<b>Figure 5.14:</b> Thickness variation of the formed part without elastic cushion from the centre to the end of blank holder <b>a)</b> along OA path, <b>b)</b> along OB path.....	83
<b>Figure 5.15:</b> Thickness variation of the formed part with 2mm elastic cushion from the centre to the end of blank holder <b>a)</b> along OA path, <b>b)</b> along OB path.....	84

---

<b>Figure 6.1:</b> Schematic of designed Multi-Point Forming die. ....	85
<b>Figure A.1:</b> True stress - strain graph of AA3015 and aluminium composite panel.....	93
<b>Figure A.2:</b> True stress - strain graph of LDPE.....	93
<b>Figure A.3:</b> Comparison of calculated strain-hardening behaviour and experimental strain-Hardening behaviour of AA3105 and 3105 aluminium composite.....	94
<b>Figure A.4:</b> Comparison of calculated strain-hardening behaviour and experimental strain-Hardening behaviour of LDPE .....	94
<b>Figure A.3:</b> Equivalent stress – strain graph of the in-plane torsion test and tensile test results.....	95
<b>Figure B.1:</b> Strain - length graph of 20 mm specimen 2 - section 1.....	96
<b>Figure B.2:</b> Determination of major and minor strain values using best-fit parabola Approximation.....	97
<b>Figure C.1:</b> Creation of AA3105 material data in Abaqus/CAE.....	98
<b>Figure C.2:</b> Assigning material orientation of AA3105 .....	99
<b>Figure C.3:</b> Material modelling of LDPE .....	99
<b>Figure C.4:</b> Creation of composite shell section .....	100
<b>Figure C.5:</b> Composite layup.....	100



## List of Tables

<b>Table 4.1:</b> Standard chemical composition of AA3105 sheets according to EN 573-3....	26
<b>Table 4.2:</b> Standard mechanical properties of AA3105 sheets according to EN 1396.....	26
<b>Table 4.3:</b> Descriptions of the dimension of tensile test specimen for AA3105 sheet and aluminium composite panel .....	32
<b>Table 4.4:</b> Descriptions of the dimension of tensile test specimen for LDPE .....	32
<b>Table 4.5:</b> Nakajima test specimen dimensions. ....	42
<b>Table 4.6:</b> Mechanical properties of AA3105, LDPE and aluminium composite panel ..	51
<b>Table 4.7:</b> Strength coefficient ( $K$ ) and strain hardening exponent ( $n$ ) values .....	54
<b>Table 4.8:</b> Strain rate sensitivity ( $m$ ) values.....	56
<b>Table 4.9:</b> The plastic strain ratio, average plastic strain ratio and planar anisotropy values for AA3105 and aluminium composite panel .....	59
<b>Table 5.1:</b> Coefficient of friction values used in numerical simulation.....	75
<b>Table B.1:</b> Values of major and minor strains for 20 mm specimen 2 - section 1 .....	97



***Dedication***

*to my beloved mother, my late father, my sister and brothers  
thanks for endless love, prayers, supports and advices*

# 1 Introduction

There are many parameters to consider for any production processes such as design, machine, assembly, manufacturing method etc. One of those parameters is the material selection. Selection of the optimum material for the right process is a vital aspect of production processes. There is a huge variety of materials nowadays available for different applications. Because of the large number of possibilities; selection of the right material also requires a lot of scientific research activities. As a result, material science is today one of the most important fields both for the industries and the academic researchers. An important part of the material science activities is focused on the composite materials which are gaining more and more attention.

Composite materials can be defined as a material which is made up by combining two or more materials with different physical and chemical properties. A composite has different material properties than the individual components. It can be produced with materials from the same material group or with materials from different material groups such as metal and plastic. Aluminium-plastic composite is one of the most used composite materials for building purpose due to reasons such as high strength-to-weight ratios of the aluminium-plastic composite, suitability of mass production of the composite and good resistance to harsh environmental conditions.

Another important parameter for the production activities is the manufacturing process. Similar to the case with material selection; there are various manufacturing processes that be employed. In addition to the traditional manufacturing processes; new methods are being developed for specific purposes as well. Therefore; the key to a successful production of a targeted part is the combination of optimum design, material, manufacturing process, machine and environment.

In this master thesis work, the formability of the aluminium composite panel is studied using multi-point forming (MPF) process. The aluminium composite panel is composed of low-density polyethylene (LDPE) layer sandwiched by two sheets of 3105 aluminium alloy using a thin adhesive layer.

Multi-point forming (MPF) process is an advanced manufacturing technology used to produce three-dimensional shaped sheet metal parts. In this forming process, the traditional die is replaced by two sets of punches. The forming process is highly flexible because the punch set can be re-adjusted to create a different kind of desired shapes. MPF process is a suitable method for the production of customized parts and small batch.

This thesis work contains seven main chapters. The first chapter introduces the topic and gives outline of the whole work. Then the up-dated background information of the concepts used in this work such as information about forming processes, formability and types of multi-point forming is given in the second chapter. The second chapter also contains the literature review on the past scientific works made to investigate on multi-point forming processes.

The third chapter explains the goals of the work, the contribution of the work to the literature and the approaches used to reach these goals. The fourth chapter begins with the introduction of 3105 aluminium composite panel, gives the physical and mechanical properties of 3105 aluminium alloy according to the European standards and explains about the production process of 3105 aluminium composite panel at ASAS aluminium company. The five different mechanical tests used in the scope of this work are also introduced in chapter four. Detailed information on specimen preparation, test setup and data analysis are described. At the end of the chapter, the results from the tests are presented and discussed.

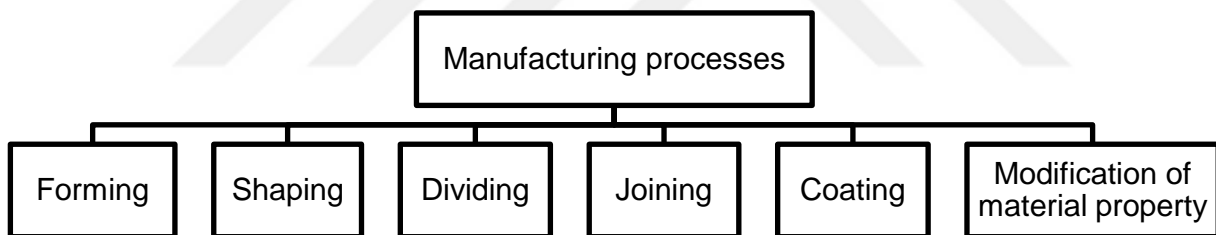
Details on punch design are introduced at the beginning of the fifth chapter. Then, a brief information on numerical simulation approach used is given starting from the element and material model of the composite panel, mesh convergence study, boundary conditions, contact interfaces and finally the results of the simulation. Chapter sixth devotes to explain the design process of multi-point forming die. In the last chapter, the summary of the results obtained from the fourth and fifth chapters is presented and suggestions on the further studies are given.

## 2 State of the Art

This chapter presents the up-to-date background information of the concepts used in this thesis work. Most of the content here comes from the literature. First, background information about forming is given in chapter 2.1. In chapter 2.2, the topic of multi-point forming (MPF) process is covered in details, then chapter 2.3 covers the topic of formability. Finally, the background information about composite material is mentioned in chapter 2.4.

### 2.1 Forming

Manufacturing processes can be classified into six main groups according to DIN 8580: primary shaping, dividing, joining, coating, modifying material property and material forming.



**Figure 2.1:** Classification of manufacturing processes according to DIN 8580

Forming is defined as manufacturing through three dimensional or plastic modifications of shape while retaining its mass and material cohesion (Schuler, 1998). In these processes, the shape of the material is modified under controlled geometry. Forming processes are chipless or non-material removal processes. The field of “forming technology” does not only include main categories of forming but also subtopics like dividing and joining through forming. Forming processes can also be combined with other manufacturing processes such as casting or laser machining.

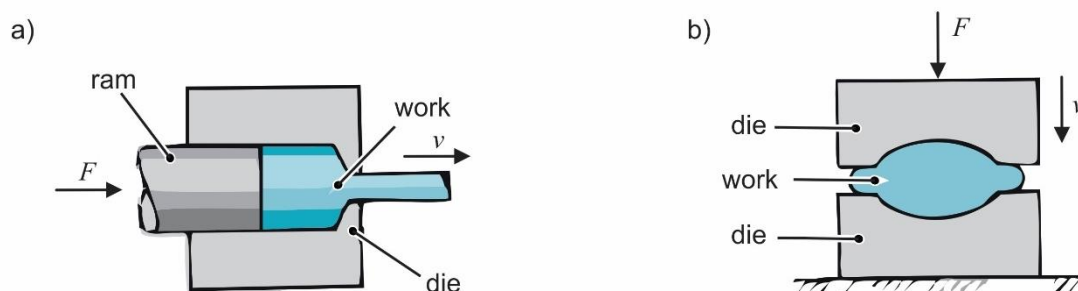
### *Classification of Forming Processes*

Based on workpiece thickness, metal forming processes can be divided into two main groups: bulk metal forming and sheet metal forming.

#### *Bulk Metal Forming*

In this manufacturing process, plastic deformation is used to change the shape of the metal workpiece between dies or tools. The workpiece is in the form of a billet, slab or rod (Semiatin, 2005). These processes involve significant amounts of plastic deformation with relatively small surface-area-to-volume ratio. Hot or warm working conditions are preferred for this type of forming process.

Extrusion and Forging (**Figure 2.2 a and b**) are among types of bulk forming processes.



**Figure 2.2 a)** Extrusion forming process, **b)** Forging forming process (Groover, 2012)

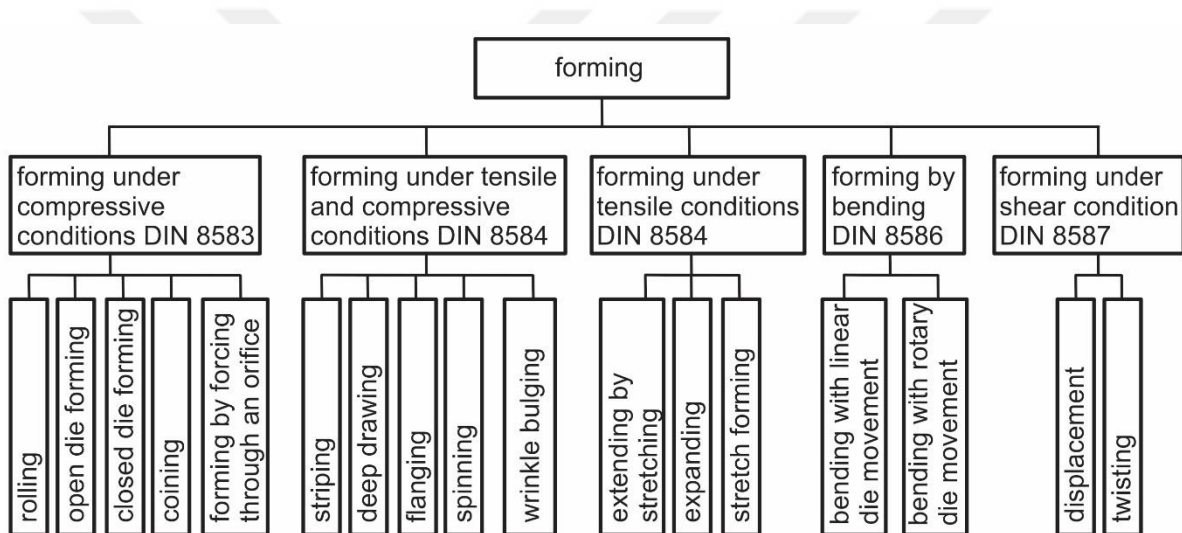
#### *Sheet Metal Forming*

In sheet metal forming, a piece of sheet metal with high cross-section-to-volume ratio is plastically deformed by forces to change the form of the workpiece (Lange, 1994). Metal sheet, coils or strips are used as workpieces. Sheet metal forming just like bulk-forming, can either be carried out at room temperature (cold forming) or the workpiece is heated to higher temperatures than the recrystallization temperature of the metal that is being formed (hot forming).

According to DIN 8582, forming techniques (sheet metal forming) can be classified depending on the main direction of applied stress (**Figure 2.3**):

- Forming under compressive conditions,
- Forming under combined tensile and compressive conditions,
- Forming under tensile conditions,
- Forming by bending,
- Forming under shear conditions (Schuler, 1998).

The DIN 8582 standard differentiated the forming process according to the workpiece geometry, die geometry and the relative movement between die and workpiece.



**Figure 2.3:** Classification of production processes used in forming under DIN 8582 (Schuler, 1998)

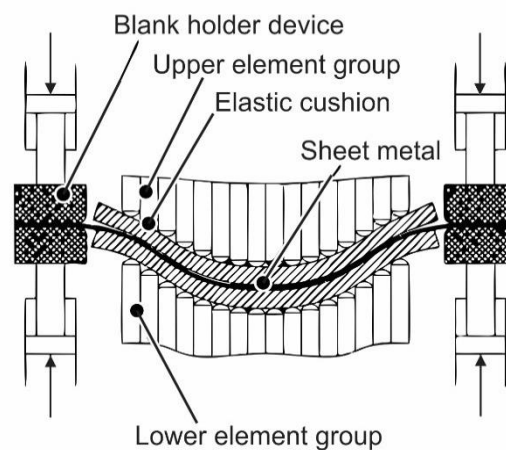
Nowadays, with the increased demand to produce complex three-dimensional parts, many advanced manufacturing technologies have been developed to fulfill this demand. Among the newly developed forming processes is the multi-point forming (MPF) process which uses punches instead of traditional die in order to save time and cost of producing conventional dies when few numbers of parts are to be produced.

## 2.2 Multi-Point Forming Process

The multi-point forming (MPF) process is an advanced manufacturing technology used to produce three-dimensional shaped sheet metal parts. An MPF integrated system can form any arbitrarily shaped parts without using conventional stamping dies given that the geometry and material information of the required part is provided. The main component of this system is a pair of matrices of punches with hemispheric ends (**Figure 2.4**). Using CAD and a control system, the desired discrete die surface is arranged by changing the positions and heights of the punches (Cai and Li, 2002).

The main characteristics of multi-point forming of sheet metal are:

- deformation of materials in MPF is not as large as that in stamping,
- bending deformation is the predominant deformation and in-plane forces are smaller than those in stamping,
- contact boundary is a multi-point, discontinuous one between sheet and punch matrices, and is much more complicated than that of stamping (Cai and Li, 2005).



**Figure 2.4:** Schematic diagram of MPF with blank-holder (Fuxing et al., 2009)



### 2.2.1 Components of Multi-Point Forming System

A typical multi-point forming integrated system is composed of four main parts:

- (i) A multi-point forming press,
- (ii) A CAD/CAE/CAM software system,
- (iii) A computer control system,
- (iv) A shape measurement system.


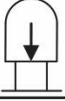
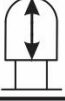
The multi-point forming (MPF) press is the central element of the system. The CAD/CAE/CAM software is used to generate the three-dimensional shape of the multi-point die and perform the numerical simulation of the forming process for prediction of the defects that may occur.

The computer control system commands the multi-point forming press to establish the forming surface of the multi-point die based on the information generated by CAD software. The shape measurement system (generally a laser coordinate measuring machine (CMM)) is used to measure the shape of the formed parts to acquire more accurate forming results (Cai and Li, 2002).

### 2.2.2 Types of Multi-Point Forming Processes

Punch adjustment methods are very critical in the multi-point forming process. They define the main features of this process. There are three types of punch adjustment methods as seen in **Figure 2.5**.

- (i) Relative fixation (fixed): Punches are adjusted to the desired height before forming.
- (ii) Passive adjustment: Punches are driven passively by pressing force of the opposed punches in the process.
- (iii) Active adjustment: Height of the punches, speed and direction can be freely adjusted during the process (Li et al., 1999).

Type	Mark	Adjusting method	Controlling force
Fixed		Before forming	Small
Passive		Be made to move in process	None
Active		Freely controlled in process	Large

**Figure 2.5:** Methods of punch adjustment (Li et al., 1999)

Based on punch adjustment methods, multi-point forming methods can be categorized into four different types (**Figure 2.6**).

#### *Multi-Point Die Forming (MPDF)*

In this method, fixed punches are adjusted to the proper position before forming, to shape the surface. During the forming process, there is no movement between the punches. This method will be used in the scope of this thesis work because the method is cost-efficient comparing to other types of MPF processes and it is easy to construct the tool. Also, the numerical analysis of this method is relatively easy compared to the other types of multi-point forming.

#### *Multi-Point Half Die Forming (MPHDF)*

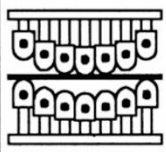

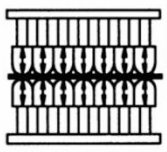
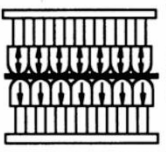
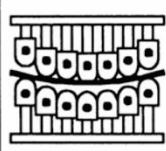
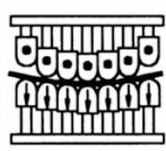
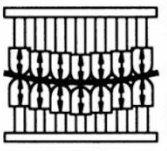
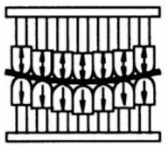
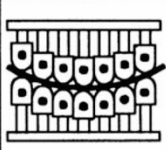

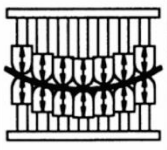
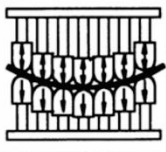
This method has both fixed and passive punches. The lower or upper punches are adjusted to the desired shape before forming, one of them being fixed. There is no relative movement between the punches. The advantage of this method is, there is a reduction of the number of the controlled punches compared to multi-point press forming and multi-point half-press forming methods because during the forming processes, the upper punches (acting as a die) are fixed and the lower punches move passively as the result of the movement of the upper punches.

### *Multi-Point Press Forming (MPPF)*

This method is made up of active upper and lower punches. To form the necessary shape of the products, punches are adjusted to the proper position during the forming process and not before the forming process like the above two methods. There is a relative movement between the punches, and each pair of punches act like a small press. The advantages of this method are; the deformation path can be changed freely to get the best deformation and the method fully displays flexible characteristics to obtain the best force state. The disadvantages are the high cost of punch and complex forming process.

### *Multi-Point Half Press Forming (MPHPF)*

The fourth method is made of active and passive punches. In this method, the movement of the active punches can be controlled freely according to necessity. The passive punches are forced to move by the pressing power of the active punches throughout the forming process (Li et al., 1999). One of the advantages of this method is the flexibility of forming process as the height of the punches can be changed at any time during the forming process. On the other hand, the cost of making the die is very high and the numerical simulation of the forming process is very difficult (Li et al., 1999).

Sorting State	Multi-point die	Multi-point half die	Multi-point press	Multi-point half press
Beginning				
Progressive				
End				

**Figure 2.6** : Classification of multi-point forming processes according to punch adjustments (Li et al., 1999)

### 2.2.3 Advantages of Multi-Point Forming

Multi-point forming is an innovative method of manufacturing sheet metal products with the following main advantages:

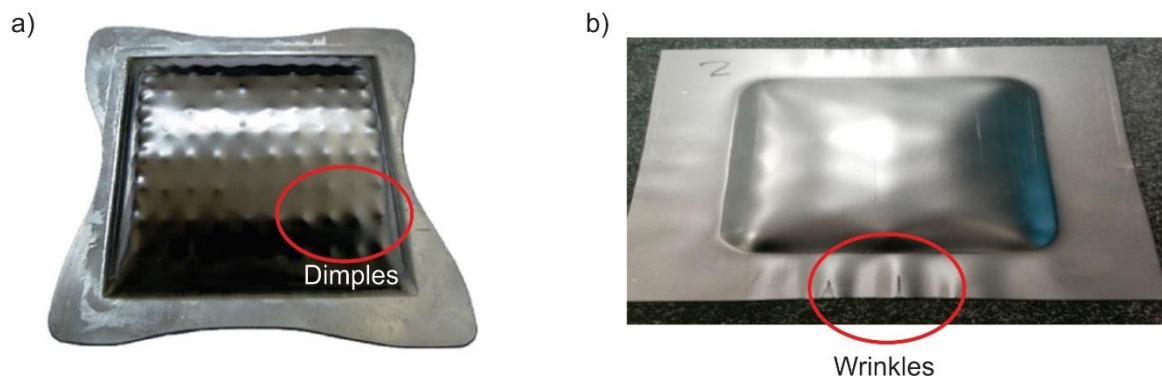
- Usage of reconfigurable discrete dies makes the process flexible.
- Complex sheet metal parts can be formed.
- Part manufacturing costs can be reduced.
- Manufacturing time is shortened substantially (Cai and Li, 2002).

### 2.2.4 Mechanical Defects in MPF Processes

Dimpling is among major mechanical defect in this process. It's mainly caused by the end contact of hemispheric punch and sheet metal surface. With the load increasing, plastic deformation occurs at the contact zone resulting in concentrated stress which produces dimpling. With using an interpolating polymer layer "elastic cushion", which is placed between sheet metal and punches, dimpling can be suppressed. The elastic cushion facilitates the distribution of the centralized load to the whole sheet and helps to produce high-quality parts with a smooth surface. (Liu et al., 2008)

Black rubber (with a shore A hardness of 50) and polyurethane pad (with a shore A hardness of 65 and 85), are among commonly used elastic cushion materials (Davoodi and Zareh-Desari, 2014). Polyurethane is mostly used because it has better wear resistance than most other polymers and is more resistant to attack by oils. Polyurethane is generally assumed to be virtually incompressible and behaves in a nonlinear elastic manner (Cai et al., 2009).

Wrinkling is another common mechanical defect in this process. It is caused by the in-plane compressive stresses. Wrinkling can be suppressed by using a blank holder to bind the blank at the periphery to provide an in-plane tensile bias (Cai and Li, 2002).



**Figure 2.7 a)** Dimpling defect on part formed by MPF process (Shen et al., 2018),  
**b)** Wrinkling defect on a formed part (Yang et al., 2018)

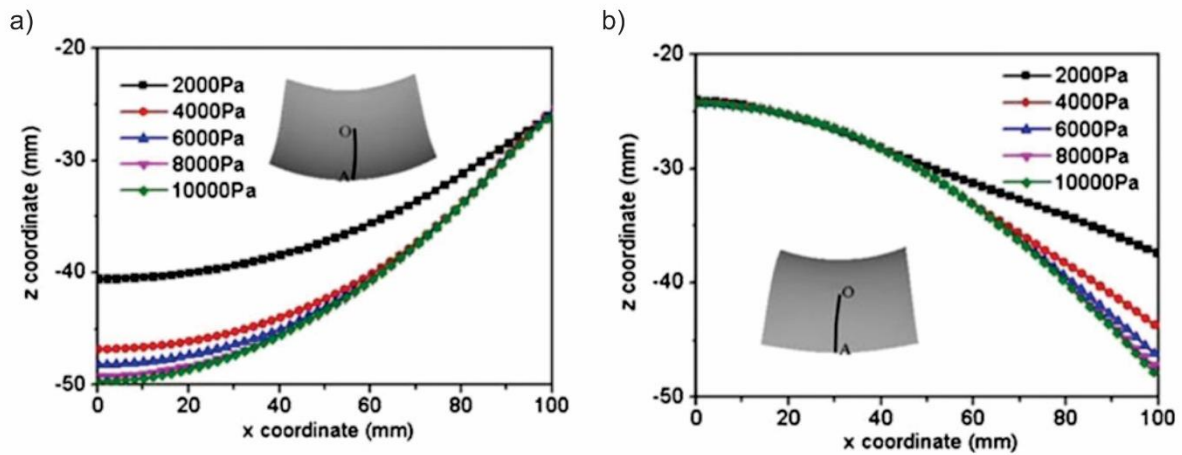
### 2.2.5 Studies on Multi-Point Forming Processes

There are many studies found in the literature about multi-point forming processes. Researchers worked to find the effect of different forming parameters on shape errors of the formed part and quality of the surface of the formed product.

#### *Effect of forming pressure*

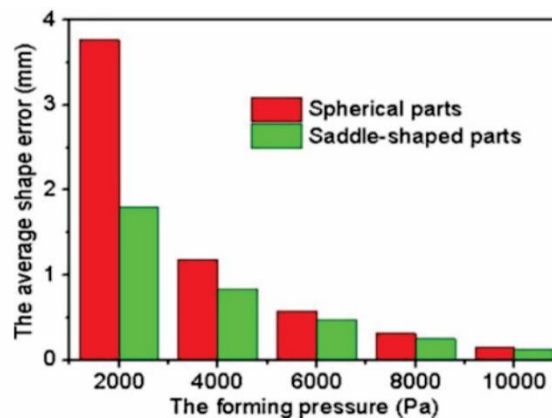
Peng et al (2013) studied the forming of polycarbonate (PC) sheet by using the multi-point forming process. They used multi-point die forming method to form a PC sheet into spherical and saddle-shaped parts. The tangent principle was used to determine the height of the punches according to the objective surface. The elastic cushion was not used in this work. The polycarbonate sheet was placed on top of the ready adjusted punch group, heated to a temperature above glass temperature and the temperature was kept for a few minutes. Then a uniform pressure was applied on top of the heated PC sheet and kept until the new product returned to room temperature. PC sheet was formed at a temperature above glass temperature because at this state the PC sheet shows good plasticity and ductility. Abaqus/Explicit software was used in FE simulation. PC material model was defined using an equation based on generalized DSGZ model. Bilinear quadrilateral three-dimensional rigid element R3D4 was used to model hemispheric end of the die punches while PC sheet was modeled with hexahedral solid element C3D8R.

Two kinds of errors were used to describe shape accuracy. Shape error ( $Z_{err}$ ) was defined by  $Z$  difference between the targeted part and formed part. The second error was average shape error ( $E_{err}$ ) which was defined as root mean square of the  $Z$  difference. The effect of five different kinds of forming pressure on forming a PC sheet, when temperature is  $160\text{ }^{\circ}\text{C}$ , punch matrix  $10 \times 10\text{ mm}$  and punch radius  $10\text{ mm}$  was then analysed.



**Figure 2.8:** The  $z$  coordinates distribution of the line OA on spherical and saddle-shaped parts with different forming pressures. **a)** Spherical part, **b)** Saddle-shaped part (Peng et al., 2013)

They found that there is a consistency on the distribution trend of  $z$  coordinate when the forming pressure is different (**Figure 2.8**). Also, the deviation between the formed part and die decreases as the forming pressure increases because large deformation occurs at high pressure (**Figure 2.9**).

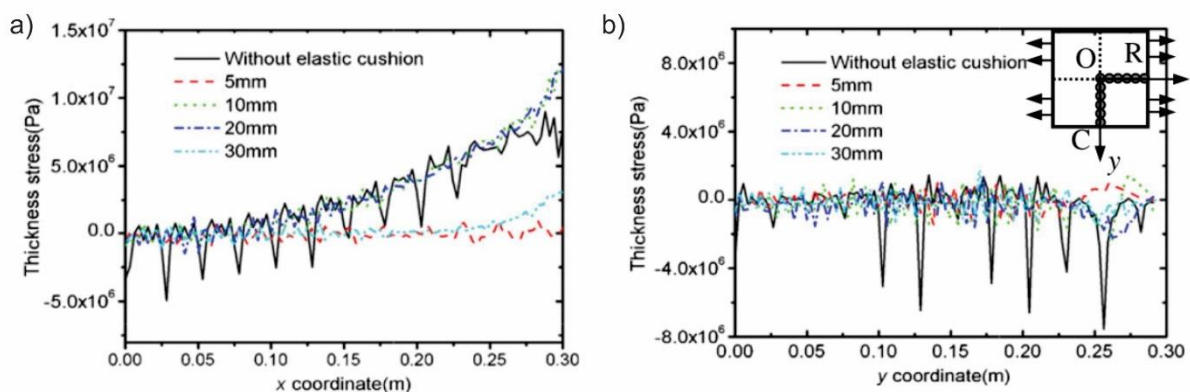


**Figure 2.9:** The average shape error of formed parts with different forming pressures (Peng et al., 2013)

### *Effect of elastic cushion*

Wang et al. (2012) used multi-point stretching die (MPSD) to investigate the effect of the thickness of elastic cushion on stress deformation and local deformation of aluminium alloy 2024-O sheet. In multi-point stretching forming (MPSF), discrete multi-point stretching die replaces the traditional fixed stretching die. Hemispherical punch with a dimension of 25 mm x 25 mm and hemispherical radius of 25 mm was used.

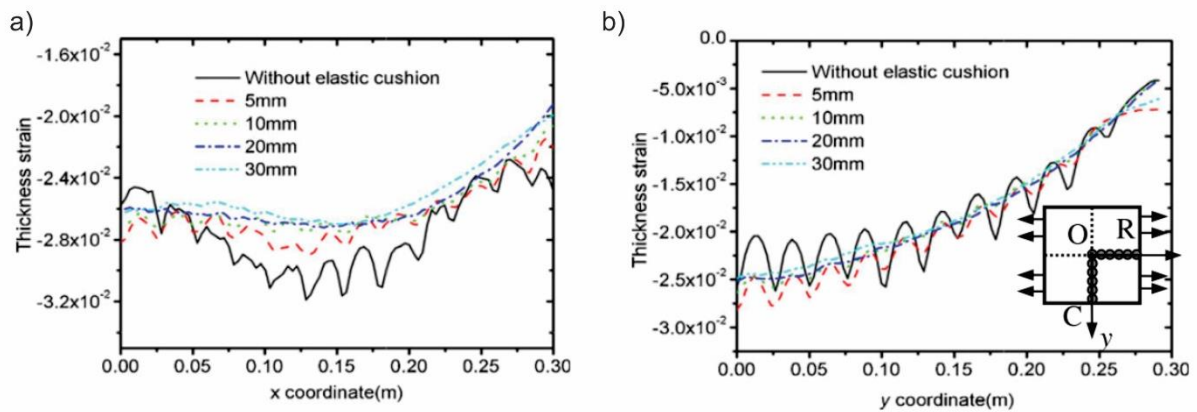
Abaqus/Explicit software was used in numerical simulation. Von Mises yield criterion and isotropic strain-hardening model was used to model the aluminium alloy. Polyurethane with a shore A hardness of 85 was used as elastic cushion provided that it had four different forms of thickness (5, 10, 20, 30 mm). Mooney-Rivlin model was used to model polyurethane. The uniaxial compression stress-strain curve obtained from a compression test of polyurethane was used as input data in the Mooney-Rivlin model. C3D8R element was used to model sheet blank and elastic cushion while die punches were modelled using R3D4 element. Sheet blank was modelled using solid element in order to analyse local deformation and stress concentration. Also, two paths (*OR* and *OC*) from the centre of the part were defined to compute thickness stress and thickness strain (**Figure 2.10 b**).



**Figure 2.10:** Thickness stress variation when four different elastic cushions are used to form a spherical part using MPSD **a)** along *OR* **b)** along *OC* (Wang et al., 2012)

For both paths, it was observed that the fluctuation of thickness stress is smaller with the increase of thickness of elastic cushion (Figure 2.10).

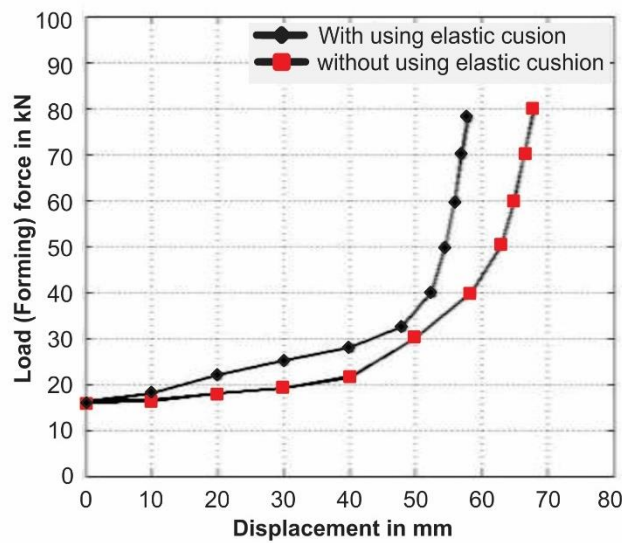
Also, the local deformation is more serious when the thickness of the elastic cushion decreases (Figure 2.11). The local deformation disappears completely when the thickness of elastic cushion is 30 mm indicating that local deformation and stress concentration can be suppressed by an elastic cushion.



**Figure 2.11:** Thickness strain variation when four different elastic cushions are used to form a spherical part using MPSD a) along OR b) along OC (Wang et al., 2012)

Kadhim and Abbas (2014) researched on experimental and numerical simulation of aluminium and steel using multi-point die forming method. ANSYS11 software was used for simulation purpose. The behaviour of elastic cushion was described using the Mooney-Rivlin hyper-elastic material model. Their results are in good agreement with the results of Wang et al. (2012). It was observed that with elastic cushion the fluctuation of thickness variation decreases due to normalization of stress variation in the shaped product. The total punch force when an elastic cushion is used is higher than without elastic cushion (Figure 2.12). They also found that the von-Mises stress values are high on the outer curved edges of the formed part because of the blank holder load and complex contact stresses between punches and parts causing these regions to have high deformation.



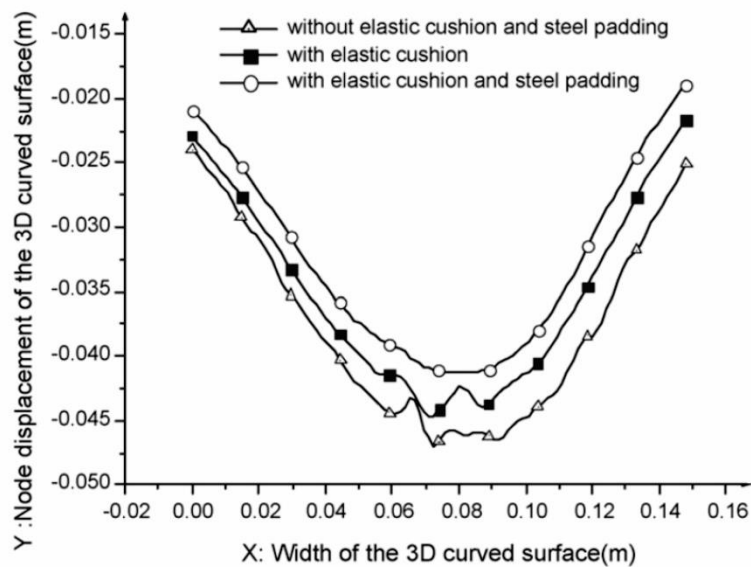


**Figure 2.12:** Graph of forming force against the displacement of the punch (Kadhim and Abbas., 2014)

(Tan et al., 2007) researched on the customization of titanium alloy cranial prosthesis using multi-point die forming process. To prevent blank holder device from damaging blank material, titanium alloy retiary sheet was placed between two pieces of steel padding made from 08AL. Then, the steel paddings were held by the blank holder device instead of placing blank material. Polyurethane was also used as an elastic cushion.

LS-DYNA software was used in FE simulation. Titanium alloy and steel padding adopted elastic-plastic model, elastic cushion adopted linear-elastic model and punch elements and blank holder device adopted a rigid body model.

From the simulation results (**Figure 2.13**), it was observed that wrinkle and dimple defects can be suppressed by the use of steel padding and an elastic cushion.

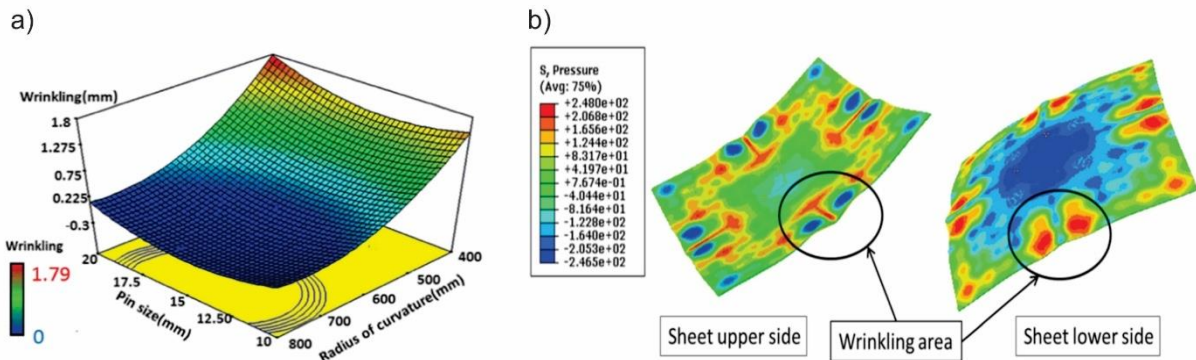


**Figure 2.13:** Graph of sectional node displacement against the width of the formed 3D curved part simulated with three different MPF modes (Tan et al., 2007)

#### *Effect of the size of punch elements*

Abosaf et al., (2017) investigated on optimisation of multi-point forming process parameters when forming 1 mm thick DC05 steel without using the blank holder. Three different types of punch tip radius (10, 15 and 20 mm) were used in numerical analysis. Abaqus/Explicit software was used in FE simulation. The blank material was assumed to be isotropic and power law equation was used to define the flow stress of the material. Polyurethane with a shore A hardness 90 (3, 6 and 9 mm thick) was used as an elastic cushion. Three material models (Neo-Hooke, Yeoh and Mooney-Rivlin) were compared with the data obtained from the uniaxial compression test results of polyurethane. Mooney-Rivlin model was observed to describe well the hyper-elastic behaviour of the used polyurethane hence used in the FE simulation to model polyurethane.

Elastic cushion and blank material were model using C3D8R quadratic solid element type while upper and lower punch set were modelled as rigid bodies using R3D4 elements. Wrinkling was measured as the normal distance between the deformed shape and target shape at every wrinkling amplitude.

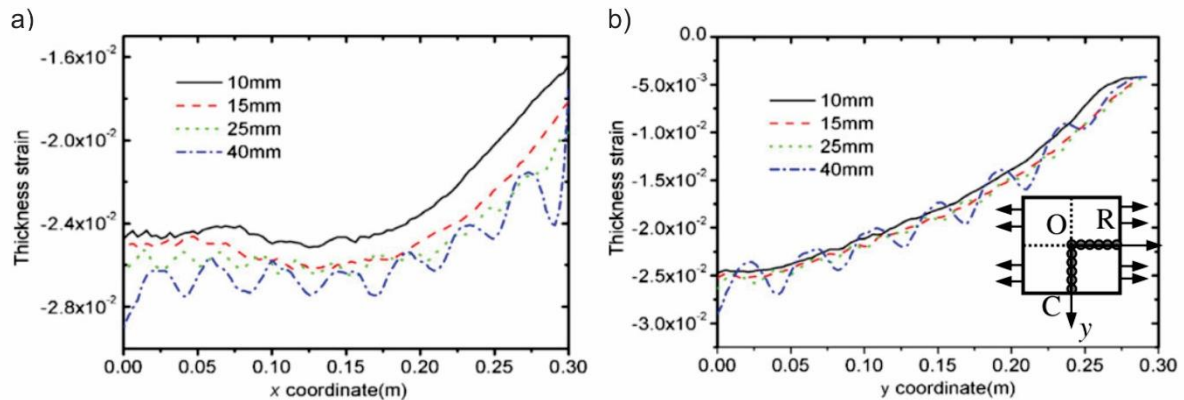


**Figure 2.14** a) Effect of the radius of curvature and pin size on wrinkling, b) Pressure distribution on both sides of the sheet when radius of curvature is 400 mm (Abosaf et al., 2017)

It was observed that as the radius of curvature decreases, wrinkling increases (**Figure 2.14 a**). The small radius of curvature causes large bending deformation and plane stress occurs as the sheet surface tries to contract under the pins. This results in wrinkling and stress instability. Effect of pin size on wrinkling varies depending on how big are the pins. Wrinkling increases when the size of the pins is less than 12.5 mm or larger than 17.5 mm. When small pins are used, the height difference between two adjacent pins (pin offset) is reduced forcing the elastic cushion to flow towards sheet edge which leads to wrinkling. Pin offset is increased when too large pin size is used causing non-uniform stress distribution on the sheet, especially on the edges (**Figure 2.14 b**). Minimal wrinkling was obtained by using a 15 mm pin size (medium size) and 800 mm radius of curvature.

Wang et al. (2012) also investigated the effect of the punch element size on the quality of the produced part. 10 mm elastic cushion and four different punch dimensions (10 x 10 mm, 15 x 15 mm, 25 x 25 mm and 40 x 40 mm) were used to simulate the MPSF process.

They observed that with 40 x 40 mm punch there is serious local deformation on the formed part and the curve fluctuate indicating that the dimples appear (a valley on the curve represents a dimple) (**Figure 2.15**). The fluctuation of the curve decreases with the decrease of the size of the punch element.



**Figure 2.15:** Effect of different punch dimensions on thickness strain of spherical part formed using MPSD a) along OR, b) Along OC (Wang et al., 2012)

#### *Effect of the blank holder (holding) force*

Yang et al. (2018) performed multi-point die forming tests to investigate the influence of process and material parameters on the quality of the aluminium alloy 1050 and low carbon sheets. Two supporting springs with different stiffness values ( $K = 87.9$  N/mm and  $38$  N/mm) were used to have two different holding (blank holder) force in order to restrain the sliding of blank materials during forming process hence better-formed part can be achieved. Polyurethane (4 mm and 8 mm thick) was selected as the elastic cushion. They used same techniques as Peng et al. (2013) to define two kinds of shape errors: shape error ( $Z_{error}$ ) and average shape error ( $E_{error}$ ) to evaluate the effect of different kind of parameters.

They found that the higher the stiffness value of the spring the lower the wrinkling defect occurs. But encourage that optimal amount of blank holder force should be selected in order to avoid over-stretching the sheet metal which might result in fractures.

They also compared the effect of blank material selection and found that steel sheet had slightly more shape errors caused by the combined effect of material's mechanical properties such as elastic modulus, yield strength and a difference in deflection amount of MPF punches caused by difference in forming forces. Their observations on the effect of elastic cushion on the shape of the formed part agree with the results from Wang et al. (2012) and Kadhim and Abbas (2014).

### *Spring back effect*

Davoodi and Zareh-Desari (2014), investigated the effect of material properties, blank thickness and anisotropy ratio on spring-back angle of AA3105. Multi-point die forming method was used to form sin-shaped geometry and V-shaped geometry. From the tensile test, AA3105 was observed to have strong anisotropic properties. Two types of elastic cushions were used in this work: rubber pad with a shore A hardness of 50 and Polyurethane with a shore A hardness of 65 and 85.

Abaqus/CAE 6.9.1 software was used in FE simulation of spring-back prediction in two stages. The first stage involved using explicit code to simulate the forming process and the second stage involved using implicit code to simulate the unloading process in order to calculate the spring-back of the formed part. The change of bending angle for V-shaped geometry and change of  $\theta_1$  (also called spring-back angle) for sin-shaped geometry were used to study the effect of the said parameters on spring back.

R3D4, C3D8R and S4R elements were used to model punches, elastic cushion and blank material respectively. The results obtained from compression tests of elastic cushions were used as input data in the Mooney-Rivlin model. Hollomon plastic flow equation was used to describe the work hardening of the AA3105 and Barlat-89 non-quadratic yield criteria used to take anisotropy behaviour of aluminium under consideration.

From the numerical simulation and experimental tests, it was observed that spring back values of AA3105 vary slightly with change in blank orientation, spring back decreases significantly when hardness of elastic layer increases, increase of thickness of blank results to decrease of spring back, the higher the amount of plastic strain ratio, the higher the values of spring back.

### *Numerical Analysis of Forming Process using Aluminium-Plastic Composite*

Parsa et al., (2010) investigated on the spring back of AA3105/polypropylene/AA3105 sandwich sheet subjected to double-curvature forming. To produce the sandwich sheet, two layers of AA3105 sandwiched a layer of polypropylene with a 200-micron thick adhesive layer on both sides. Abaqus/Explicit software was used in FE simulation.

The explicit procedure was used to simulate the loading process while unloading process was simulated using implicit procedure.

Polypropylene (PP) was assumed to have isotropic behaviour because PP completely melts during the production of the sandwich sheets and it solidifies smoothly. Isotropic hardening rule was used to model polypropylene an AA3105. Tensile test results of AA3105 sheet and PP showed that both materials have isotropic behaviour. Hollomon plastic flow equation was used to describe work hardening of both materials. Die and punches were modelled as rigid parts. The friction at the interfaces between die surface, punch and sheet were assumed to be based on Coulomb's law.

The experimental and simulation results showed that the sandwich sheet could be bent around a radius of 60-120 mm without causing any damage. Due to the non-uniformity of shear strain distribution in the PP layer, the sandwich sheet had non-uniform curvature after unloading. The sandwich sheet had lesser spring-back than monolayer aluminium sheet of the same flexural stiffness meaning the sandwich could sustain greater strain than aluminium sheet. The amount of spring-back increases as the thickness of the sandwich sheet increases.

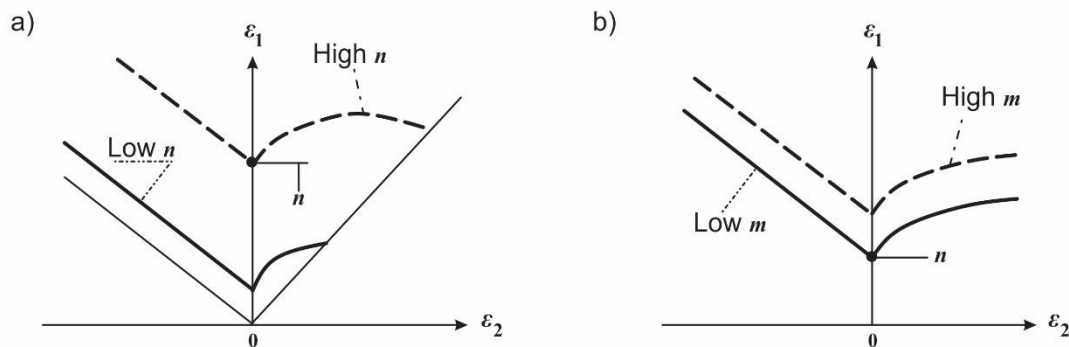
### **2.3 Formability**

Formability is the ability of a metal to adopt the desired shape without fracture or necking. The formability of a material is not a fixed quantity but highly depends on the mean hydrostatic pressure ( $P_m$ ) exerted during the forming operation. The formability of materials increases with increasing hydrostatic pressure. (Marciniak et al., 2002)

One way to measure the formability of metal is by using the forming limit curve (FLC). Forming limit curve (FLC) is a curve which indicates the onset of observed necking or fracture in the principal strain space (in the sheet plane).

With FLC, it is possible to validate the finite element simulation results, whether the forming process will run successfully (without crack formation) or any changes to the process parameters are required to obtain better results. Nakajima test (covered in chapter 4.5) is among mechanical tests used to compute FLC for metals.

Strain-hardening ( $n$ ), strain rate sensitivity ( $m$ ), ductile fracture and inhomogeneity are among factors affecting the forming limit curve (FLC) (Marciniak et al., 2002). The height of the FLC decreases as the values of  $n$  and  $m$  decrease (**Figure 2.16 a and b**).



**Figure 2.16 a)** Effect of strain-hardening ( $n$ ) on FLC, **b)** Effect of strain rate sensitivity ( $m$ ) on FLC (Marciniak et al., 2002)

## 2.4 Composite Materials

A composite can be defined as a material formed by combining two or more materials in order to achieve better properties (physical, chemical, etc.) than those of the constituents. Composites are mainly made of the matrix and the reinforcement. The matrix protects the fibres and carries some of the loads (i.e. intralaminar shear stress, transverse stress and bearing stress) while fibres, on the other hand, provide most of the stiffness and strength (Barbero, 2011). Reinforcements are usually discontinuous, stiffer and stronger while matrixes are less stiff but continuous.

Advantages of composites over monolithic materials are low density, long fatigue life, high strength, high stiffness and adaptability to the intended function of the structure.

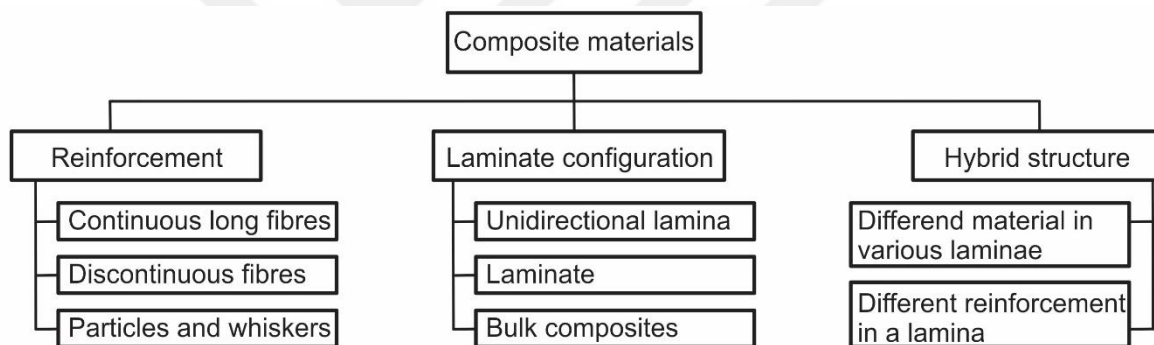
The superior structural performance of composite materials is based on high specific stiffness (modulus to density ratio) and high specific strength (strength to density ratio). The properties of a composite material depend on the properties of the constituents, their geometry, and the distribution of the phases (Daniel and Ishai, 2006).

### 2.4.1 Classification of Composite Materials

There are many ways to categorize composite materials. **Figure 2.17** shows the classification of composite materials according to reinforcement materials, laminate configuration and hybrid structure.

Unidirectional lamina is made up from a single lamina (also called *layer* or *ply*), or several laminae (plural) with the same material and orientation in all laminae. Laminate is made up of several laminae, with at least some laminae having different material or orientation, stacked and bonded together.

The composite with laminae which cannot be identified is called bulk composite. This includes bulk moulding compound composites and particle-reinforced composites (Barbero, 2011).



**Figure 2.17:** Classification of composite materials (Barbero, 2011)

Composite materials can also be categorized according to their uses such as airplane composite, automotive composite and building composite.

### 2.4.2 Composites in Building Applications

Due to factors like high strength-to-weight ratios, resistance to environmental attack, suitability for mass production and ability to be moulded into different shapes, plastic and reinforced plastic composites have become one of the most used building materials especially for making facades. Plastic composites are formed by combining plastic resins and reinforcing materials.



Various thermoplastic or thermosetting resins are used as structural plastics to produce plastic composites. Fillers or various additives may be added so to improve durability, fire resistance or stiffness of the composite. The properties of the plastic composite are highly influenced by manufacturing method used (Mortensen, 2007).

Among mostly used plastic composite for building application are aluminium composites. They are mainly made from two thin aluminium sheets and plastic materials (mainly Polyethylene). 3105 aluminium composite panel is the main material used in this work in order to investigate its formability by using the multi-point forming (MPF) process.



### **3 Goal of the Work**

The goal of this master thesis work is to investigate the formability of the 3105 aluminium composite panel by means of the multi-point forming process. The first approach in this work is to study the literature regarding the effect of forming parameters on the multi-point forming (MPF) processes.

Material characterization of aluminium composite panel will be conducted using five different mechanical tests. The first test to be performed is the T-peel stripping test. In this test, the behaviour of the bond between AA3105 sheets and LDPE layer will be investigated. Then, tensile tests of AA3105 sheet, LDPE and aluminium composite panel will be performed in order to obtain mechanical properties of each component of the composite such as strain rate sensitivity, anisotropy values and flow stresses. In addition, fracture analysis of the aluminium composite panel tensile test specimens will be conducted using a scanning electron microscope (SEM) to investigate on the bond condition between LDPE and AA3105 sheets before fracture.

In-plane torsion test will be conducted in order to obtain a flow curve of AA3105 sheet up to high strains. Nakajima test will be conducted to obtain the forming limit curve (FLC) of the aluminium composite panel. Finally, friction test will be performed to investigate on contact condition between aluminium composite panel, MPF die and elastic cushion.

The numerical analysis will be done in two stages: first to find the height of the punches with reference to the targeted surface to be formed and second to simulate the loading process of MPF process using a commercial finite element software Abaqus/Explicit 6.14. In finite element (FE) simulation, the effect of the selected forming parameters on the forming process will be investigated under different conditions. Multi-point forming die will be designed using SolidWorks® software.

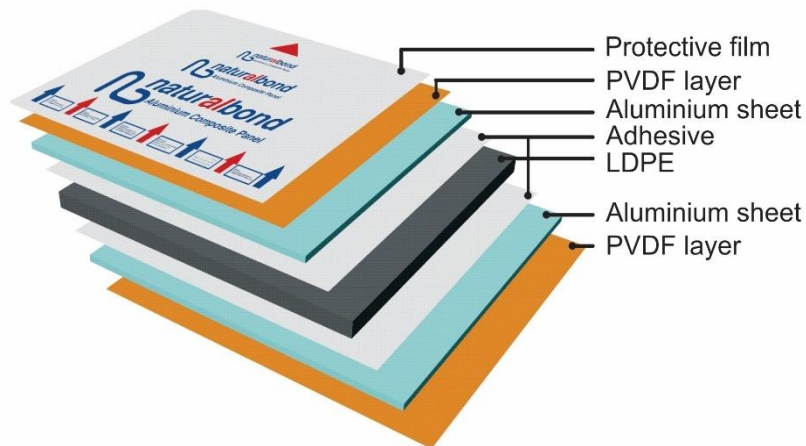
This work aims to contribute to the literature on numerical simulation of 3105 aluminium composite panel using multi-point forming process as there is no literature found regarding formability analysis of this kind of material using MPF process.

## 4 Material Characterization

### 4.1 3105 Aluminium Composite Panel

An aluminium composite panel produced by ASAS aluminium company in Turkey with the commercial name NATURALBOND® is used in this thesis. NATURALBOND® is a contemporary building material with a smooth, aesthetic, chic appearance used in the design of architectural buildings and also as protective coating materials. It's a three-ply sandwich sheet composed of non-heat treatable 3105-H46 aluminium alloy as face sheets and low-density polyethylene (LDPE) as central material. LDPE is used because of its good performance and low production costs.

A standard NATURALBOND® aluminium composite panel is made of two 0.5 mm thick AA3105 sheets and 3 mm thick LDPE layer. NATURALBOND® aluminium composite panels are produced by a continuous hot-pressing method. **Figure 4.1** shows different layers of the composite panel. For simplicity, 3105 aluminium composite panel will be used to refer to the composite panel instead of using the commercial name of the product.



**Figure 4.1:** Layers of NATURALBOND® composite panel (ASAS aluminium)

The protective film needs to be removed right after the mounting of the panel. Among the advantages of these composite panels are:

- They are 40% lighter compared to aluminium sheets with similar resistance,
- High material resistant to atmospheric terms (against corrosion and wind load),

- Smooth surface.

#### 4.1.1 Physical and Mechanical Properties of 3105 Aluminium Alloy

AA3105 sheets are produced by cold rolling processes under temper H46 according to EN 573-3 (chemical composition) and EN 1396 (mechanical properties) standards. AA3105 sheet is used as ply material because of it is high resistance to corrosion and high dyeing ability. **Table 4.1** and **Table 4.2** contain standard chemical compositions and standard mechanical properties of AA3105 sheets respectively.

**Table 4.1:** Standard chemical composition of AA3105 sheets according to EN 573-3

Elements	Si	Fe	Cu	Mn	Mg	Cr	Zn	Ti	Al
Composition (wt%)	0.6	0.7	0.3	0.30- 0.80	0.20 - 0.80	0.2	0.40	0.10	Rest

The upper surface of the aluminium sheet is coated by Polyvinylidene Fluoride (PVDF) coating. PVDF coatings are mainly used to coat aluminium and steel for architectural purpose in order to last for a long time without colour changes or coating chalk.

**Table 4.2:** Standard mechanical properties of AA3105 sheets according to EN 1396

Material	$R_{p0,2}$ , MPa	$R_m$ , MPa		Elongation at fracture $A_t$ (%) min. for specified thickness $t$ mm		
	Min	Min	Max	$t \leq 0.5$	$0.5 < t \leq 1.5$	$t > 1.5$
AA3105 [Al Mn0.5 Mg0.5] Temper H46	150	175	225	2	2	3

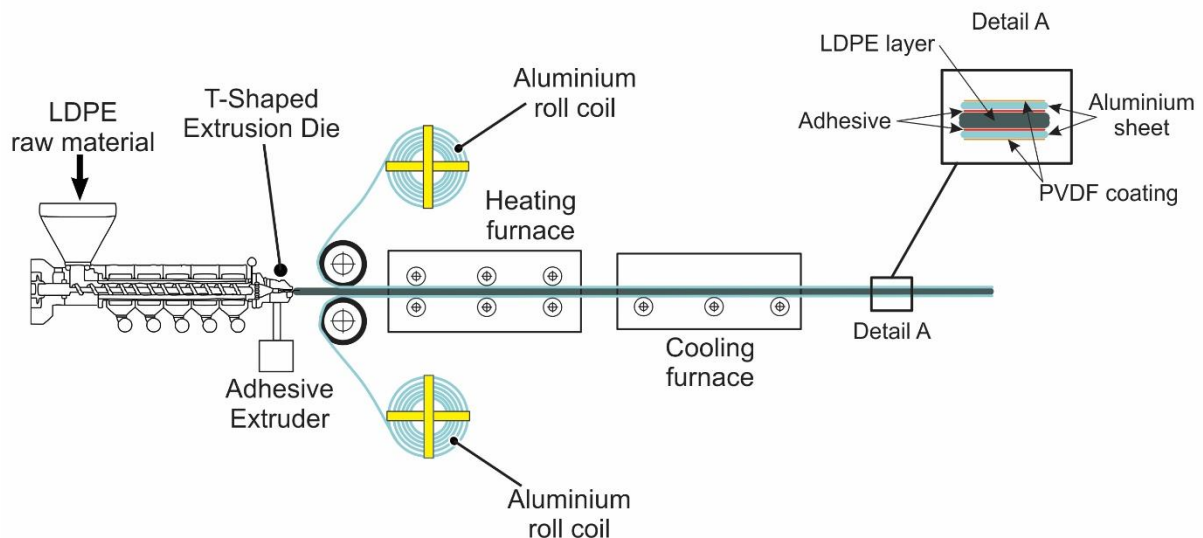
LDPE, which is the first synthesized polyethylene, is produced by plastic extrusion process without any preferred material orientation then directly bonded between two AA3105 sheets using a thin adhesive layer. According to ASTM D 1248 standard, LDPE has a nominal density range of 910 – 925 kg/m<sup>3</sup> and tensile strength ( $R_m$ ) of 9.7 MPa.

Tensile tests of AA3105, LDPE and 3105 aluminium composite panel at different strain rates are conducted later in this work to experimentally determine mechanical properties of the AA3105, LDPE and 3105 aluminium composite panel.

#### 4.1.2 Production Process of the 3105 Aluminium Composite Panel

The 3105 aluminium composite panels are produced on continuous hot-press production lines, ensuring excellent impact strength, peel strength and superior flatness. **Figure 4.2** illustrates the production process.

Firstly, an LDPE layer is extruded from T-shaped extrusion die at around 190 °C temperature. Then, a hot-melt BYNEL® 3000 series adhesive layer with a thickness of 70 microns is directly deposited on the top and the bottom of the LDPE layer by adhesive extruders which are directly connected to the die. Two PVDF coated aluminium sheets are roll bonded with LDPE layer through continuous hot-pressing machines under controlled temperature until cooled down. The temperature of aluminium sheets at the beginning of the roll bonding process is around 170° C. At the end of the production process, a protective layer is placed at the top surface of the produced composite panel.



**Figure 4.2:** Production process of aluminium composite panel (ASAS aluminium)

In order to determine different mechanical properties of AA3105, LDPE and 3105 composite panels under different conditions, five types of mechanical tests are used. Those tests are: (i) T-peel stripping test, (ii) tensile test, (iii) in-plane torsion test, (iv) Nakajima test and (v) friction test.

The T-peel stripping test is used to characterize the bond between AA3105 sheets and LDPE. The tensile test is used to determine the mechanical properties of AA3105 sheets, LPDE and Aluminium composite panels under uniaxial loading condition. The in-plane torsion test is used to determine the flow curve of AA3105 sheets up to high strains. The Nakajima test is used to determine the forming limit diagram (FLD) of aluminium composite panel and the friction test is used to determine values of the coefficient of friction between aluminium composite panel, elastic cushion and MPF die punches during multi-point forming processes.

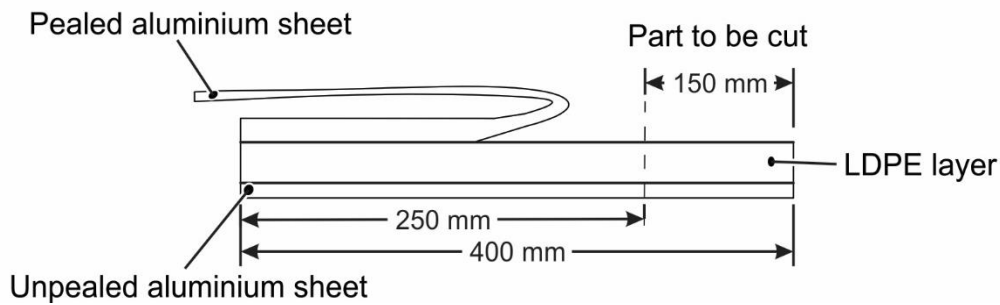
## **4.2 T-Peel Stripping Test**

Before starting the work on characterizing composite materials, it is important to investigate the quality of adhesive bonds between the core layer and face layers. The T-peel stripping test is among the common test methods used to determine the stripping characteristics of adhesive bonds found between the core and face layers. In this work, the peel strength of the adhesive bonds found between AA3105 sheets and LDPE is investigated using this test method. Peel strength is the average load per unit width of bond line required to separate progressively one member from the other over the adhered surfaces at a separation angle of approximately  $180^\circ$  and a separation rate of 152mm/min (ASTM D 903-98). It is expressed in newton per millimetre of the specimen width. This test is conducted in the material laboratory of ASAS aluminium company.

### **4.2.1 Specimen Preparation**

Specimen are prepared according to ASTM D 903-98 standard by cutting aluminium composite panel to stripes of 400 mm x 25 mm, using a Durma® shearing machine. Ten specimens are used in this test.

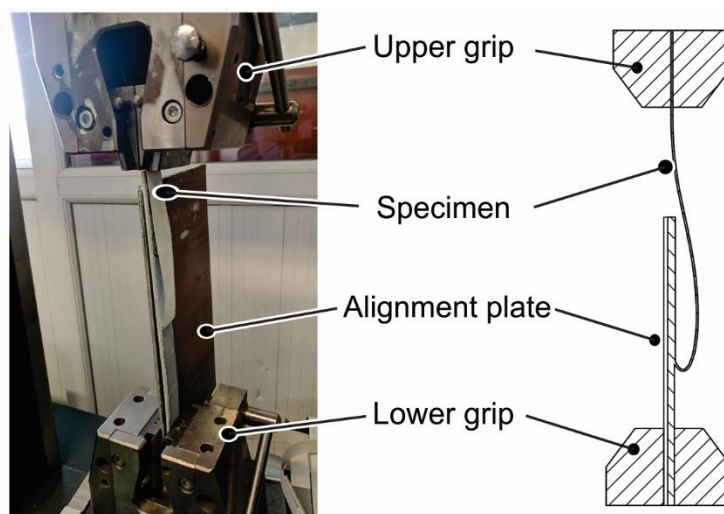
On one side of the specimen, the aluminium sheet is manually peeled for about 220 mm and turned  $180^\circ$  to be parallel with LDPE layer. Finally, the open side of the specimen is cut for about 150 mm (**Figure 4.3**).



**Figure 4.3:** T-Peel stripping test specimen geometry according to ASTM D 903-98

#### 4.2.2 Experimental Setup

Tests are conducted using Zwick/Roell Z050 machine at room temperature. Firstly, the pealed aluminium sheet is clamped to the upper grip. Then, the open side of the specimen is clamped to the lower grip together with the alignment plate after the force is set to zero. Alignment plate (**Figure 4.4**) is used to hold the specimen in order to maintain the specimen in the plane of the clamps. To record the stripping strength values, the pealed aluminium sheet is stripped for about 180 mm before stopping the machine. TestXpert software found in the computer connected to the machine calculates the peel strength and plots the graph of force in N/25 mm (Newton per width of the specimen) against path in mm.



**Figure 4.4:** T-Peel test setup according to ASTM D 903-98

### 4.2.3 Data Analysis

TestXpert software creates a graph of force in N/25 mm against path in mm and calculates the average value of peel strength for the specific specimen. The average value of the peel strength for all ten specimens is calculated as the arithmetic mean of the peel strength values of each specimen.

According to the Turkish standard institution, the mean peel strength for the ten specimens should be at least 175 N/ 25 mm (TS 13777).

## 4.3 Tensile Test

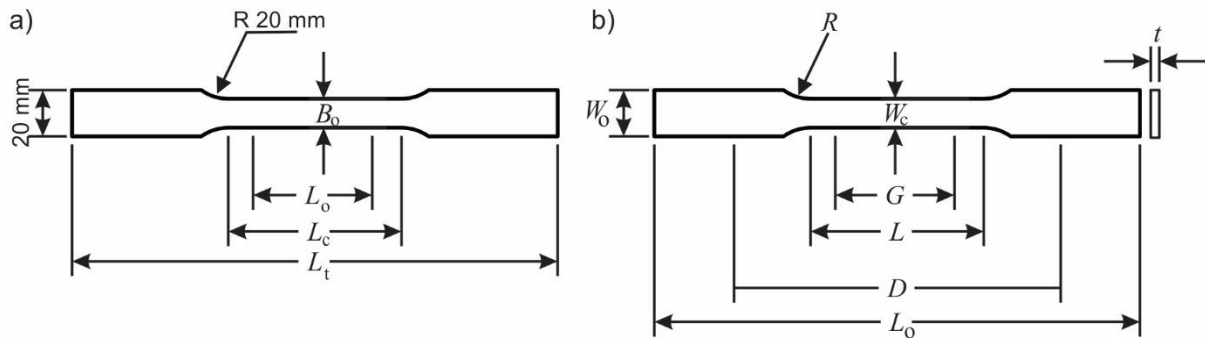
The tensile test is a common test method used to determine mechanical properties of materials such as yield strength ( $R_{p0.2}$ ), tensile strength ( $R_m$ ), elongation at maximum load ( $A_g$ ), elongation at fracture ( $A_t$ ) and Young's modulus ( $E$ ). In this test, a sample specimen is subjected to a controlled tension until failure. In this work, tensile tests for AA3105 sheets and aluminium composite panels are conducted according to (DIN EN ISO 6892-1) standard while tensile tests for LDPE are conducted according to (ASTM D 638-14) which is a standard used for the preparation of tensile testing of plastics at room temperature. Some of the aluminium composite specimens are tested up to the pre-defined strain, the test is stopped and then the fracture analysis of the same specimens is conducted to study the nature of the bond between AA3105 sheet and LDPE before fracture. All tensile tests are performed in IUL at TU Dortmund while the fracture analysis is conducted in ASAS aluminium company.

### 4.3.1 Specimen Preparation

AA3105 sheet and aluminium composite panel specimens are prepared according to DIN EN ISO 6892-1 standard. This standard is used for the preparation of tensile testing of metallic materials at room temperature. LDPE specimens are prepared according to ASTM D 638-14, specimen type I for rigid and semi-rigid plastics. Type I specimen is mostly used for plastic specimens of thickness 7mm or less (ASTM D 638-14).



**Figure 4.5 a** illustrates the geometry of the standard specimen according to DIN EN ISO 6892-1 while **Figure 4.5 b** illustrates the geometry of the standard specimen according to ASTM D 638-14.



**Figure 4.5 a)** Tensile test specimen geometry according to DIN EN ISO 6892-1,  
**b)** Type I tensile test specimen geometry according to ASTM D 638-14

Using a press machine, AA3105 sheet and aluminium composite panel specimen are cut according to the rolling direction angles ( $0^\circ$ ,  $45^\circ$  and  $90^\circ$ ) of the AA3105 sheet so as to observe the anisotropic behaviour of aluminium alloy for both specimens.

LDPE layer specimens are prepared by cutting the aluminium composite panel using a press machine then manually peeling both layers of AA3105 sheets to get a 3 mm layer of LDPE. **Table 4.3** contains the description of the dimension of the tensile test specimen for AA3105 sheet and aluminium composite panel and **Table 4.4** contains that of LDPE.

For the sake of accuracy, three specimens are prepared for each rolling direction. Each specimen is labelled with the degree of rolling direction, material type and specimen number as seen in **Figure 4.7**.

**Table 4.3:** Descriptions of the dimension of tensile test specimen for AA3105 sheet and aluminium composite panel

Symbol	Description	Dimension (mm)
$t_{o,Al}$	Initial thickness of an AA3105 flat test piece	0.5
$t_{o,comp}$	Initial thickness of an aluminium composite flat test piece	4
$B_o$	Initial width of the parallel length of a flat test specimen	12.5
$L_o$	Original gauge length	50
$L_c$	Parallel length	75
$L_t$	Initial total length of the specimen	210

**Table 4.4:** Descriptions of the dimension of tensile test specimen for LDPE

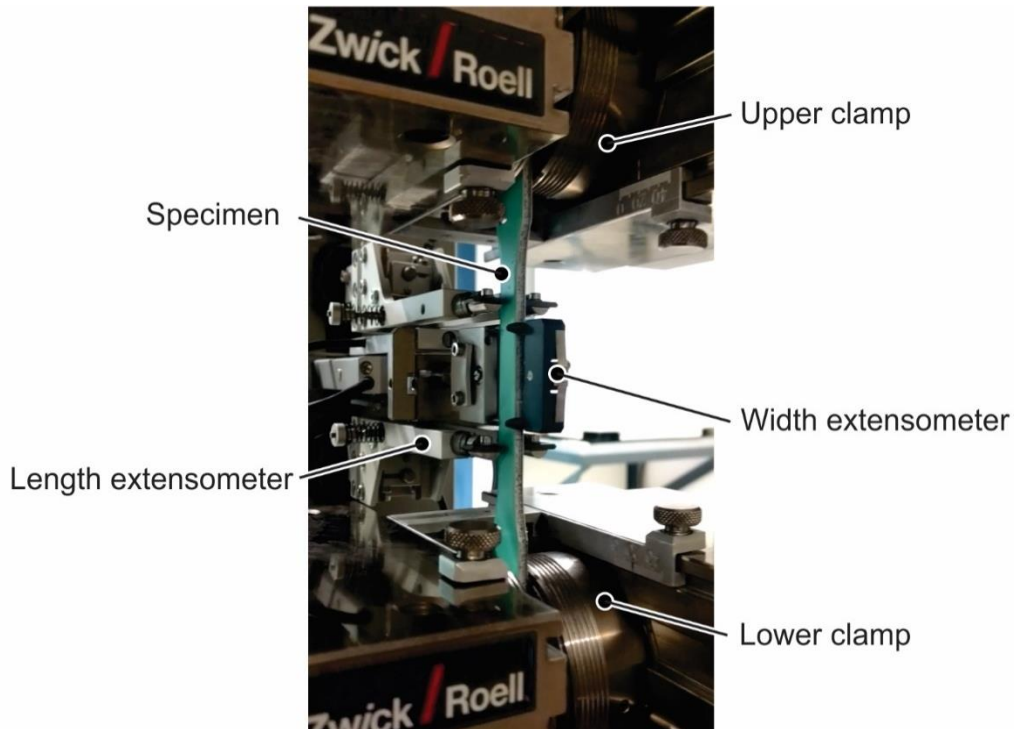
Symbol	Description	Dimension (mm)
$t$	Thickness of the specimen	3
$W_c$	Width of narrow section	12.5
$W_o$	Width overall, min	20
$G$	Gage length	50
$L$	Length of narrow section	70
$D$	Distance between grips	115
$L_o$	Initial total length of the specimen	210
$R$	Radius of the fillet	20

### 4.3.2 Experimental Setup

Zwick/Roell Z250 universal testing machine is used for this test at room temperature.

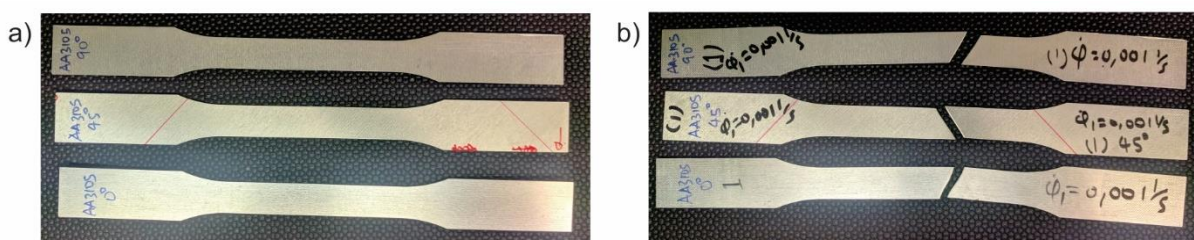
**Figure 4.6** illustrates the test setup. All specimens are cleaned to remove any dirt and/or dust on the surface and then the exact dimensions of the specimen are measured.

The measured dimensions are used as input data in TestXpert II software before clamping the specimen to the machine. The clamps are used to tighten the specimen evenly and firmly to prevent slippage of the specimen during the test.



**Figure 4.6:** Tensile test setup using Zwick/Roell Z250 machine

Before starting the test, the machine is set to zero and the distance between the clamps is set according to the type of material (115 mm for LDPE and 135 mm for AA3105 sheet and aluminium composite panel). The specimens are then positioned between the clamps and the upper grip is closed first. Tensile tests for AA3105 sheet and aluminium composite panel are conducted at 0.001 1/s, 0.01 1/s and 0.1 1/s strain rates. Tensile tests for LDPE are conducted at 0.00167 1/s and 0.01667 1/s strain rates. The specimen elongation is measured directly on the test specimens by means of a tactile macro-extensometer with a gauge length of 50 mm (Figure 4.6). The extensometer also measures changes at the specimen width. Throughout the test, the TestXpert II Software records load, extension in length and width of the specimen. The specimen which break outside of the original gauge length are considered invalid.



**Figure 4.7:** AA3105 tensile test specimens **a)** before the test, **b)** after the test

### 4.3.3 Data Analysis

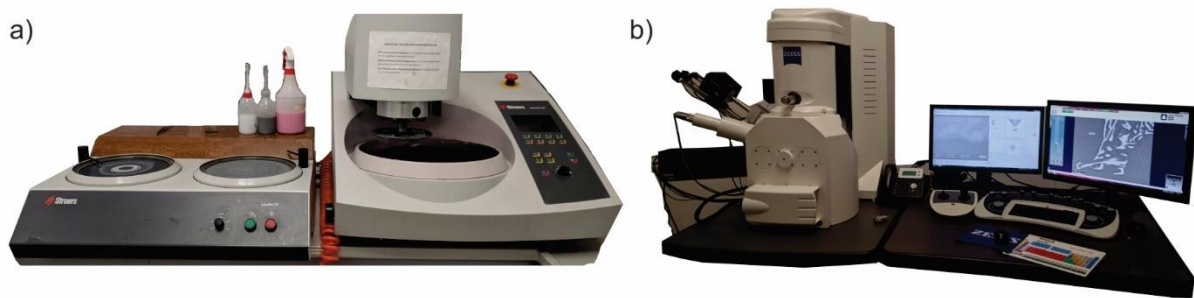
The force-displacement data obtained from the tensile test are analysed using Microsoft Excel program. Both engineering stress-strain graphs and true stress-strain graphs are computed. A mean curve for every three specimens of the same test parameters is drawn. The values of elastic modulus ( $E$ ), yield stress ( $R_{p0.2}$ ) and tensile strength ( $R_m$ ) are obtained directly from the TestXpert II software. Yield stress ( $R_{p0.2}$ ) is calculated by the software using the offset method in which a line is drawn parallel to the linear line (found in the elastic region) with 0.2% offset value. The value at the point of intersection between the stress-strain curve and offset line is a yield stress ( $R_{p0.2}$ ). At the yield point, materials start to deform plastically while at tensile strength ( $R_m$ ) necking starts.

### 4.3.4 Fracture Analysis with Scanning Electron Microscope

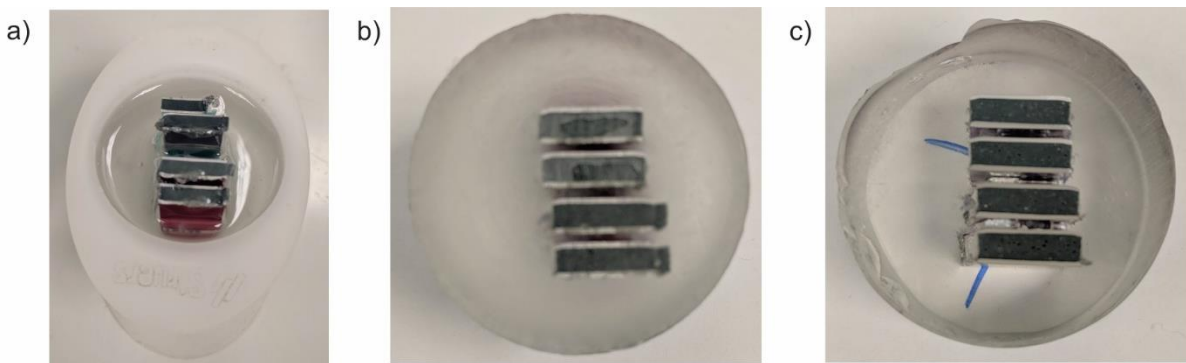
Fracture analysis is very important in order to learn more about the bond condition between the composite laminates just before a fracture occurs. In this study, the fracture analysis was done using Zeiss EVO MAT 15 scanning electron microscope (**Figure 4.8 b**) found in the material laboratory at ASAS aluminium company. Eight aluminium composite panel specimens from tensile tests, which differ from one another by their rolling direction, test strain rate and amount of strain at which the test was stopped, are prepared for this analysis.

#### *Specimen preparation*

The specimens are cut close to the fracture formation zone then mixed with EpoFix resin and EpoxFix hardener to form a Bakelite (**Figure 4.9 a and b**). The formed Bakelite is ground using silicon carbide (SiC) abrasive papers with different grit sizes, then polished using colloidal silica (SiO<sub>2</sub>) (Figure 4.9 c). Finally, the Bakelite is coated with gold in order to improve the surface conductivity.



**Figure 4.8** a) grinding and polishing machines used for the preparation of Bakelite, b) Zeiss EVO MAT15 scanning electron microscope used for fracture analysis

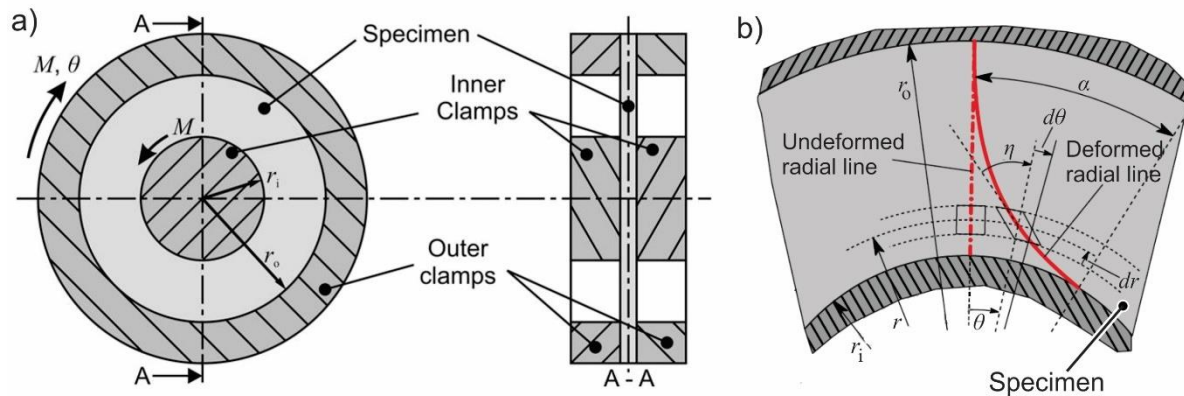


**Figure 4.9:** SEM specimen preparation procedures a) preparation of the Bakelite b) condensed Bakelite 12 hours after preparation c) Bakelite after several grinding and polishing

#### 4.4 In-plane Torsion Test

The in-plane torsion test is a shear test for material characterization of planar sheet and also for arbitrarily shaped components. Marciniak first used this test to determine the Bauschinger effect in copper sheets and determination of the forming limit. This test is used to determine flow curves with an equivalent plastic strain of up to 1.0 by (Tekkaya et al., 1982). In this test, a circular specimen is clamped on the outer rim as well as in the centre (**Figure 4.10 a**), then the outer clamp is rotated against the inner clamps. As a result, the total free area between the clamping devices is loaded with simple shear in the sheet plane (Traphöner et al., 2017).

**Figure 4.10 b** illustrates the deformation of the radial line on the surface of the specimen during testing (Traphöner et al., 2018).



**Figure 4.10 a)** Schematic design of the in-plane torsion test (Yin et al., 2015b),  
**b)** Deformation of a radial line during testing (Traphöner et al., 2018)

Classical experiments such as uniaxial tensile test have disadvantages like material fracture at lower plastic strains, the formation of necking on specimens results to an inhomogeneous stress and strain state. In-plane torsion test on the other hand not only allows the determination of characteristic values up to high true strains but also allow possibilities of determination of several flow curves on only one specimen (Yin et al., 2015a).

The following can be achieved with this test method:

- The determination of flow curves for high strains,
- The determination of multiple cyclic flow curves with only one specimen in one test,
- The characterization of the forming limit with a specially grooved specimen,
- The determination of flow curves on curved components with form-fitted clamping's
- The non-destructive determination of the local strength for arbitrarily shaped parts (Traphöner et al., 2017).

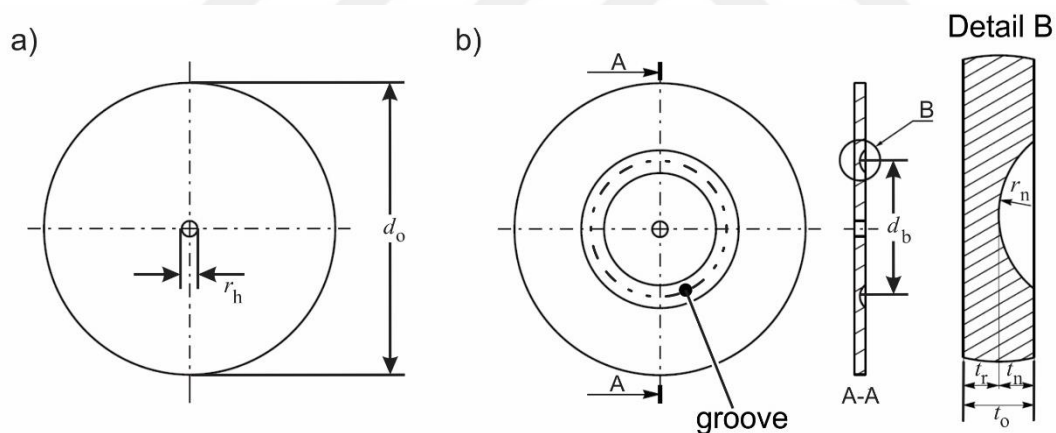
Some of the disadvantages of this test method are:

- Averaging of the planar anisotropy over the circumference of the specimen,
- The occurrence of slipping of the punch when sheet thickness or the material flow stress is too high (Traphöner et al., 2017).

In the scope of this work, the in-plane torsion test is used to determine the flow curve of AA3105 sheet up to high strains and to compare the results from this test with the results of AA3105 sheet obtained from the tensile test.

#### 4.4.1 Specimen Preparation

Three types of specimen geometries are used in this test: (i) uncoated and non-grooved specimen, (ii) coated and non-grooved specimen, (iii) coated and grooved specimen (Figure 4.11).



**Figure 4.11** a) Design of the non-grooved in-plane torsion specimens, b) Details of the grooved specimen (Yin et al., 2015a)

The thickness of the specimen  $t_o = 0.5$  mm, diameter  $d_o = 80$  mm while the radius of the centre hole  $r_h = 4.1$  mm (Figure 4.11). The groove is defined by the groove depth  $t_n = 0.25$  mm, the groove radius  $r_n = 4$  mm and the diameter of the circular milling path  $d_b = 34$  mm.

A circumferential annular groove on the specimen helps to overcome process limits which hinder the determination of characteristic values up to the forming limit. Those process limits are: too early failure, indents in the sheet caused by pyramidal profiling of the punches and a superposition of compressive stresses to the homogeneous shear stress results from high clamping forces. Groove moves the deformation area away from the inner clamping and due to the circumferential reduction of the specimen cross-section, the shear deformation can be shifted to the region of the groove until crack formation occurs. The main disadvantages of this specimen geometry are the complex manufacturing process of the groove geometry including its measurement and more effort is needed for the test evaluation (Traphöner et al., 2017).

A laser cutting device is used for cutting the blank. The groove is cut from one side of the in-plane torsion specimen by the milling process. During the milling process, the specimen is positioned using a centring hole and the groove is created by using a 4 mm radius spherical ball cutter. Finally, a stochastic pattern is applied on the surface of the specimen using matt white and black coloured sprays (Yin et al., 2015a).

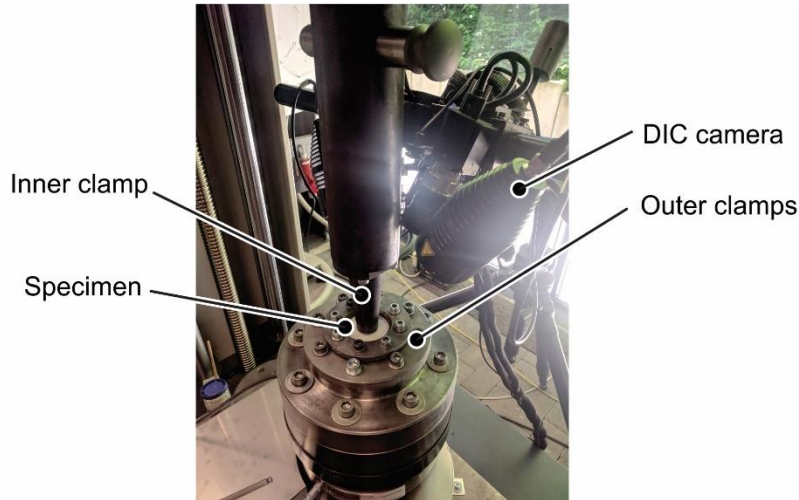
#### 4.4.2 Experimental Setup

A Zwick/Roell Z250 universal testing machine integrated with a torsion device is used for this test (**Figure 4.12**). The inner clamping tool has a radius of  $r_i = 15$  mm and the outer clamping tool has a radius of  $r_o = 30$  mm (Figure 4.11 a). The specimen is clamped in the centre area and on the outer rim. The inner clamping is connected to the machine while the outer clamping is rotated by means of a servomotor with a worm gear. The inner clamping force of 20 kN is applied to the centre of the specimen by the upper punch. Outer clamping force ( $F_o$ ) is provided by the screw connections. The rotation speed of 100 rpm is applied.

The free circular area between the clamps is loaded by planar simple shear as the results of planar rotation of the outer fixture against the inner ones. A GOM ARAMIS 5M DIC system is used for 3D optical strain measurement.



The DIC cameras are placed 200 mm away from the measured area in order to evaluate the local strain in the test area of the specimen. During loading, the camera takes one picture per second.



**Figure 4.12:** Set up of in-plane torsion test integrated into a Zwick/Roell Z250 machine

In the post-processing of the measurement, a section cut is created every 0.1 mm in the area of  $r = 15.0$  mm to  $r = 20.0$  mm. The local shear strain between two measured radii can be calculated using **equation (4.1)** by tracking the averaged rotation angle of each section cut (Yin et al., 2015b).

#### 4.4.3 Data Analysis

The in-plane shear stress  $\tau$  at any radial position  $r$  can be analytically calculated by

$$\tau = \frac{M}{2\pi \cdot t \cdot r^2} \quad (4.1)$$

where  $M$  is the currently applied torque and  $t$  is the sheet thickness. The shear stress quadratically decreases with increased distance to the rotation centre.

The highest stress is located near the inner clamps (Yin et al., 2015a). Shear strain  $\gamma$  can be calculated from any change of slope of an initially straight radial line (Figure 4.10 b).

$$\gamma = r \cdot \frac{d\theta}{dr} \quad (4.2)$$

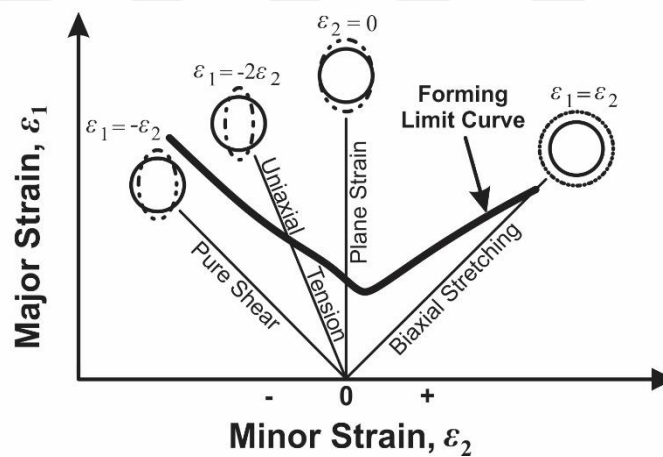
where  $\theta$  is the angle of rotation.

The flow stress and the equivalent plastic strain can be calculated using the Hill anisotropic yield criterion taking account of the influence of the normal anisotropy  $r_n$ . For Isotropic material  $r_n = 1$  (Yin et al., 2015b).

$$\sigma_f = \sqrt{3} \cdot \tau \sqrt{\frac{2(2r_n+1)}{3(r_n+1)}} ; \epsilon_{eq} = \frac{\gamma}{\sqrt{3}} \cdot \sqrt{\frac{3(r_n+1)}{2(2r_n+1)}} \quad (4.3)$$

#### 4.5 Nakajima Test

The Nakajima test is a stretch forming-based test which allows the analysis of stretching at different stress conditions. It is a well-known test and widely used in the determination of forming limit diagram (FLD), the most common tool for analysing the formability of sheet metals. The forming limit diagram is used to determine critical strain states that limit formability of sheet metals, hence help modelling and designing of different forming processes (Emanuela and Marion, 2017).



**Figure 4.13:** Forming limit diagram (Z. Hasan et al., 2011)

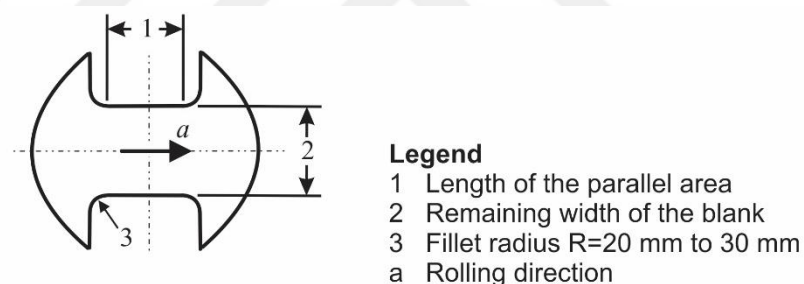
Forming limit diagram records the principle strain values on the surface of the specimen which is subjected to formability tests along different strain-paths under plane-stress conditions (Schwindt et al., 2015). Hence, the boundary between unsafe area (where thinning and necking may happen) and safe area (where there is no risk of excessive thinning or necking) can be established.

The boundary between these two areas is a line manually drawn from measured strain values which is called forming limit curve (FLC). The curve is a function of the major strain ( $\epsilon_1$ ) and minor strain ( $\epsilon_2$ ) expressed on the surface of the sheet metal. **Figure 4.13** shows an example of forming limit diagram (FLD) with important information gained from the diagram.

In this work, the Nakajima test is conducted in IUL at TU Dortmund to experimentally determine the forming limit diagram (FLD) of the aluminium composite panel.

#### 4.5.1 Specimen Preparation

Test specimens are prepared according to (DIN ISO 12004-2) standard. This standard guide is also used for the preparation of test setups and the evaluation of the acquired data. **Figure 4.14** illustrates the standard geometry used in the test.



**Figure 4.14:** Nakajima test specimen geometry according to DIN ISO 12004-2

The specimen has a central parallel recess which should have a length of at least 25% of the die diameter. For aluminium alloy, the sheet orientation is parallel to  $0^\circ$  rolling direction. A water jet cutting machine is used to cut the specimen because this cutting method does not cause changes in microstructure, work hardening or cracks on the surface of the aluminium composite panel, especially to the LDPE layer.

Six different geometries are used. **Table 4.5** contains the different dimensions of specimens. The limitation in thickness of the specimen up to 4 mm is proposed in the standard, giving a maximum allowable thickness to the punch diameter ratio.

**Table 4.5:** Nakajima test specimen dimensions.

Symbol	Description	Dimensions (mm)
1	Length of the parallel area	50
2	Remaining width of the blank	20, 40, 70, 100, 130, 200
3	Fillet radius	25

The surface of the specimen is cleaned by acetone and then a matt white colour and black colour are sprayed respectively creating a stochastic pattern which is required by ARAMIS software to measure major and minor strains of the specimens.

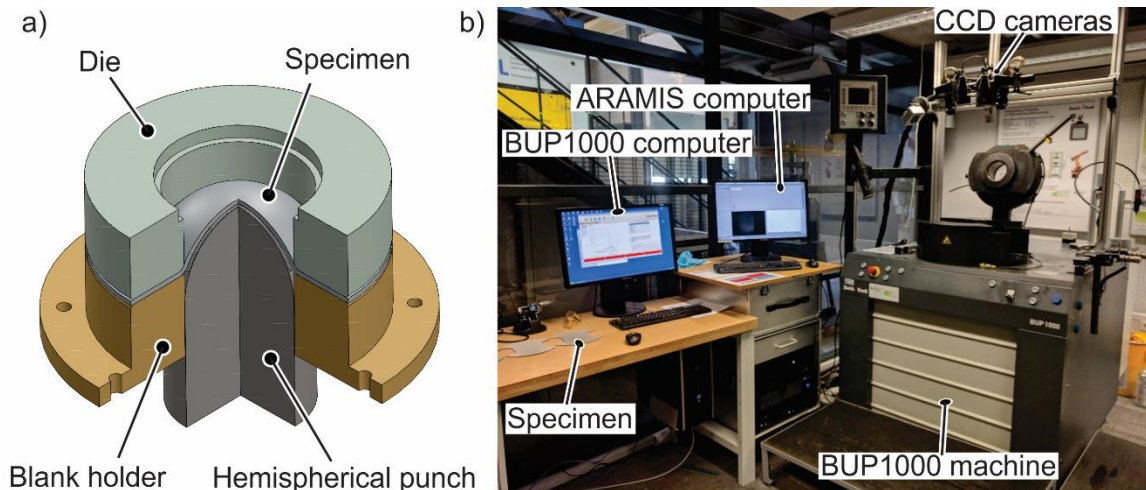
#### 4.5.2 Experimental Setup

A Zwick/Roell BUP1000 machine integrated with ARAMIS system for optical deformation analysis is used for this test. ARAMIS system is a 3D optical strain measurement system which uses two high-speed, high-resolution CCD cameras to develop a three-dimensional image of a part and helps to calculate major and minor strains on the surface of the specimen. **Figure 4.15 a** illustrates the schematic design of Nakajima test.

The CCD cameras of the ARAMIS system are calibrated before starting the test in order to make sure that accurate results are recorded. After the calibration process, the test parameters are entered into the TestXpert II software.

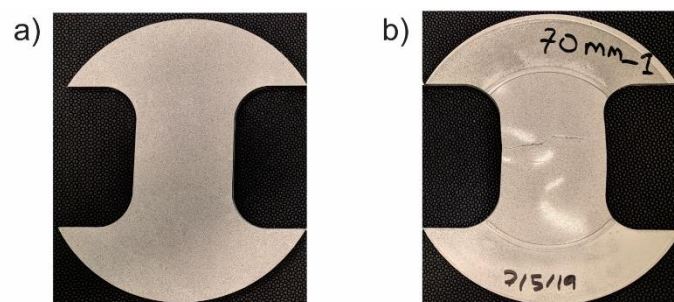
Followings are the parameters used in this test: punch speed = 1.5 mm/s, hemispherical punch diameter = 100 mm, maximum punch stroke = 55 mm, blank holder force = 350 kN and maximum punch force = 700 kN.

Lubrication is applied to the top of the hemispherical punch followed by the placement of a 2 mm thick PVC foil on top of the lubricated punch. Then, the upper surface of the PVC foil is lubricated and the specimen is placed on top of the blank holder. Lubricant is applied to reduce friction between the specimen and the punch.



**Figure 4.15** a) Schematic design of the Nakajima test, b) Test set up for the determination of the FLC

The specimen is clamped with locking beads to the BUP1000 machine before starting the test. The specimen is then deformed by the hemispherical punch until fracture occurred. BUP1000 machine and the ARAMIS software work simultaneously during the experiments. After the failure of the specimen (crack formation), the machine stops and the punch force starts to drop and CCD cameras are manually shut down. Once the test is finished, ARAMIS software is used to calculate minor and major strains. The specimen before and after the tests are shown in **Figure 4.16 a and b**.



**Figure 4.16** a) Nakajima test specimens before the test, b) after the test

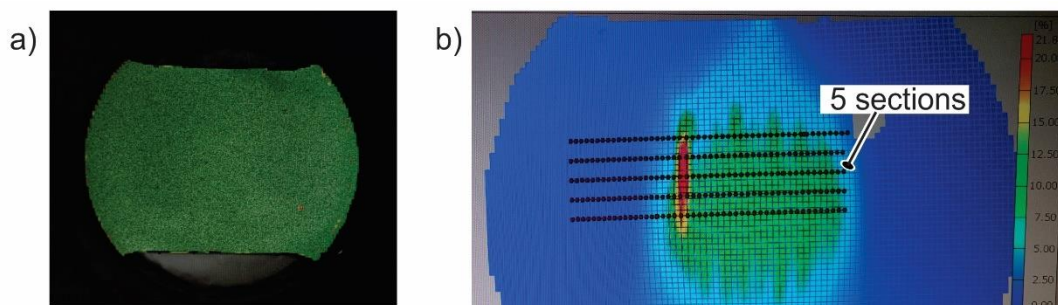
Tests of up to 36 specimens are performed. The tests of a single specimen geometry (i.e. 70 mm) are repeated until the geometry has three successful experimental results.

An experiment is successful when the crack occurs within a range of 15 mm left or right from the middle of the parallel area of the specimen (DIN ISO 12004-2). Validity control of the test results is conducted for each test experiment.

### 4.5.3 Data Analysis

ARAMIS software is used to analyse the images taken by CCD cameras during the experiments and calculating the major and minor strain values. From the ARAMIS software, an image of the specimen before the fracture formation is selected and five parallel sections are created perpendicular to the fracture with the first one passing through the centre of the crack (**Figure 4.17 b**). These sections define the region with major and minor strain values needed for obtaining the forming limit diagram (FLD).

ARAMIS software computed the minor and major strain values along different sections. The position of pairs (major strain  $\varepsilon_1$ , minor strain  $\varepsilon_2$ ) for each specimen geometry forms the forming limit curve (FLC).



**Figure 4.17 a)** Selection of the specimen deformed surface area before creating sections, **b)** creation of five sections on an image before the specimen formed a crack

## 4.6 Friction Test

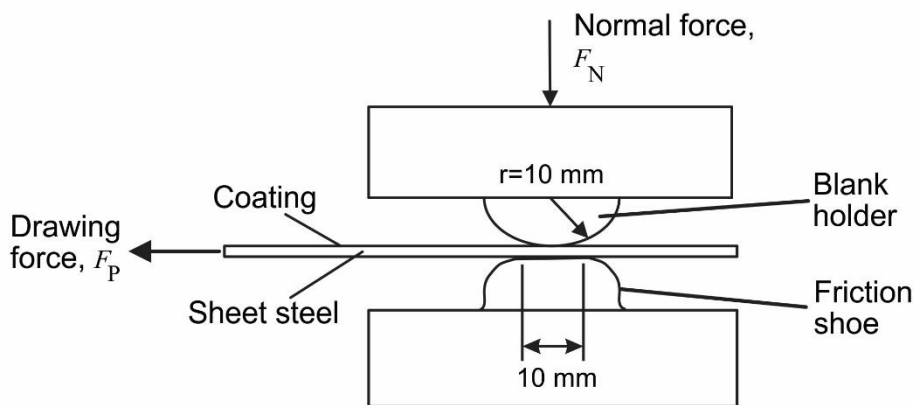
Friction plays an important role in the metal forming processes. Friction is a resistive force that prevents two objects from sliding freely against each other. In the multi-point forming process, friction is present in the contact area between the workpiece with punches, the workpiece with elastic cushion and between the elastic cushion with the blank holder. In this work, the friction test is conducted to determine the coefficient of friction between MPF die punches and aluminium composite panel and between elastic cushion and aluminium composite panel. These values will be used as input data in numerical simulation.

The apparatus used to measure friction forces and their effects is called tribometer. According to the principle of measurement, the methods for the determination of friction can be divided into six categories: direct linear force measurement, gravitation-based tests (e.g. tilting-plane apparatus), torque measurement (e.g. disk brakes), oscillation decrement devices (e.g. pendulum-type devices), tension-wrap devices and indirect indications (e.g. vibration sensors) (Blau, 2001).

Some of the processes used to investigate coefficient of friction in sheet metal forming are: rotating disc assemblies, stripe drawing test, stripe drawing test with deflection, ring compression test, bar tensile test by Pawelski and Renault procedure and Reihle test. In the scope of this thesis, the Renault procedure is used to investigate the coefficient of friction under different test parameters.

The Renault procedure (**Figure 4.18**) is mainly used to perform a friction test to evaluate different lubrication states. A stripe sheet is drawn in five sections between a friction shoe and a semi-spherical blank holder under a certain normal force and sliding speed. To calculate the coefficient of friction through **equation (4.4)**, the normal force  $F_n$  and mean value of the pulling (friction) force  $F_p$  for each section are measured throughout the tests (Doege and Behrens, 2007).

$$\mu = \frac{F_p}{2F_n} \quad (4.4)$$

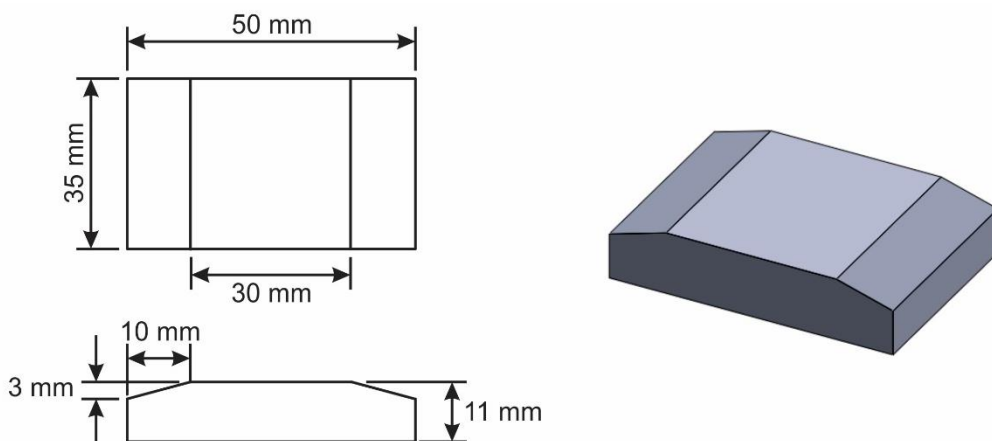


**Figure 4.18:** Renault procedure (Doege and Behrens, 2007)

#### 4.6.1 Specimen Preparation

Aluminium composite panels are cut in strips of 300 x 30 mm, using a Durma® shearing machine. Elastic cushions are also cut in stripes of 200 mm x 30 mm. For the sake of accuracy, three specimens are prepared for each test parameters.

The friction pad must be made of the same material as that of the multi-point forming die punches. For this reason, 6060-T6 aluminium alloy is used to prepare the friction pads. SolidWorks® software is used for generation of the CAD modelling (**Figure 4.19**) according to Renault Procedure.

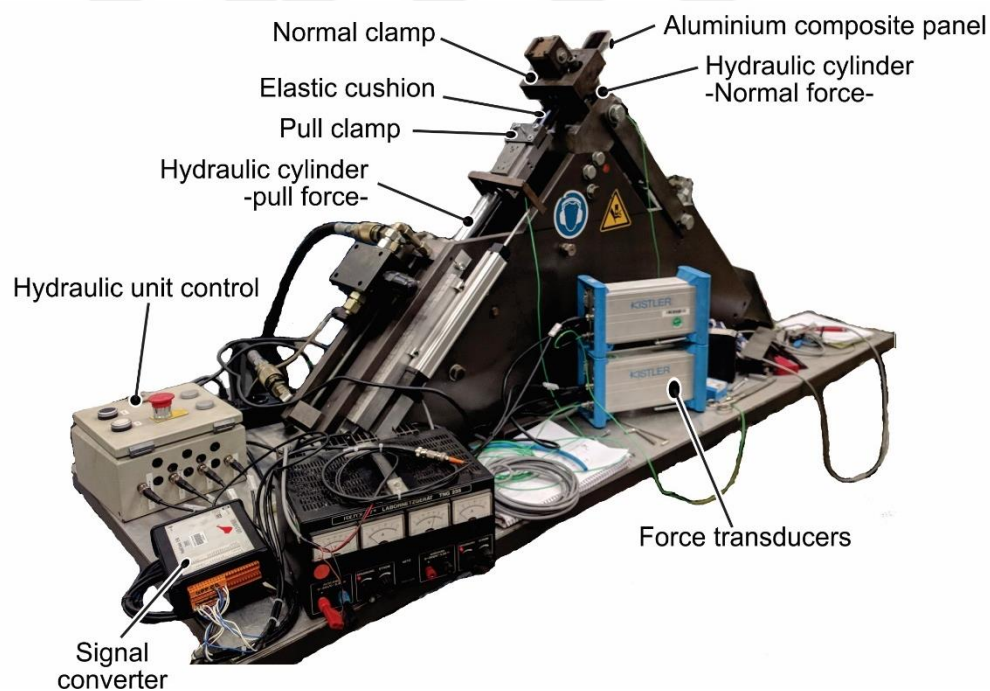


**Figure 4.19:** Geometry of the planar shaped friction pad



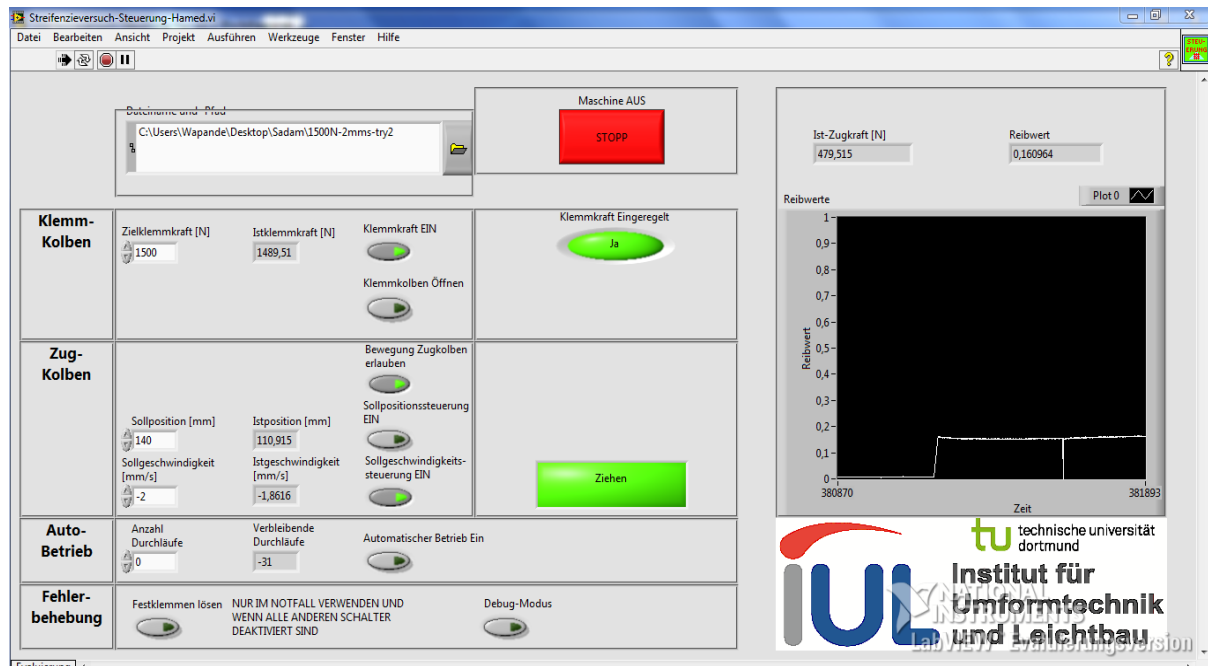
## 4.6.2 Experimental Setup

**Figure 4.20** shows the device used to perform friction tests at IUL. The device has hydraulic cylinders to apply the normal and pulling forces over the aluminium composite panel. To avoid relative movements during the tests which might increase the error in measurements, an aluminium composite panel is firmly clamped to the pull clamp using five screws. To assure that the pulling force is only used to overcome the resistance imposed by the normal force on the contact zone, the following measures are taken before starting every test: checking the avoidance of contacts between the parts of the equipment and the aluminium composite panel or/and elastic cushion (polyurethane), proper fixation of the specimen and the correct alignment of the aluminium composite panel to the pulling direction.



**Figure 4.20:** Devices used during friction test

The device is also connected to sensors which measure displacement, sliding velocity, pulling and normal forces. LabView® interface (**Figure 4.21**) control the hydraulic unit, which perform displacements and forces of the device. LabView® interface also records and saves all the results to be used in data analysis.



**Figure 4.21:** LabView interface used to control the equipment during friction tests

Two experimental parameters (normal force and sliding speed) are then introduced in LabView® interface to control movement conditions of the equipment.

### *Normal force*

The normal load of the friction tests is correspondent to the forming force during the multi-point forming process. An investigation from a literature review was done to learn about the influence of normal force on the MPF process of Aluminium alloy and obtain some reference values of the variable. (Kadhim and Abbas, 2014) and (Abosaf et al., 2017) investigated the experimental and numerical simulation of the sheet metal forming process based on multi-point die for aluminium and steel. They found that the maximum predicted forming forces when the upper and lower dies are fully closed are 80 kN and 88 kN respectively.

The appropriate contact area between the punches and aluminium alloy sheet was calculated (280 mm x 280 mm), obtaining a value of 78400 mm<sup>2</sup>. With an applied forming force of 80 kN, the applied pressure is around 1.02 MPa. The contact area of the friction pad with the specimen is around 1000 mm<sup>2</sup>, using this value and applied pressure value, the computed normal loads for the friction tests would start from 1020 N. The selected values of normal force for the friction tests are 1000 N and 1500 N.

### *Sliding speed*

The selected sliding speeds for the present work are: 1 mm/s and 4 mm/s.

The tests are performed along a length of 56 mm. Starting from the beginning of the test, the LabView® interface computes the friction coefficient ( $\mu$ ) using equation 4.4 above.

### **4.6.3 Data Analysis**

Throughout the test, the LabView® interface records pulling (friction) force  $F_p$ , normal force  $F_n$ , the coefficient of friction, displacement, speed and time. Using Excel program, the mean graph of coefficient of friction (COF) against displacement in mm from three specimens of the same test parameters is drawn considering the following criteria:

- Deviation of the normal force is not bigger than  $\pm 5\%$  of the average value,
- Deviation of sliding velocity is not bigger than  $\pm 0.5$  mm/s of the average value.

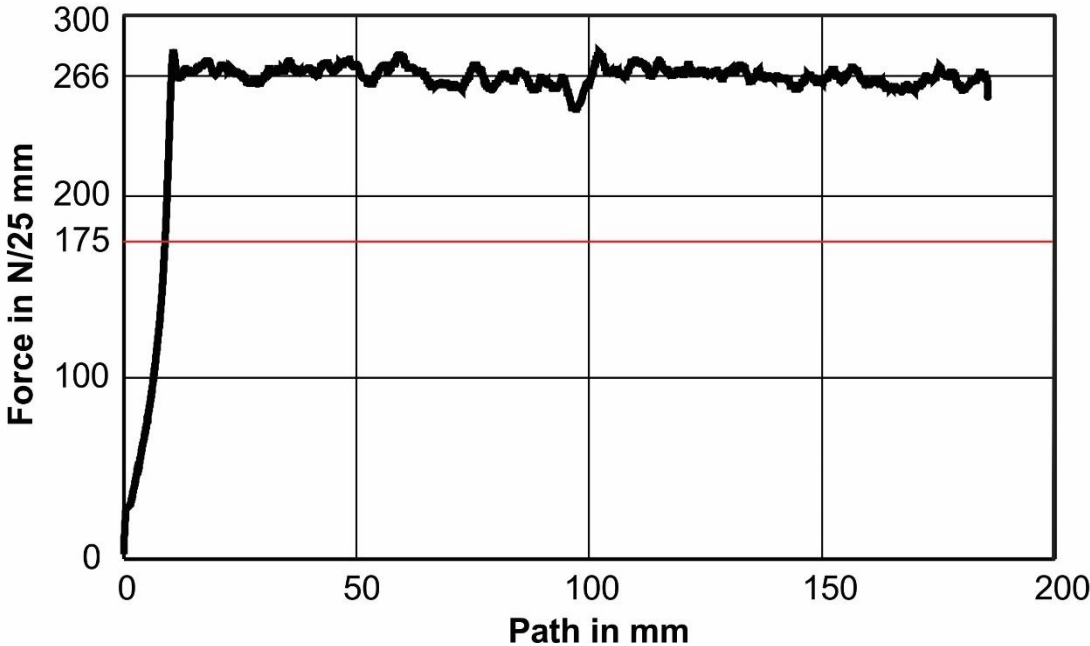
Then, the value of the mean coefficient of friction (COF) for a test is calculated considering values of COF for at least 25 mm of the displacement.

### 4.7 Results

#### 4.7.1 T-Peel Stripping Test Results

The results of the T-Peel stripping test (**Figure 4.22**) show that the quality of the bond between AA3105 sheet and LDPE is good because the force is stable throughout the experimental path. The quality of the bond is considered bad when there is high fluctuation of the force on the graph. This means that the specimens for other tests and forming experiments can be taken from any place of the composite panel and they are expected to have the same bond properties.

The average mean peel strength (266 N/25 mm) from the ten specimens is higher than the minimum peel strength value (175 N/25 mm) according to TS 13777 standard.



**Figure 4.22:** The average graph of Force in N/25mm against path in mm

#### 4.7.2 Tensile Test Results

Mechanical properties of AA3105, LDPE and aluminium composite panel obtained from the tensile tests are found in **Table 4.6**. These values are calculated by TestXpert II software. Stress-strain curves are drawn from the average results of three successful tested specimens. The mean standard deviation (MSD) for each curve is also noted down inside the graphs.

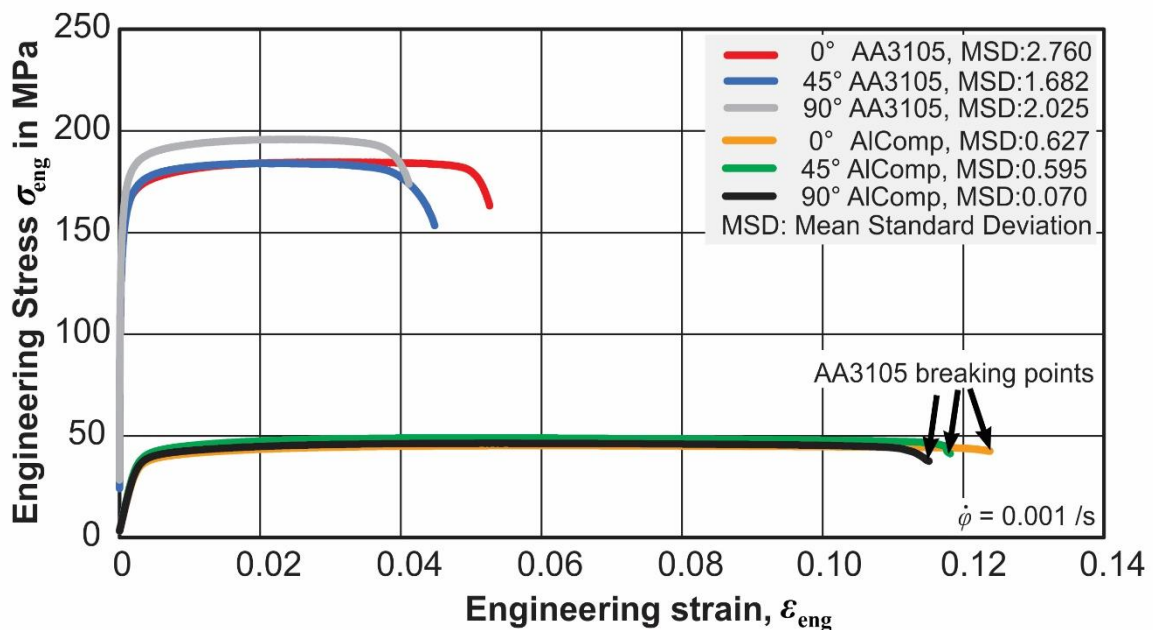
**Table 4.6:** Mechanical properties of AA3105, LDPE and aluminium composite panel

Properties	AA3105			Aluminium composite panel			LDPE
	Rolling direction			Rolling direction			
	0°	45°	90°	0°	45°	90°	
Elastic modulus, $E$ (GPa)	70	65	68	14	15	15	0.29
Yield stress, $R_{p0,2}$ (MPa)	169	169	182	38	43	39	N/A
Upper yield stress, $R_{eH}$ (MPa)	N/A	N/A	N/A	N/A	N/A	N/A	9.11
Tensile stress, $R_m$ (MPa)	185	183	196	45	49	46	9.11
Fracture stress, $R_t$ (MPa)	110	110	110	4.98	4.89	4.65	4.65
Elongation at maximum load, $A_g$ (%)	1.97	1.94	2.01	5.77	4.90	5.54	14.7
Elongation at fracture, $A_t$ (%)	4.31	4.59	5.37	19.97	23.80	17.80	113.89
Poisson ratio, $\nu$	0.33			N/A			0.46
Density, $\rho$ (kg/m <sup>3</sup> )	2700			N/A			920

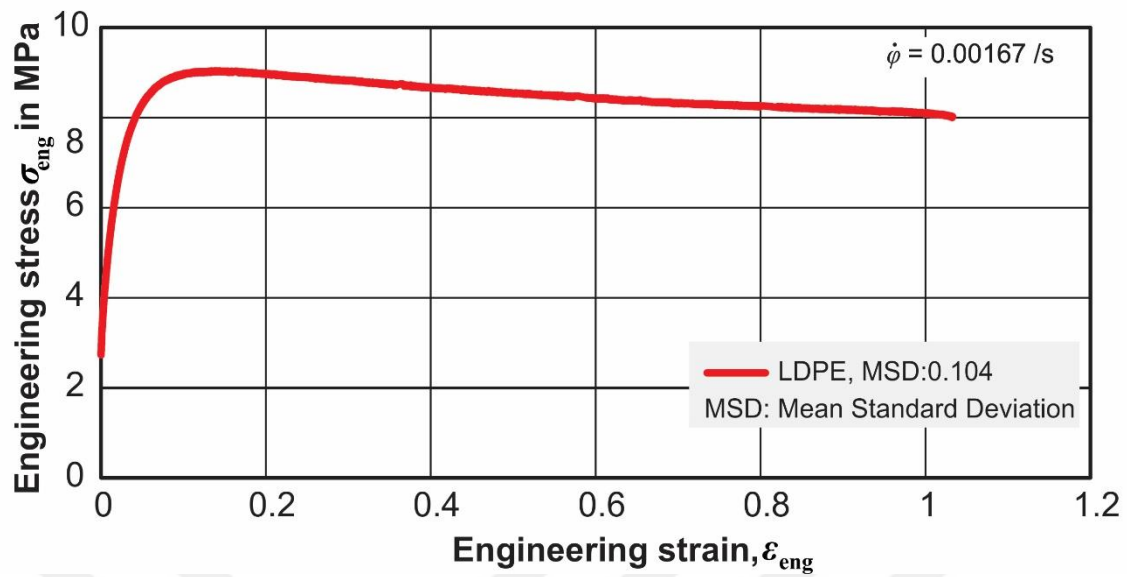
The Poisson ratio ( $\nu$ ) and density ( $\rho$ ) values of AA3105 are taken from (ASM International, 1990) and the values of LDPE are taken from (ASTM D 1248-05) standard. The mean engineering stress-strain graphs for each material (**Figure 4.23**, **Figure 4.24** and **Figure 4.25**) are drawn using force and displacement data obtained from the TestXpert II software. **Equation 4.5** is used to calculate engineering stress and engineering strain.

$$\sigma_{eng} = \frac{F}{A_0} ; \quad \varepsilon_{eng} = \frac{\Delta l}{l_0} \quad (4.5)$$

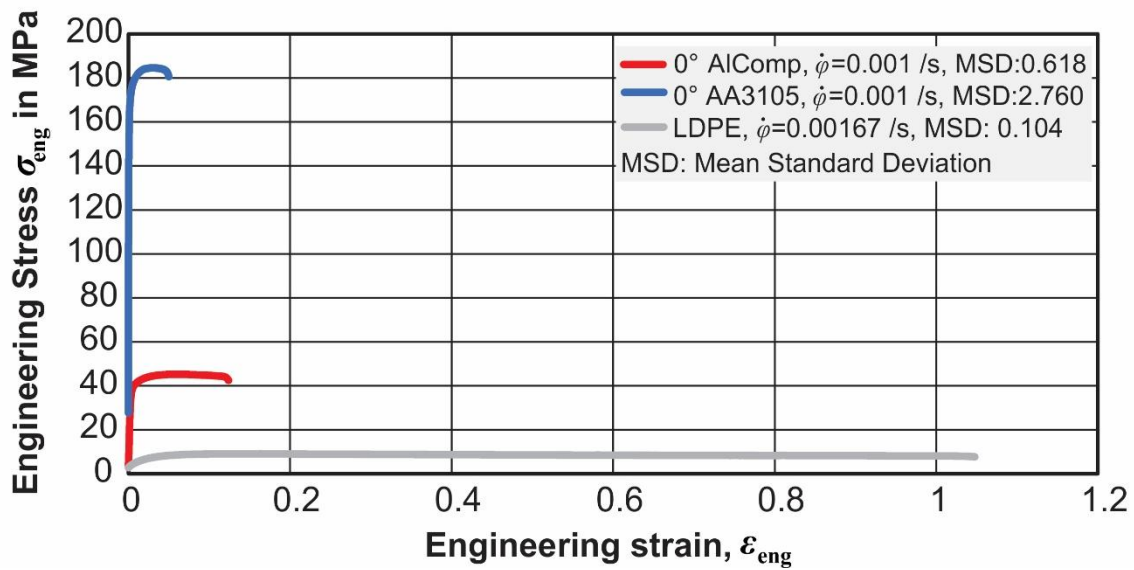
From the tensile tests of aluminium composite panel, it has been observed that one of the AA3105 sheets starts to crack first followed by the drop of the stress until the other AA3105 sheet cracks. The LDPE layer is then pulled until it fractures. The LDPE specimens were prepared by delaminating them from aluminium composite panel with different rolling direction and the results obtained from all three specimens are similar with a standard deviation of 0.104 MPa. Hence, the LDPE is assumed to have isotropic behaviour in all directions (Parsa et al., 2010). The engineering stress - strain graph plotted (Figure 4.23) is up to when the first AA3105 sheet cracks.



**Figure 4.23:** Engineering stress - strain graph of AA3105 sheet and aluminium composite panel



**Figure 4.24:** Engineering stress - strain graph of LDPE



**Figure 4.25:** Engineering stress - strain graphs of AA3105, LDPE and aluminium composite panel

True stress – strain graphs (**Appendix A**) can be plotted by first calculating true stress and true strain values using **equation 4.6**.

$$\sigma = \frac{F}{A_i} = \sigma_{eng} \cdot (1 + \varepsilon_{eng}) \quad ; \quad \varphi = \ln\left(\frac{l_i}{l_o}\right) = \ln(1 + \varepsilon_{eng}) \quad (4.6)$$

### Flow curve

True stress - strain curve provides more direct material behaviour in the plastic flow range. Hollomon equation is used to plot flow curves of AA3105, LPDE and aluminium composite panel (Parsa et al., 2010).

$$\sigma = K\varepsilon^n \quad (4.7)$$

Where  $\sigma$  is the true stress,  $\varepsilon$  is the true strain,  $K$  is the strength coefficient and  $n$  is the strain hardening coefficient. Taking logarithms of both sides of the equation,  $\log s = \log K + n \cdot \log \varepsilon$ , a graph of  $\log s - \log \varepsilon$  is drawn to determine  $n$  and  $K$  values (Table 4.7). The flow curve can then be plotted using  $n$  and  $K$  values obtained from the calculation (Figure 4.26 and Figure 4.27).

**Table 4.7:** Strength coefficient ( $K$ ) and strain hardening exponent ( $n$ ) values

Properties	AA3105			Aluminium composite panel			LDPE
	Rolling direction			Rolling direction			
	0°	45°	90°	0°	45°	90°	
Strength coefficient, $K$ (MPa)	311.17	338.92	356.20	108.29	131.92	111.97	14.70
Strain-hardening exponent, $n$	0.1121	0.1287	0.1259	0.2386	0.2626	0.2393	0.2217

The calculated strain-hardening behaviour using Hollomon equation was compared to the experimental strain-hardening behaviour of AA3105, LDPE and 3105 aluminium composite panel (Appendix A). It is observed that the calculated strain-hardening behaviour has a correlation with the experimental strain-hardening behaviour hence the calculated strain-hardening behaviour can be used in numerical simulation.



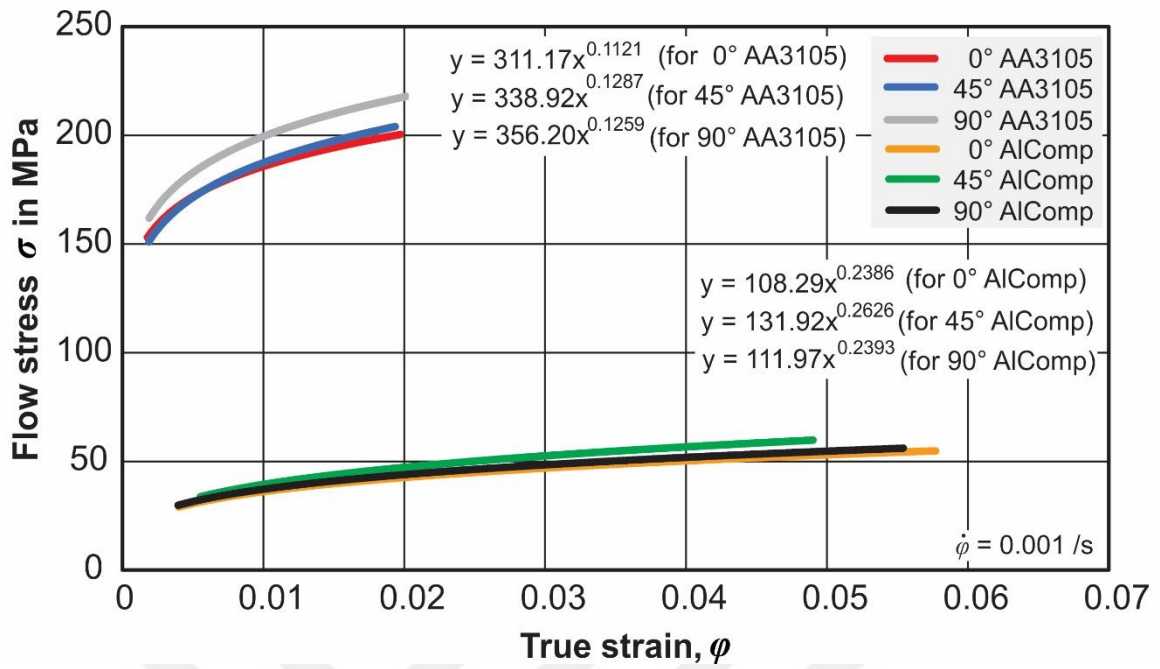


Figure 4.26: Flow curve of AA3105 sheet and aluminium composite panel

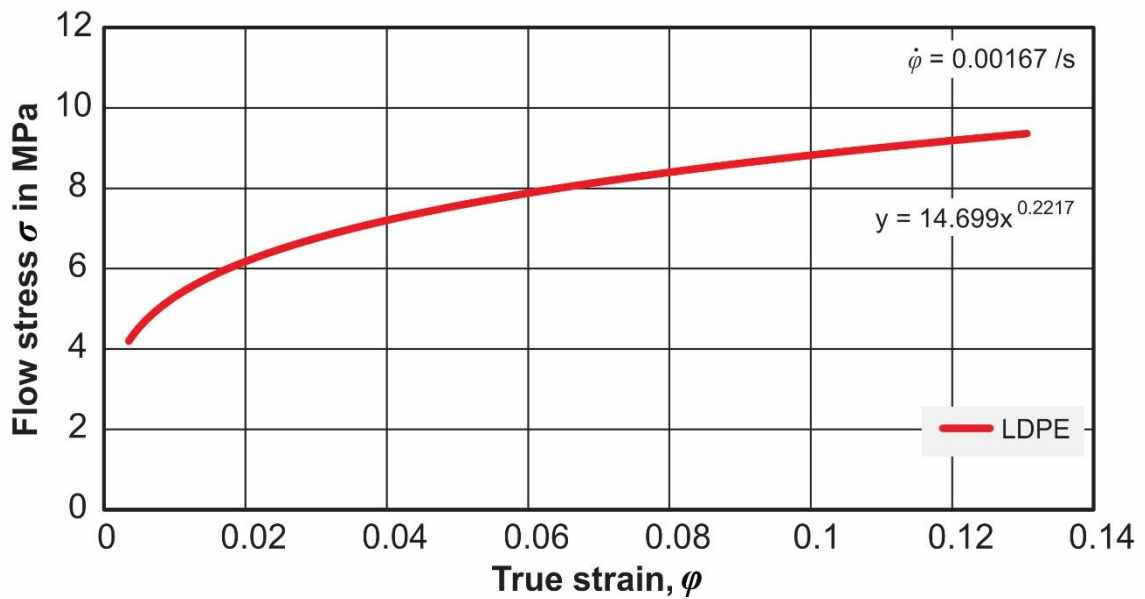


Figure 4.27: Flow curve of LDPE

*Strain rate sensitivity,  $m$* 

A material's flow stress depends on strain rate and temperature. An increase in strain rate normally causes an increase in flow stress. (Hosford and Caddell, 2011). At constant strain, the strain rate effect can be approximated by;

$$\sigma = C \dot{\phi}^m \quad (4.8)$$

Where  $\sigma$  is the flow stress,  $\dot{\phi}$  is the strain rate,  $m$  is the strain-rate sensitivity of the flow stress and  $C$  is a strength constant that depends upon the temperature, strain, and the material. The ratio of flow stresses at two strain rates is;

$$\frac{\sigma_2}{\sigma_1} = \left( \frac{\dot{\phi}_2}{\dot{\phi}_1} \right)^m \quad (4.9)$$

By taking logarithms of both sides, the value of  $m$  can be calculated by;

$$m = \frac{\ln\left(\frac{\sigma_2}{\sigma_1}\right)}{\ln\left(\frac{\dot{\phi}_2}{\dot{\phi}_1}\right)} \quad (4.10)$$

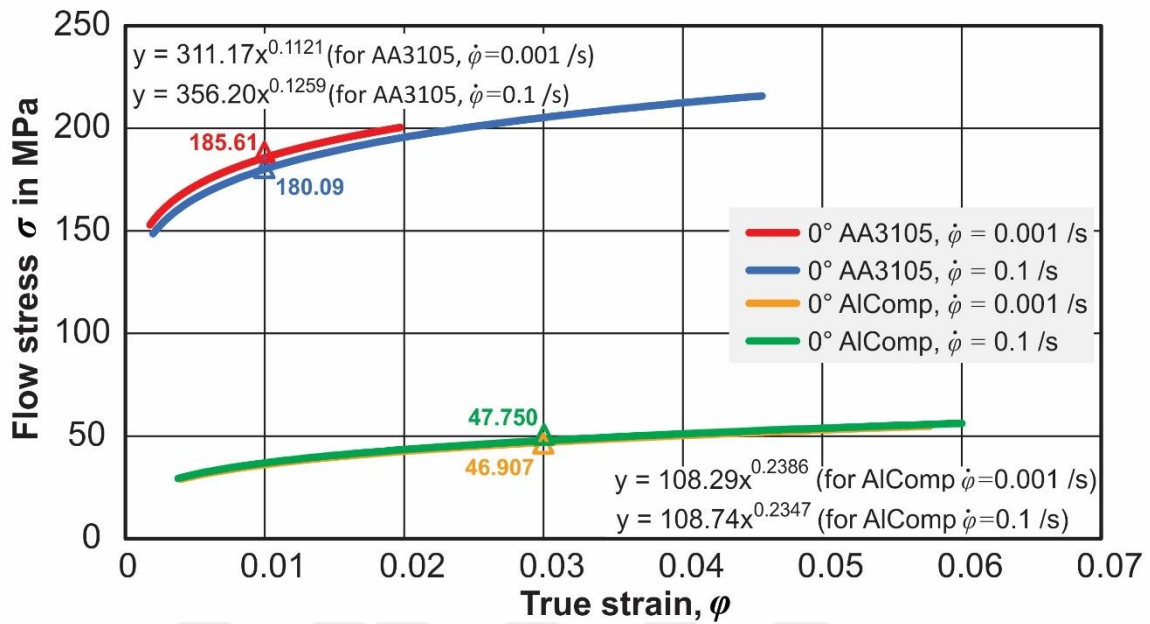
Three continuous flow stress – strain graphs (**Figure 4.28 and Figure 4.29**) at two different strain rates ( $\dot{\phi}_1 = 0.001$  /s and  $\dot{\phi}_2 = 0.1$  /s for AA3105 and aluminium composite panel,  $\dot{\phi}_1 = 0.00167$  /s and  $\dot{\phi}_2 = 0.01667$  /s for LDPE) are created to find the value of strain rate sensitivity ( $m$ ) at the same strain.

The values of strain rate sensitivity,  $m$  for AA3105 sheet, aluminium composite panel and LDPE are calculated at true strain values of 0.01, 0.03 and 0.06 respectively.

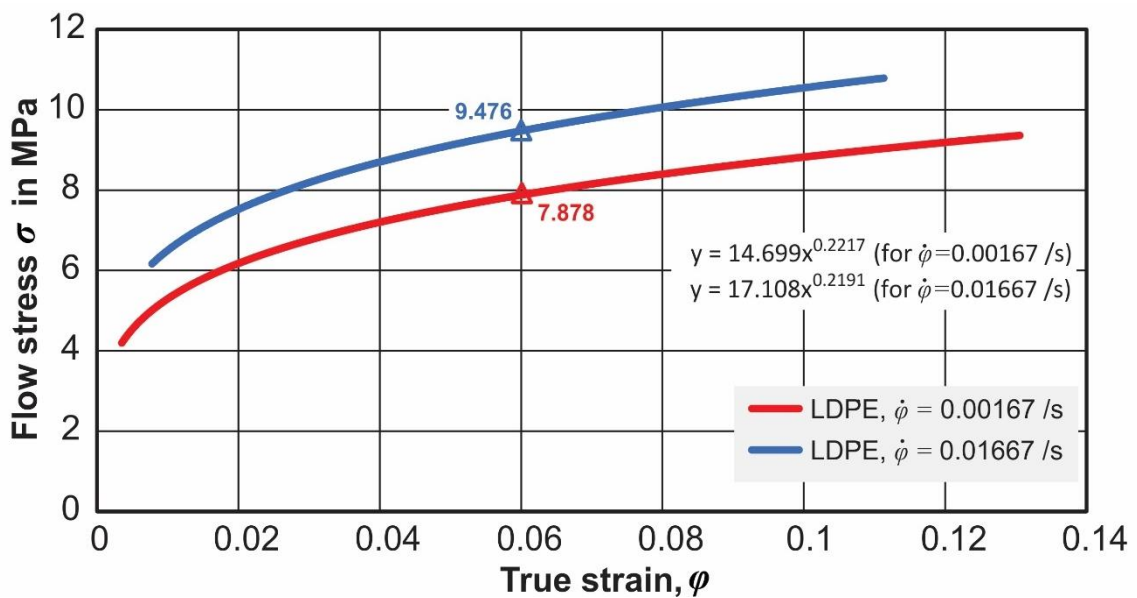
**Table 4.8** shows the results of strain rate sensitivity for the three tested materials.

**Table 4.8:** Strain rate sensitivity ( $m$ ) values

Properties	AA3105	Aluminium composite panel	LDPE
Strain rate sensitivity, $m$	-0.0066	0.0039	0.0802



**Figure 4.28:** Flow curves of AA3105 sheet and aluminium composite panel at a different strain rate



**Figure 4.29:** Flow curves of LDPE at a different strain rate

### Anisotropy

Plastic strain ratio ( $r$ ), also called anisotropy coefficient or Lankford coefficient, is a ratio of the true plastic width strain to the true plastic thickness strain in a test piece that has been subjected to uniaxial tensile stress (DIN ISO 10113).

It can be calculated by **equation (4.11)** where  $\varepsilon_a$  is the true plastic thickness strain and  $\varepsilon_b$  is the true plastic width strain.

$$r = \frac{\varepsilon_b}{\varepsilon_a} = \frac{\ln\left(\frac{b}{b_0}\right)}{\ln\left(\frac{L_0 b_0}{L b}\right)} \quad (4.11)$$

Where  $L_0$ ,  $b_0$ ,  $L$  and  $b$  are the initial length, initial width, current length and current width of the specimen respectively. The values of  $b_0$ ,  $L_0$ ,  $L$ , and  $b$  are recorded by an extensometer during the tests. The weighted average plastic strain ratio ( $\bar{r}$ ) and planar anisotropy ( $\overline{\Delta r}$ ) are calculated using **equation 4.12** and **equation 4.13** respectively.

$$\bar{r} = \frac{r_{0/20} + r_{90/20} + 2r_{45/20}}{4} \quad (4.12)$$

$$\overline{\Delta r} = \frac{r_{0/20} + r_{90/20} - 2r_{45/20}}{2} \quad (4.13)$$

$r$  is supplemented by the angle which characterizes the orientation of the specimen and the strain level at which measurements are taken. In this work, the  $r$  values of AA3105 and 3105 aluminium composite panel are taken at strain value of 1.5%, hence  $r$  symbol for  $0^\circ$ ,  $45^\circ$  and  $90^\circ$  material orientation can be re-written as  $r_{0/1.5}$ ,  $r_{45/1.5}$ ,  $r_{90/1.5}$  respectively. **Table 4.9** contains the calculated values of  $r$ ,  $\bar{r}$  and  $\overline{\Delta r}$  for AA3105 and aluminium composite panel.

**Table 4.9:** The plastic strain ratio, average plastic strain ratio and planar anisotropy values for AA3105 and aluminium composite panel

Rolling direction	AA3105			Aluminium composite panel		
	0°	45°	90°	0°	45°	90°
Plastic strain ratio, $r$	0.1409	1.6590	1.0592	0.5198	0.4806	1.6035
Average plastic strain ratio, $\bar{r}$	1.1295			0.7711		
Planar anisotropy, $\bar{\Delta r}$	-1.0589			0.5811		

### *Evaluation of the Tensile Test Results*

AA3105 fracture at very low strain due to its brittleness nature caused by the manufacturing process (cold rolling). The elastic modulus of AA3105 at 0° and 90° rolling direction shows similarities to the values from the literature (ASM International, 1990) while the elastic modulus value of AA3105 at 45° rolling direction shows some slight deviation. The values of yield stress ( $R_{p0.2}$ ) and tensile strength ( $R_m$ ) are within the expected range according to EN 1396 standard ( $R_{p0.2}^{min}$  150 MPa,  $R_m^{min}$  175 MPa and  $R_m^{max}$  225 Mpa).

The values of yield stress and tensile strength for AA3105 at 90° rolling direction are higher than that of 0° and 45° rolling direction. This is because it is more difficult to deform material at 90° rolling direction than at 0° or 45° rolling directions due to grain orientations (Najib et al., 2015). The values of % elongation at maximum load ( $A_g$ ) and at fracture ( $A_t$ ) are almost the same for 0°, 45° and 90° rolling direction specimens. The value of average plastic strain ratio for AA3105 ( $\bar{r}=1.1295$ ) is closed to 1, implying that there is a slight amount of anisotropic behaviour in AA3105.

The strain rate sensitivity of AA3105 is a negative value (Table 4.8). This can be attributed to segregation of aluminium alloy solute to dislocation at a low strain rate. This lowers their energy so that the forces required to move the dislocations are higher than those required for solute-free dislocations (Hosford and Caddell, 2011).

The strain rate sensitivity values for LDPE and aluminium composite panel are both positive values but too small that their effect on flow stresses can be neglected (Hosford and Caddell, 2011).

The hook region of LDPE does not show an ideal linear behaviour, because of this, the upper yield stress ( $R_{eH}$ ) was determined instead of 0.2% yield stress ( $R_{p0.2}$ ). LDPE shows high ductility and due to this, the % elongation at fracture ( $A_t$ ) of aluminium composite panel is higher than that of AA3105 sheet. The value of tensile strength ( $R_m=9.11$  MPa) is within the range stated by ASTM D 1248 standard ( $R_m=9.7$  MPa).

The values of yield stress ( $R_{p0.2}$ ) and tensile strength ( $R_m$ ) of aluminium composite panel does not show agreement with the results of Najib et al. (2015). The 45° rolling direction specimens have higher ( $R_{p0.2}$ ) and ( $R_m$ ) than 0° and 90° rolling direction specimens. This might be because of the effect of LDPE on the composite panel. The values of % elongation at fracture ( $A_t$ ) is also higher for 45° rolling direction specimens than 0° and 90° rolling direction specimens.

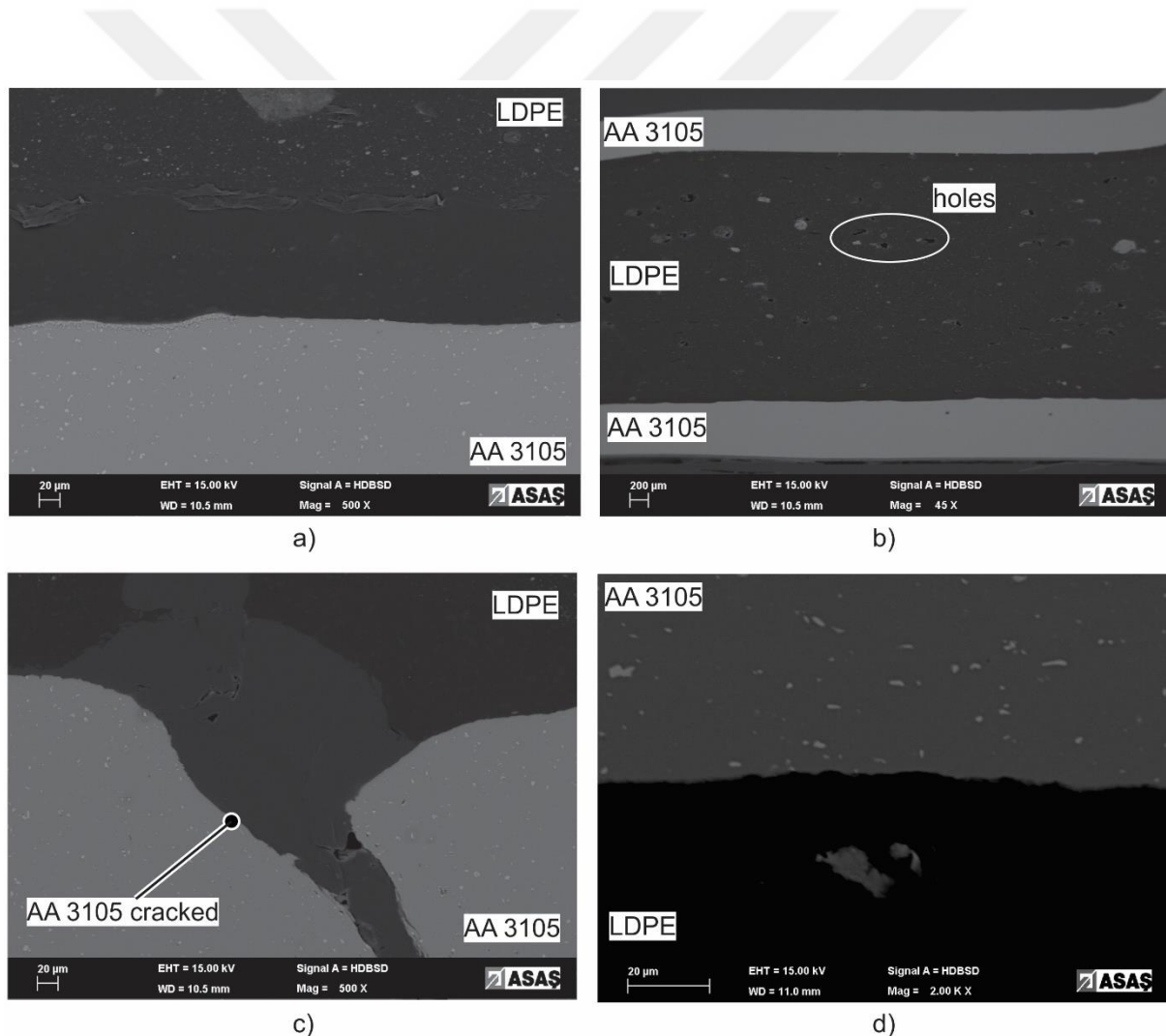
The value of average plastic strain ratio for aluminium composite panel ( $\bar{r}=0.7711$ ) is not closed to 1, this means the composite shows some anisotropy behaviour and this behaviour should be taken under consideration in numerical simulation by using a yield criterion which takes anisotropy behaviour under consideration. Aluminium composite panel is expected to have higher formability than AA3105 because it is strain rate sensitivity and strain hardening exponent values are higher than that of AA3105 sheet (Marciniak et al., 2002)

#### *Fracture Analysis with Scanning Electron Microscope (SEM) Results*

During the analysis, the working distance (WD), which is the distance between the specimen on stage inside the SEM and lens, was set to 10.5 mm or 11 mm and electron high tension (EHT) was set to 15 kV. The images were taken at a magnification between 38x and 7kx. **Figure 4.30** shows some of the pictures taken by SEM from the eight tensile test specimens.

From the analysis, it has been observed that the AA3105 sheets and LDPE layers are still intact before the fracture of the aluminium sheet (Figure 4.30 a) and there is no slip between the layers. LDPE is deformed plastically due to the high stresses compared to its yield stress (9.11 MPa) and this can be seen by the holes formed on the LDPE (Figure 4.30 b).

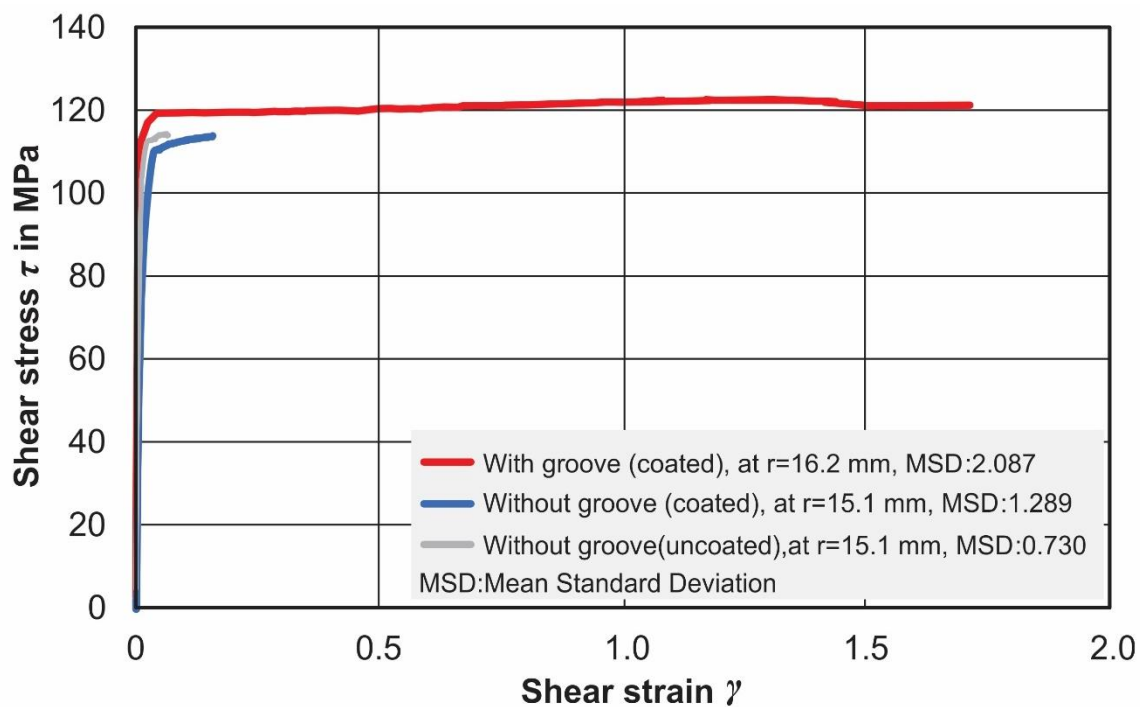
When the aluminium sheet cracks (Figure 4.30 c), the LDPE rapidly flows through the gap but still LDPE looks to be intact with AA3105 sheet. Also, the thickness of AA3105 layer does not significantly decrease. The difference between specimen tested at high strain rate and that tested at low strain rate is insignificant.



**Figure 4.30:** SEM pictures from, **a and b)** aluminium composite specimen with AA3105-0° tested at 0.001 /s, strain 11.5%; **c and d)** aluminium composite specimen with AA3105-0° tested at 0.01 /s, strain 14.5%

### 4.7.3 In-Plane Torsion Test Results

Equivalent stress and equivalent strain of the three different specimens are calculated using **equation 4.3**. The value of normal anisotropy ( $r_n=1.1295$ ) obtained from the tensile test (Table 4.9) is used in the calculation. **Figure 4.31** shows the shear stress–strain graphs of in-plane torsion test specimens and **Figure 4.33** shows the comparison of the results obtained from the tensile test of AA3105 and in-plane torsion results of grooved (coated) specimens.

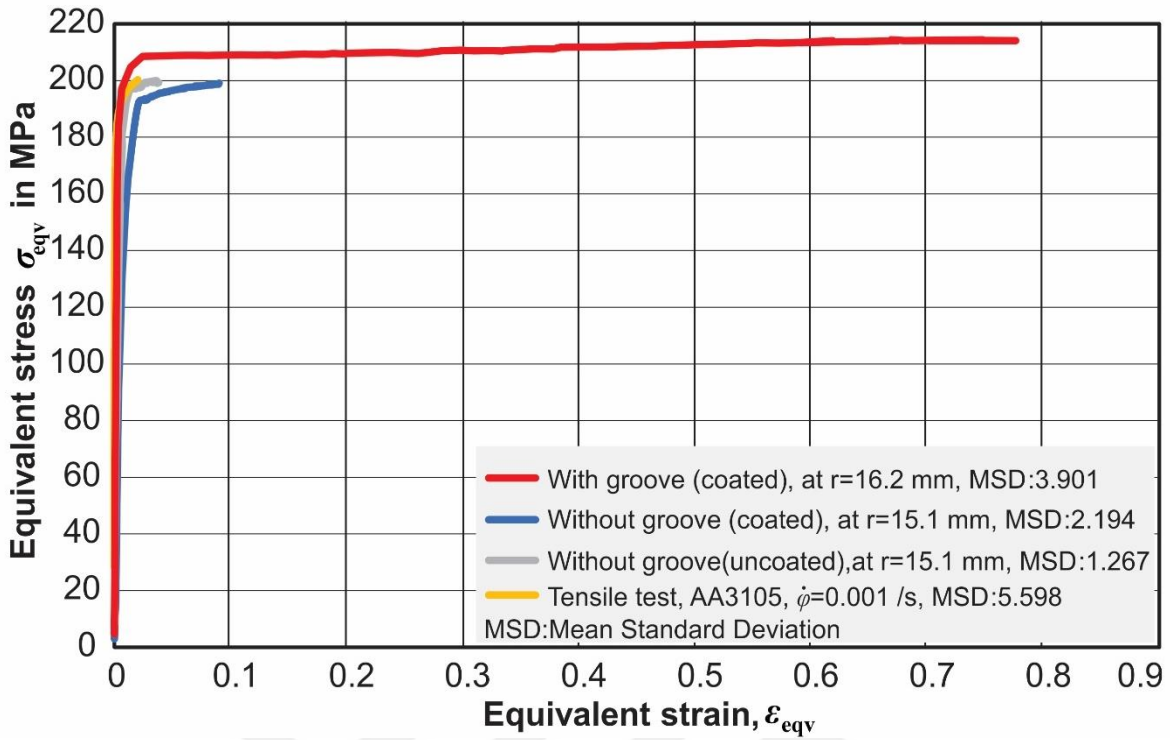


**Figure 4.31:** Shear stress – shear strain graph of the three specimen geometries

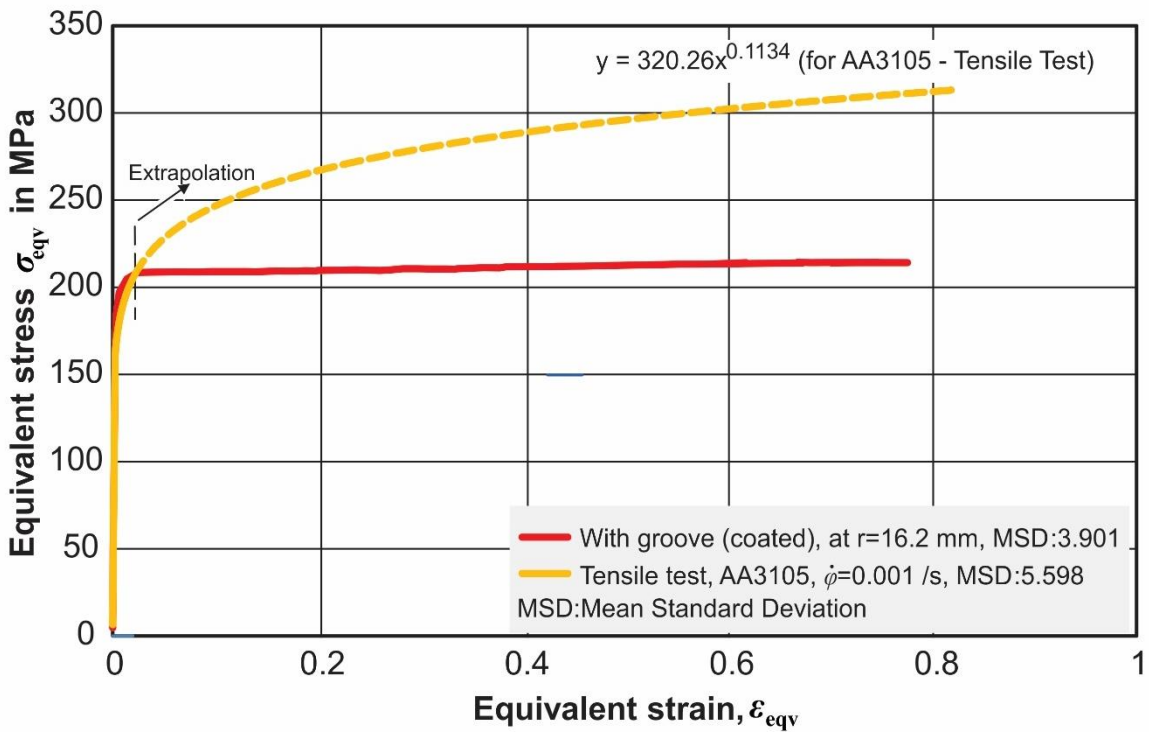
#### *Evaluation of the In-plane Torsion Test Results*

The specimens without a groove (both coated and uncoated) does not show higher equivalent strain than that of mean tensile test results while grooved (coated) specimen reach almost 0.8 equivalent strain (**Figure 4.32**). The equivalent stress–strain curve of the grooved (coated) specimen shows good agreement with the results of the AA3105 tensile specimens up to tensile strength ( $R_m$ ) of aluminium sheet (Figure 4.33). As the AA3105 fracture at the low strain in the tensile test, the flow curve obtained from the grooved specimen can be used in simulation as material data of aluminium alloy instead of applying extrapolation to the flow curve obtained from the tensile test.





**Figure 4.32:** Equivalent stress - strain graphs of in-plane torsion test specimens and tensile test specimen

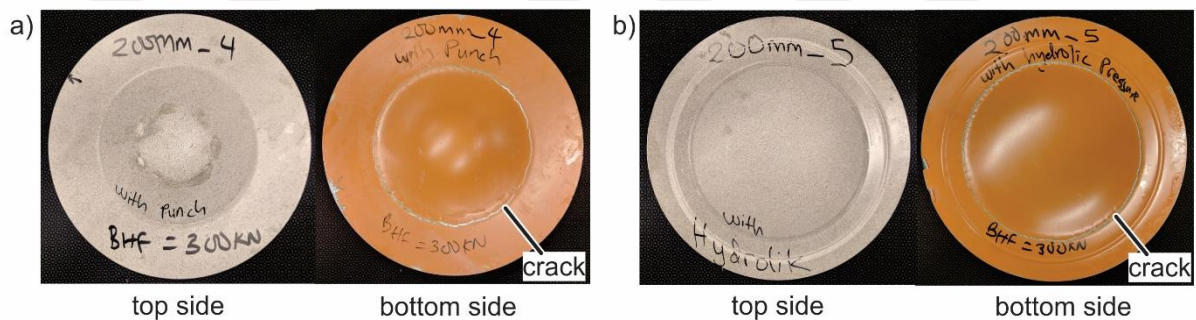


**Figure 4.33:** Comparison of the AA3105 grooved (coated) specimen and AA3105 tensile test specimens results

#### 4.7.4 Nakajima Test Results

##### *Invalid specimens*

During the test, it was observed that the 200 mm specimens do not crack on the top of the specimen but rather crack on the bottom side close the blank holder (**Figure 4.34 a**). The hemispherical punch was changed and hydraulic oil was used instead (**Figure 4.34 b**). In this condition, the results were still the same as the ones observed when the hemispherical punch was used. Due to this, the 200 mm specimens have been concluded to be invalid and the results obtained from the tests were not used to compute the forming limit curve.

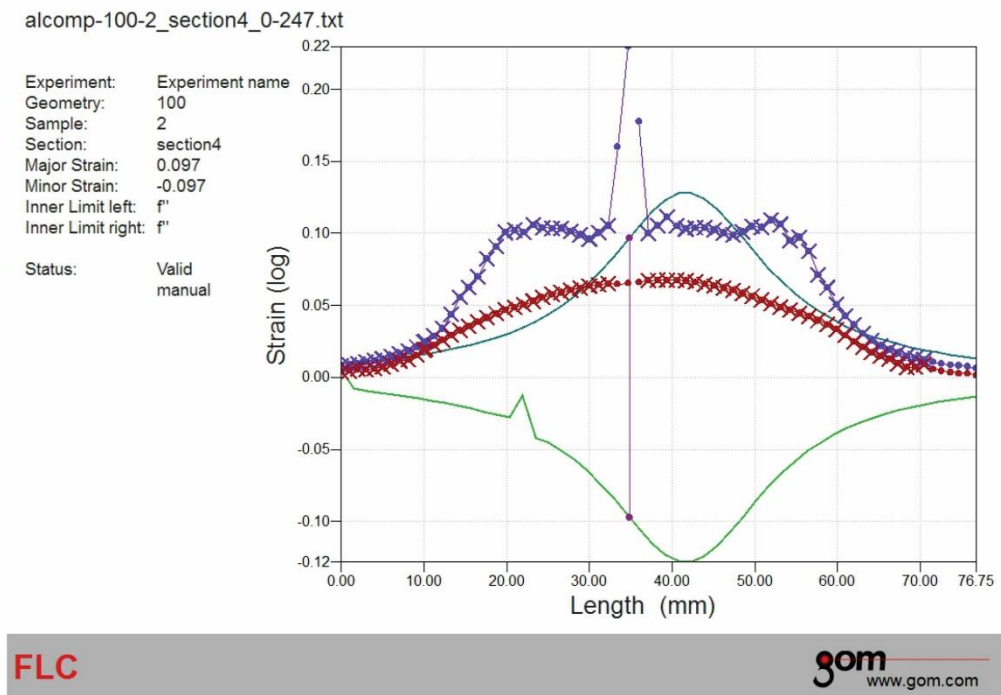


**Figure 4.34 a)** 200 mm Nakajima specimen when hemispherical punch used, **b)** 200 mm Nakajima specimen when hydraulic pressure used

##### *FLC computation*

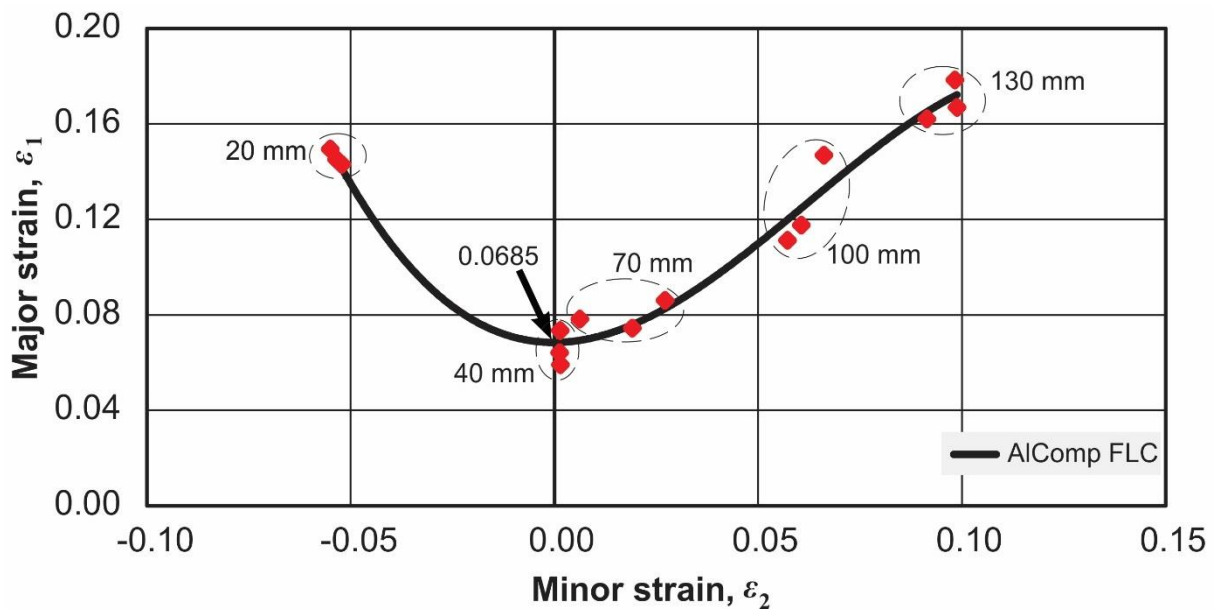
Due to inhomogeneous deformation of aluminium composite panel, multiple peaks are formed on the strain - length curve (**Figure 4.35**) of the created sections in ARAMIS software. Because of this, ARAMIS software cannot be used to automatically compute FLC, instead the section data have to be analysed manually using best-fit parabola approximation (ISO 12004-2:2008) by employing Excel software (**Appendix B**).

**Figure 4.36** is the forming limit diagram (FLD) of aluminium composite panel after the manual computation of all section data. The FLD contains the results from 20 mm, 40 mm, 70 mm, 100 mm and 130 mm specimens. The lowest point of forming limit curve (when minor strain,  $\varepsilon_2 = 0$ ) is 0.0685.



**Figure 4.35:** Multiple peaks on the strain-length curve of the 100 mm geometry section obtained from ARAMIS software

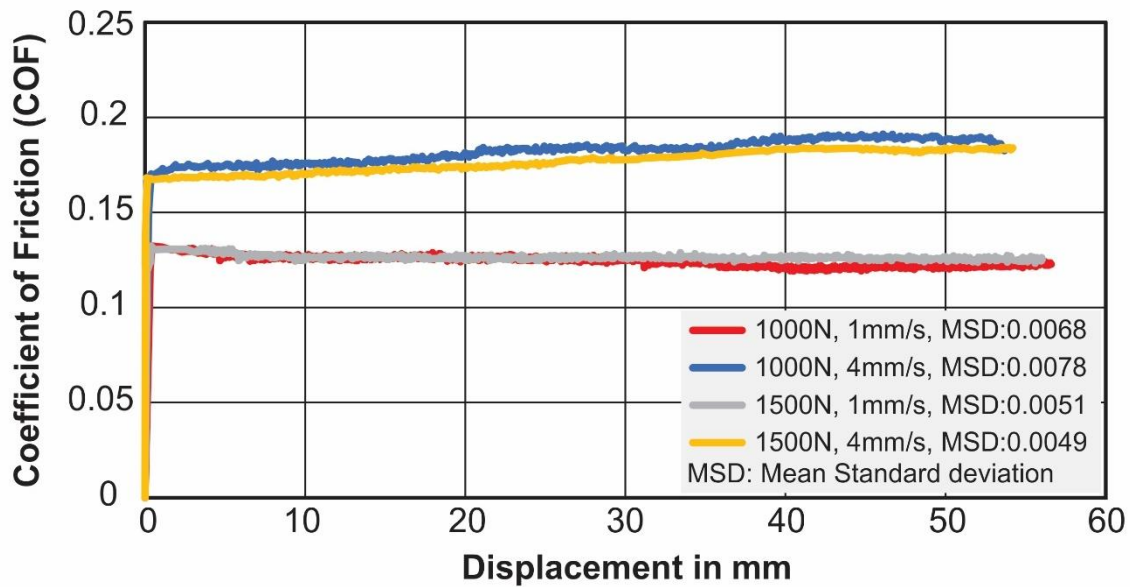
On FLC (Figure 4.36), 40 mm specimen points are along with zero minor strain (plane strain state). Normally 40 mm specimen points are closer to the 20 mm specimen points than to the 70 mm specimen points.



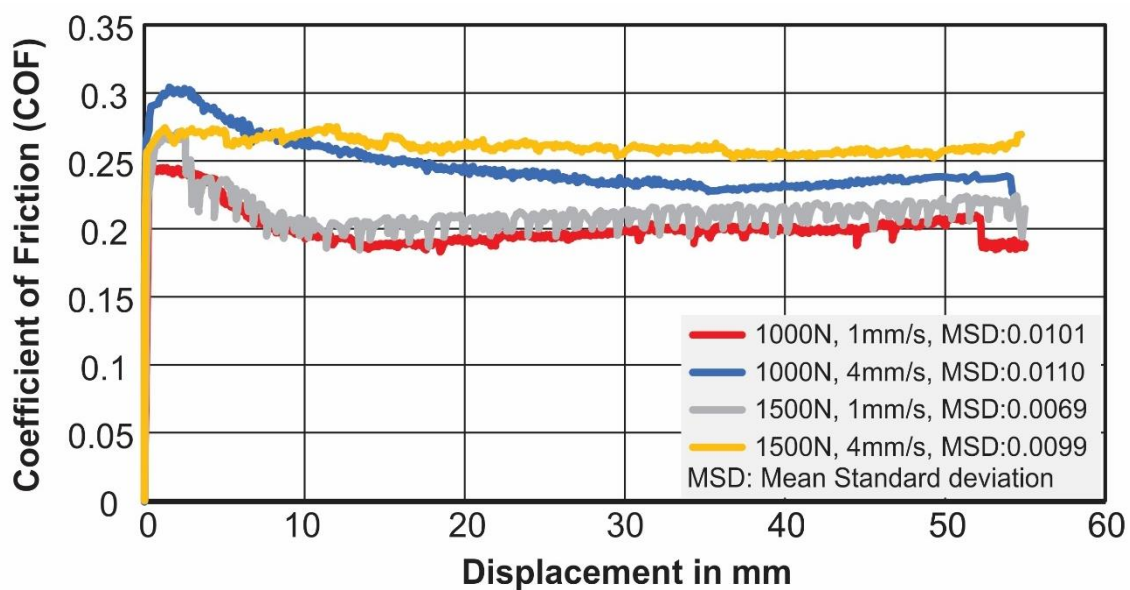
**Figure 4.36:** Forming limit diagram of aluminium composite panel

### 4.7.5 Friction Test Results

The friction test between aluminium composite panel and MPF die material and that of aluminium composite panel and polyurethane layer have been performed and using equation 4.4 the coefficient of friction was calculated throughout the test with the help of LabView software. The graphs of the coefficient of friction (COF) against displacement were then drawn as seen in **Figure 4.37** and **Figure 4.38**.

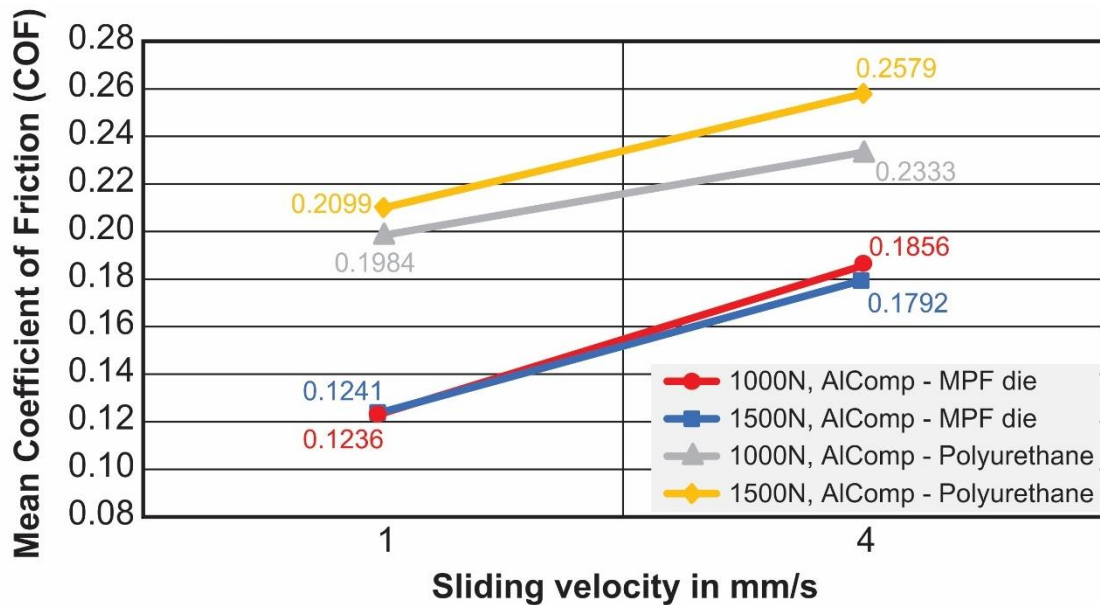


**Figure 4.37:** Friction test results of aluminium composite panel and MPF die material



**Figure 4.38:** Friction test results of aluminium composite panel and a polyurethane layer

An interaction plot for the mean values of COF is also drawn to show the effect of normal force and sliding velocity on the COF (**Figure 4.39**).



**Figure 4.39:** Interaction plot for COF between sliding velocity and normal force

#### *Evaluation of the Friction Test results*

From interaction plot (Figure 4.39), all the lines are almost parallel, that means there is no remarkable interaction between sliding velocity and normal force for both tests.

For the friction test between aluminium composite panel and MPF die material, at 1 mm/s sliding velocity the mean value of COF is almost the same for 1000 N and 1500 N normal force. At 4 mm/s sliding velocity the mean value of COF increases slightly with increase of normal force. Overall, the change in sliding velocity affects the mean value of COF more than the change of normal force (Fu et al., 2012).

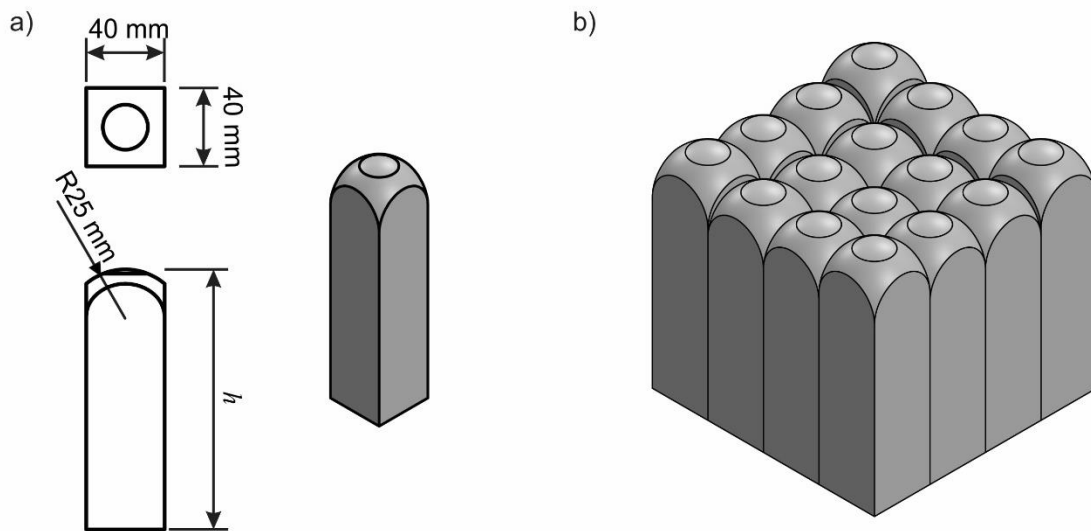
For the friction test between aluminium composite panel and elastic cushion (polyurethane), when the normal force increases the mean value of COF slightly increases. But when sliding velocity increases the mean value of COF highly increases. The lowest and highest COF values obtained from both experiments will be used in numerical simulation in order to investigate the effect of COF on the forming process.

## 5 Numerical Analysis

### 5.1 Punch Design

The multi-point die forming (MPDF) method (chapter 2.2.2) is used in this work because of the low cost of tool production and easy control of forming process as both of the punch set are fixed to the upper and lower plates. Both upper and lower punches are fixed and there is no movement between punches during the forming process.

Based on the material available in the factory, AA6060-T6 is selected as punch material. The dimension of the punch is 40 mm x 40 mm with 25 mm hemispherical radius (Figure 5.1 a). Each punch set is made of 16 total punches with a network of 4x4 punches (Figure 5.1 b).



**Figure 5.1** a) Geometry of Multi-Point Die Forming (MPDF) punch, b) Schematic design of lower MPDF punch set

The punch geometry in MPDF depends on the contact points between the blank and the part. To form the required shaped part, the pins positions are given by the heights which they occupy in relation to the part to be formed (Paunoiu et al., 2011). The  $x$  coordinate and  $y$  coordinate of all punches are stationary while only the  $z$  coordinate changes.

The  $z$  coordinate of each punch can be calculated based on the tangent principle between the objective surface and punch surface (Peng et al., 2013).

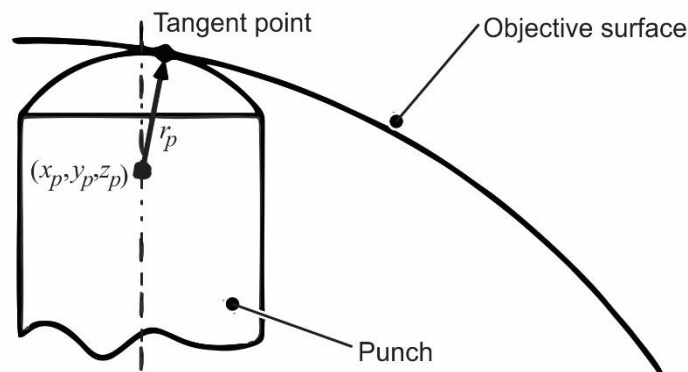
The function of punch surface can be calculated by:

$$\varphi(x, y, z_p) = \pm \sqrt{r_p^2 - (x - x_p)^2 - (y - y_p)^2} + z_p \quad (5.1)$$

where  $r_p$  is the spherical radius of punch and  $(x_p, y_p, z_p)$  is the central coordinate of the punch. At tangent point (**Figure 5.2**), the  $z$  coordinate of the objective surface is the same as the  $z$  coordinate of the punch. The partial derivatives of the objective surface and punch surface for  $x$  and  $y$  are the same. The  $x$  and  $y$  coordinate of the tangent point and the  $z$  coordinate of the punch can be calculated using the following equations.

$$\begin{aligned} F_1(x, y, z_p) &= f(x, y) - \varphi(x, y, z_p) = 0 \\ F_2(x, y) &= \frac{\partial f}{\partial x} - \frac{\partial \varphi}{\partial x} = 0 \\ F_3(x, y) &= \frac{\partial f}{\partial y} - \frac{\partial \varphi}{\partial y} = 0 \end{aligned} \quad (5.2)$$

where  $f(x, y)$  is the function of the objective surface. Based on the **equation (5.2)**, the central coordinate of the punch can be calculated using the Newton-Raphson method (Peng et al., 2013).

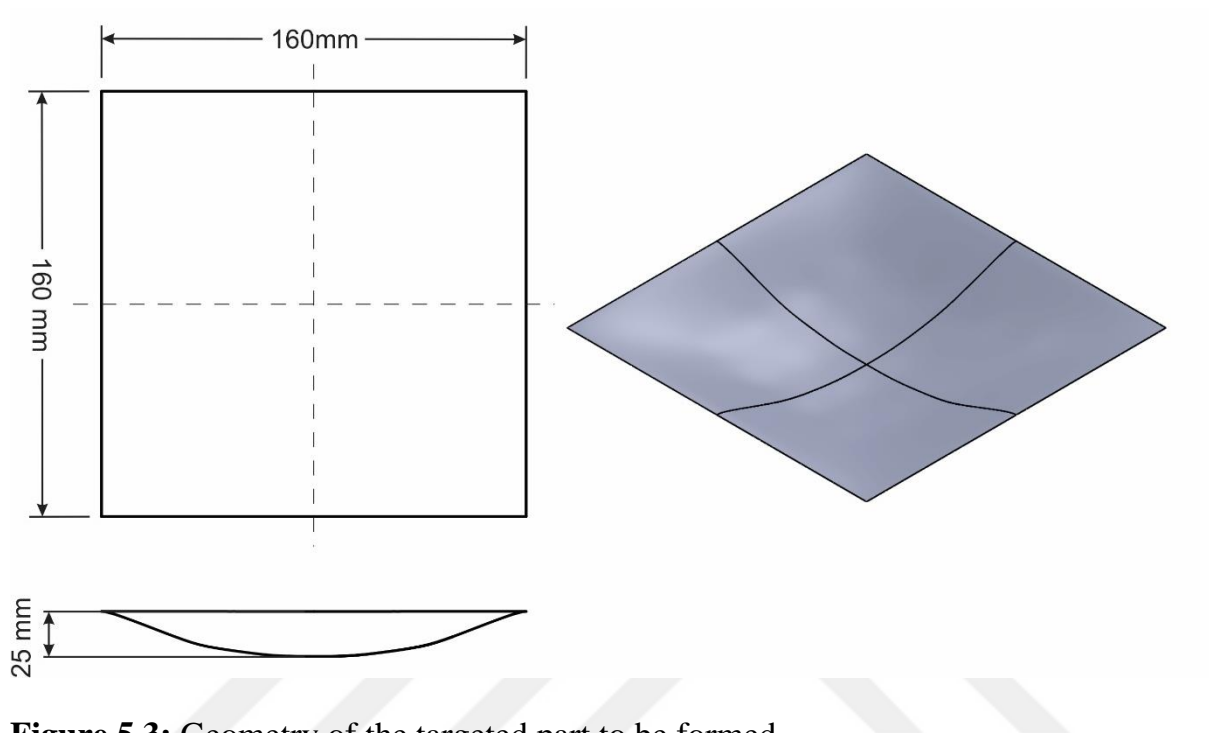


**Figure 5.2:** Location of the punch (Peng et al., 2013).

In this work, the punch heights are calculated using AutoForm® Software based on the above principle. The blank dimensions are then extended to 430 mm x 430 mm according to the blank holder design (Chapter 6.1.2).

## 5.2 Targeted Part Geometry

The targeted part to be formed is a symmetrically curved part with dimensions of 160 mm x 160 mm. **Figure 5.3** illustrates the dimensions of the part to be formed.



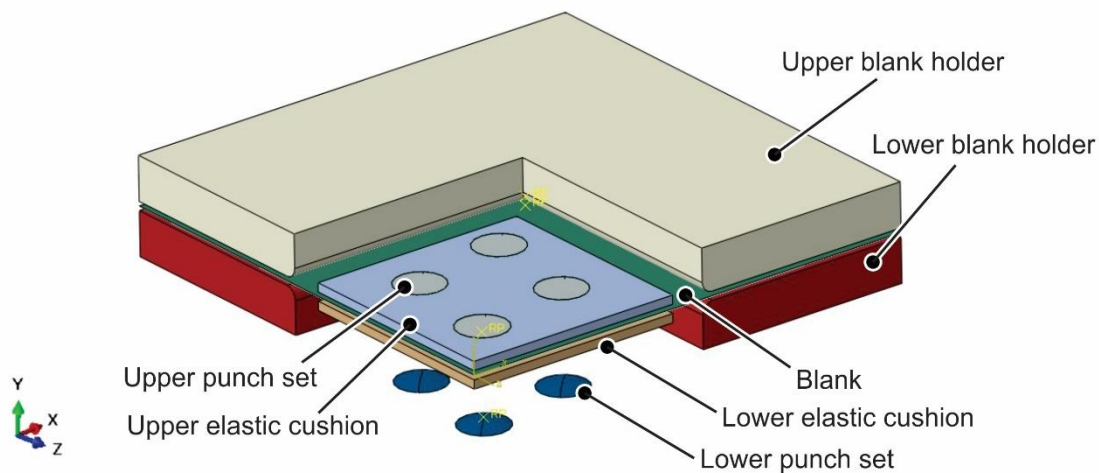
**Figure 5.3:** Geometry of the targeted part to be formed

## 5.3 Numerical Simulation

A commercial finite element software Abaqus/Explicit 6.14 is used for numerical simulation. With explicit formulation, complex contacts in MPF process can be efficiently handled and small workstation can be used to solve large problems (Cai and Li., 2002). An elastic-plastic model (**Figure 5.4**) made from only one quarter of the composite panel is created to reduce computation time because the formed part is symmetric. The movement of the upper punch set is controlled by velocity same as the forming velocity of the hydraulic press machine to be used in forming experiments.

The upper and lower punch sets are imported from STEP file model designed in SolidWorks® software. Only the hemispheric ends of the punches are imported to simplify the model and save simulation time.





**Figure 5.4:** Schematic design of a quarter of the MPDF simulation in Abaqus/Explicit software.

### 5.3.1 Element Model

Both of the die sets are treated as rigid bodies during the simulation. The element R3D4, a bilinear quadrilateral three-dimensional rigid element with four nodes, is used to model the die sets. Mesh control is also assigned to control the element shapes using Quad-dominated Medial axis algorithm. Blank holders are modelled like punch sets with R3D4 element and also assigned mesh control.

The elastic cushion (polyurethane) is modelled using C3D8R elements. The C3D8R is a hexahedral solid element with eight nodes, reduced integration, hourglass control and linear displacement interpolation. It is formulated for large strains and deformations (Davoodi and Zareh-Desari, 2014).

The blank is modelled using finite shell element S4R with reduced integration. The S4R is a four-nodded, doubly curved quadrilateral shell element, it includes large rotations, transverse shear deformations and finite membrane strains (Davoodi and Zareh-Desari, 2014). A default hourglass control technique is also used to avoid the spurious deformation modes during finite element simulations. The shell element is used because of the large surface-to-volume ratio of the blank (Banabic and Tekkaya, 2006).

Mesh convergence analysis is conducted to study the effect of mesh size on the numerical analysis results. The same MPDF process without elastic cushion is simulated using 196, 484, 1849, 5184 and 11664 total number of blank elements. Point O (Figure 5.12), located at the centre of the blank, is selected as the reference point and the values of von Mises stress and equivalent plastic strain at point O when the upper and lower punches are fully closed are taken. The graphs of von Mises stress and equivalent plastic strain against a total number of blank elements are then drawn (Figure 5.5).

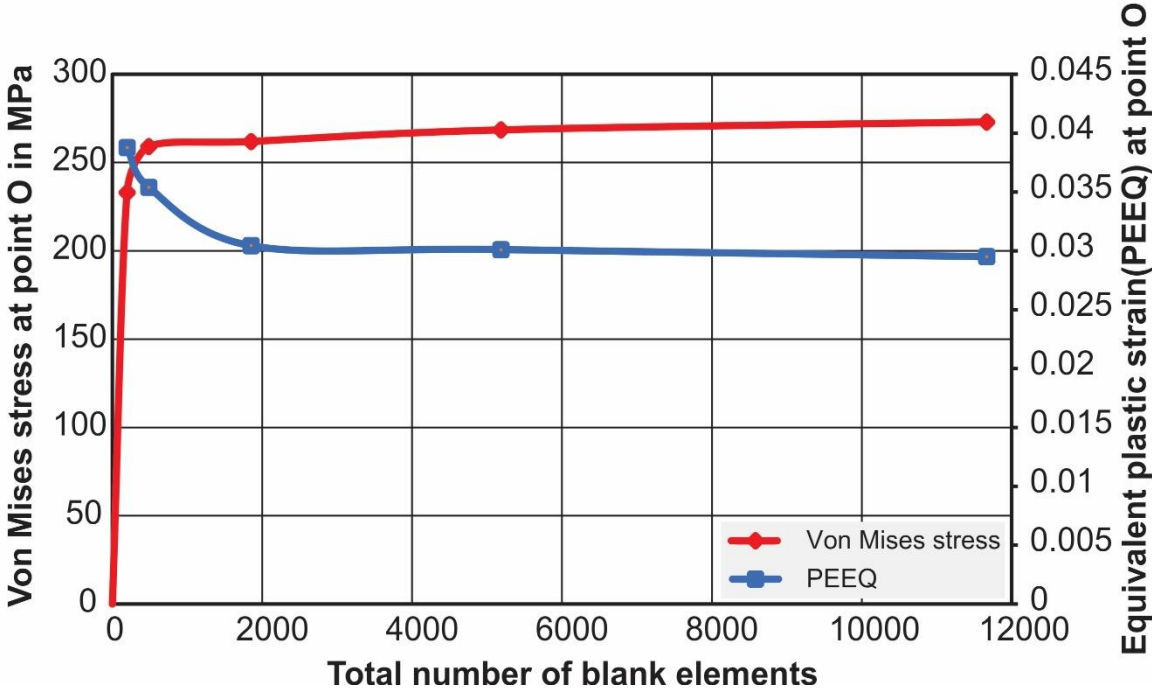


Figure 5.5: Graph of von Mises stress and equivalent plastic strain at point O against the total number of blank elements

From Figure 5.5, it can be observed that the values of von Mises stress and equivalent plastic strain for total number of blank elements bigger than 1849 are insensitive to the number of elements. Therefore, the total number of blank elements was chosen to be 1849 for the rest of the FE simulation. After meshing, the total number of elements of the elastic cushion, each die set, and blank holder are 5000, 4200 and 3741 respectively.

### 5.3.2 Material Model

The upper and lower punch sets and blank holders adopt the rigid material model.

The Mooney-Rivlin model is used to describe the elastic cushion material (polyurethane) which behaves in a non-linear elastic manner and is generally assumed to be virtually incompressible (Wang et al., 2012). The Mooney-Rivlin (hyper-elastic) model can be expressed using the following equation:

$$W = C_{10}(I_1 - 3) + C_{01}(I_2 - 3) \quad (5.3)$$

where  $W$  is the strain energy per unit volume,  $I_1$  and  $I_2$  are the first and second invariants of the deviatoric strain tensor and  $C_{10}$  and  $C_{01}$  are the temperature-dependent material properties obtained from a uniaxial compression test (Abosaf et al., 2017).

In Abaqus/Explicit, either the stress-strain curve of the hyper-elastic material or the constants of Mooney-Rivlin model constants ( $C_{10}$  and  $C_{01}$ ) can be used as input data for this model (Cai et al., 2009). In this work, the values of  $C_{10}$  and  $C_{01}$  obtained by Abosaf et al. (2017) who conducted uniaxial compression tests of polyurethane with a shore A hardness of 90, are used because the same type of polyurethane is used in this work. The values of  $C_{10}$  and  $C_{01}$  are 0.861 and 0.354 respectively.

AA3105 is modelled using Hill's quadratic yield criterions taking consideration of anisotropic behaviour of the material as follows (Bagherzadeh et al., 2015).

$$f(\sigma) = \sqrt{F(\sigma_{22} - \sigma_{33})^2 + G(\sigma_{33} - \sigma_{11})^2 + H(\sigma_{11} - \sigma_{22})^2 + 2L\sigma_{23}^2 + 2M\sigma_{31}^2 + 2N\sigma_{12}^2} \quad (5.4)$$

where  $F$ ,  $G$ ,  $H$ ,  $L$ ,  $M$  and  $N$  are material parameters and  $\sigma_{ij}$  is the stress component.

$$F = \frac{1}{2} \left( \frac{1}{R_{22}^2} + \frac{1}{R_{33}^2} - \frac{1}{R_{11}^2} \right), \quad G = \frac{1}{2} \left( \frac{1}{R_{33}^2} + \frac{1}{R_{11}^2} - \frac{1}{R_{22}^2} \right), \quad H = \frac{1}{2} \left( \frac{1}{R_{11}^2} + \frac{1}{R_{22}^2} - \frac{1}{R_{33}^2} \right),$$

$$L = \frac{3}{2R_{23}^2}, \quad M = \frac{3}{2R_{13}^2}, \quad N = \frac{3}{2R_{12}^2} \quad (5.5)$$

$R_{ij}$  is the anisotropic yield stress ratio which can be calculated from plastic strain ratio( $r$ ) obtained from the tensile test of AA3105 (Table 4.9).

By assuming  $R_{11} = R_{13} = R_{23} = 1$  (Bagherzadeh et al., 2015),  $R_{22}$ ,  $R_{33}$  and  $R_{12}$  can be calculated as follows:

$$R_{22} = \sqrt{\frac{r_{90}(r_0+1)}{r_0(r_{90}+1)}}, R_{33} = \sqrt{\frac{r_{90}(r_0+1)}{(r_0+r_{90})}}, R_{12} = \sqrt{\frac{3(r_0+1)r_{90}}{(2r_{45}+1)(r_0+r_{90})}} \quad (5.6)$$

The calculated yield stress ratios of AA3105 are  $R_{22} = 2.0408$ ,  $R_{33} = 1.0035$  and  $R_{12} = 0.8364$ . These six yield stress ratio values are used as input data of AA3105 material model in Abaqus/Explicit. **Equation 5.7** is used to describe the work hardening of AA3105 (Davoodi and Zareh-Desari, 2014).

LDPE is modelled by isotropic von Mises model. The work hardening of material is described by Hollomon plastic flow equation below (Parsa et al., 2010).

$$\sigma = K\varepsilon^n \quad (5.7)$$

where  $\sigma$  is the true stress,  $\varepsilon$  is the true strain,  $K$  is the strength coefficient and  $n$  is the strain hardening coefficient. Finally, a composite conventional shell section with 3 plies (0.5 mm AA3105 – 3 mm LDPE - 0.5mm AA3105) is created and assigned to the blank. For more details about composite material modelling see **appendix C**. Forming limit curve (FLC) of aluminium composite panel (Figure 4.36) could not be used in material modelling because it is not possible to assign FLC to a composite conventional shell section. In Abaqus/Explicit, it is only possible to assign FLC to ductile metals.

### 5.3.3 Contact Interfaces

The friction at the interfaces is assumed to be based on Coulomb's model (Wang et al., 2012). The coefficient of friction (COF) between punches and aluminium composite and that between elastic cushion (polyurethane) and aluminium composite panel are experimentally determined (Figure 4.39). The smallest values of COF obtained from friction test between aluminium composite panel and elastic cushion and that between aluminium composite panel and MPF die are taken as the minimum (low) values in the numerical analysis.

The highest COF values obtained from the same experiments are taken as maximum (high) COF in the simulation (**Table 5.1**). The coefficient of friction between elastic cushion (polyurethane) and punches could not be experimentally determined because the elastic cushion was sliding between the pull clamps (Figure 4.20). The coefficient of friction between aluminium composite panel and blank holder was not experimentally determined because blank holder material was not available at the time friction test was conducted. Hence the COF values from literature (Cai et al., 2009), (Davoodi and Zareh-Desari, 2014) are used.

**Table 5.1:** Coefficient of friction values used in numerical simulation.

Parameters	Levels	
	Low	High
Coefficient of friction (AlComp - polyurethane)	0.1984	0.2579
Coefficient of friction (AlComp – MPF die)	0.1236	0.1856
Coefficient of friction (AlComp – blank holder)	0.1	
Coefficient of friction (polyurethane – MPF die)	0.2	

The interaction properties are set to surface-to-surface contact (Explicit), finite sliding for sliding formulation and “Hard” contact for pressure-overclosure and penalty contact method for mechanical constraint formulation. Penalty contact method searches for edge into edge and node into face penetrations and also it can model some types of contact that the kinematic method cannot.

### 5.3.4 Boundary Conditions

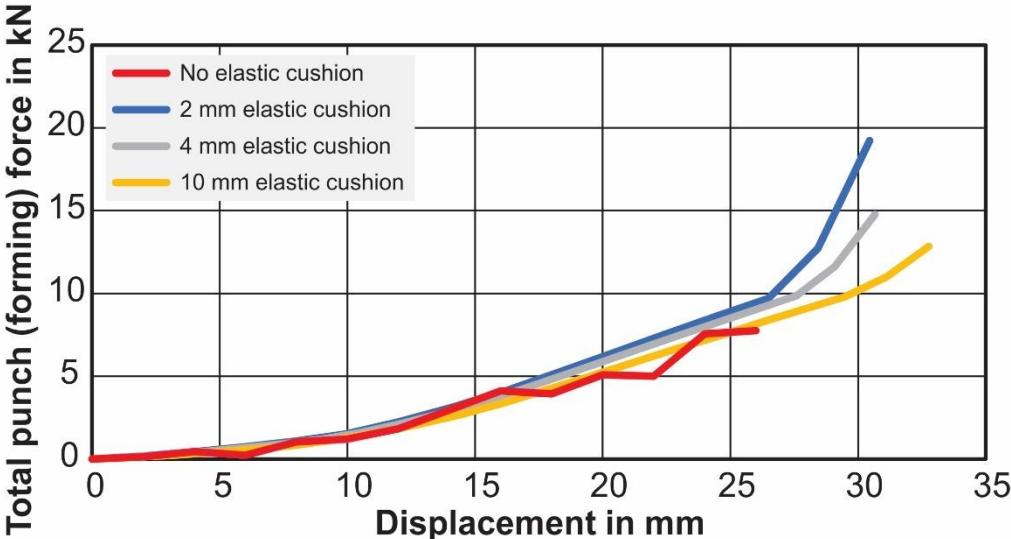
The lower punch set and lower blank holder (**Figure 5.4**) are constrained in all directions because they don't move during the forming process. The upper blank holder is assigned with blank holder force of 10 kN in y-direction while constrained in all other directions. The upper die is assigned with a velocity of 20 mm/s in y-direction same as the maximum forming speed of the hydraulic press used in the forming experiments.

The blank and elastic cushions are constrained using symmetrical boundary conditions on *XOY* and *YOZ* symmetrical planes.

### 5.4 Numerical Analysis Results

#### 5.4.1 Punch (Forming) Force

The graph of total punch force (for all punches) against displacement when there is no elastic cushion, 2 mm, 4 mm and 10 mm elastic cushion is drawn (**Figure 5.6**). From the graph, it can be observed that the total punch force is higher when an elastic cushion is used than without elastic cushion. These results are in good agreement with the results obtained by Kadhim and Abbas (2014).

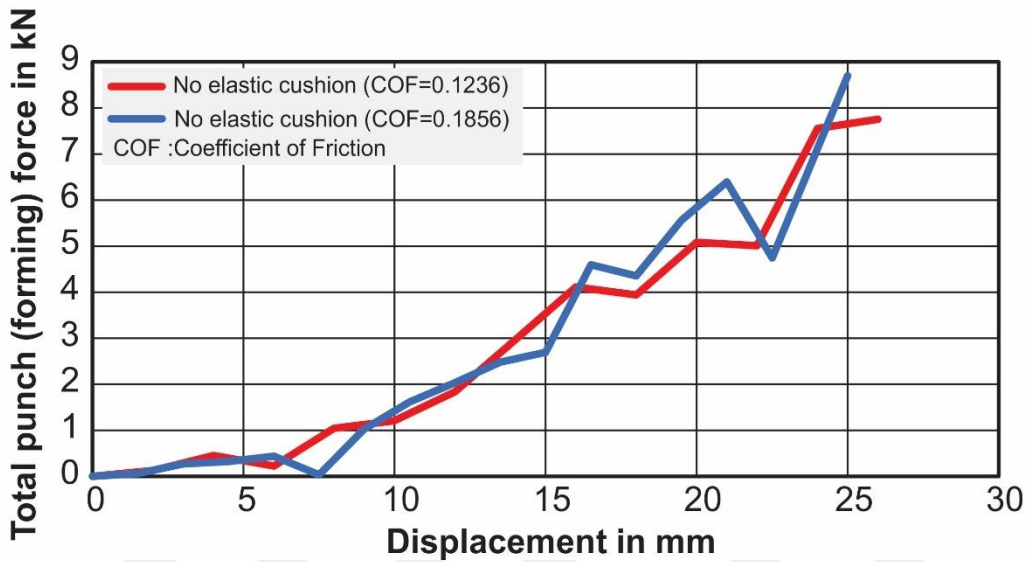


**Figure 5.6:** Total punch force-displacement graph for different elastic cushion

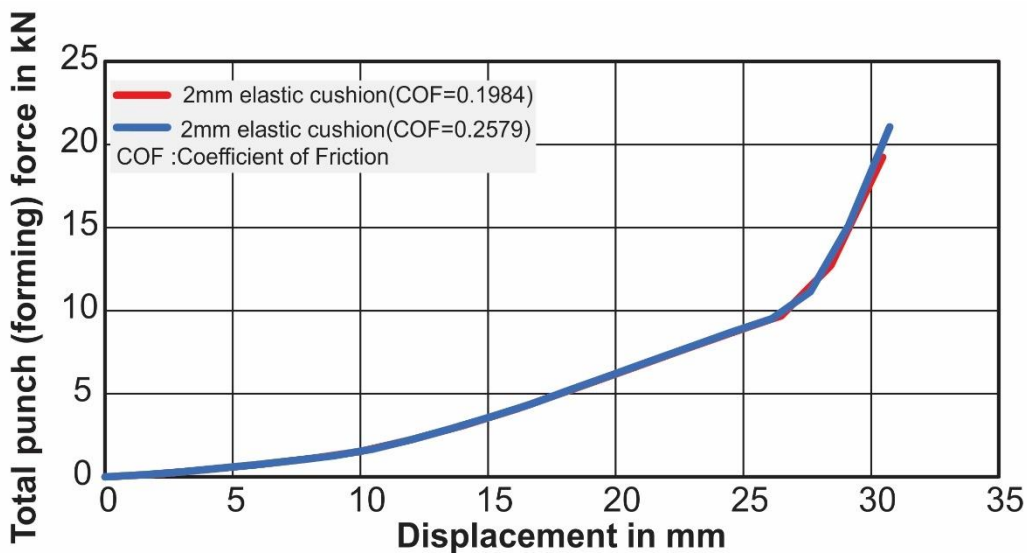
Also, it can be observed that the total punch force increases as the displacement increases and as more punches make contact with the blank. The punch force reaches its maximum when all the punches make contact with the blank. When the elastic cushion is not used, the punch force is not uniform, this might be caused by the high discrete concentration force on contact points between the punch and aluminium composite panel.

*Effect of Coefficient of Friction on Punch Force*

To investigate the effect of the coefficient of friction (COF) on punch force, the forming process is simulated using the same conditions but only different values of COF according to data in Table 5.1. It is observed that the effect of COF on the punch force is insignificant especially when the elastic cushion (**Figure 5.8**) is used.



**Figure 5.7:** Total punch (forming) force - displacement graph for different COF values without cushion

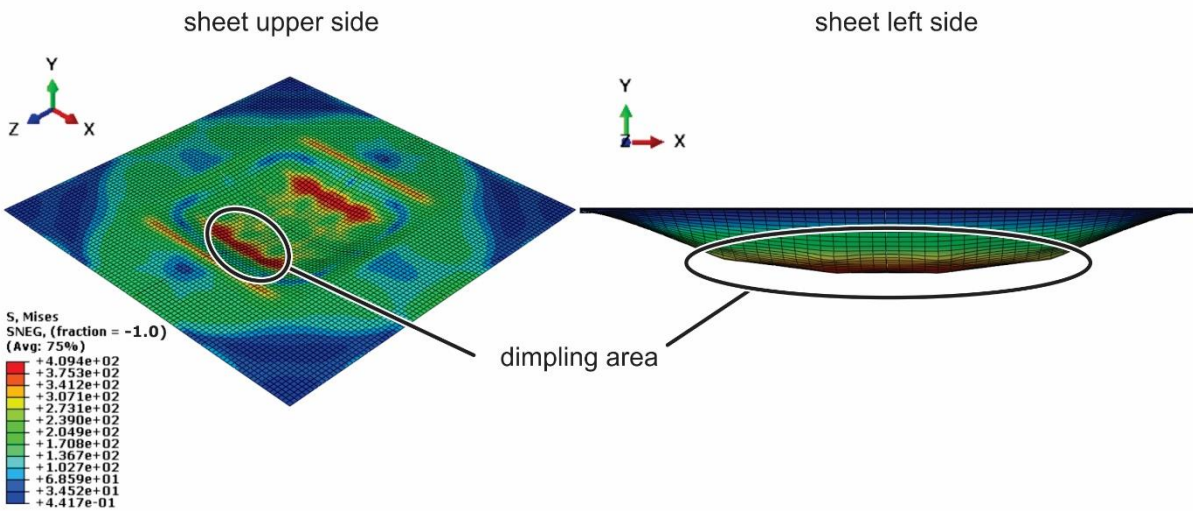


**Figure 5.8:** Total punch (forming) force - displacement graph for different COF values with 2mm cushion

### 5.4.2 Stress Distribution

#### *Without Elastic Cushion*

**Figure 5.9** shows the stress (Mises) distribution on both sides of the aluminium composite panel when the elastic cushion is not used. Dimpling, which results from discontinuous contacts between the blank and punches, can be seen with high visibility on the outer sides of the formed part (red areas) while wrinkling is not formed due to the effect of blank holder force. The stress concentration appears on the outer zones (outer punches) because of the complex contact stresses in these areas (Kadhim and Abbas, 2014). The maximum von Mises stress value is 409.4 MPa. The stress values at contact point between the blank and punches are higher than the stress values between the punches.

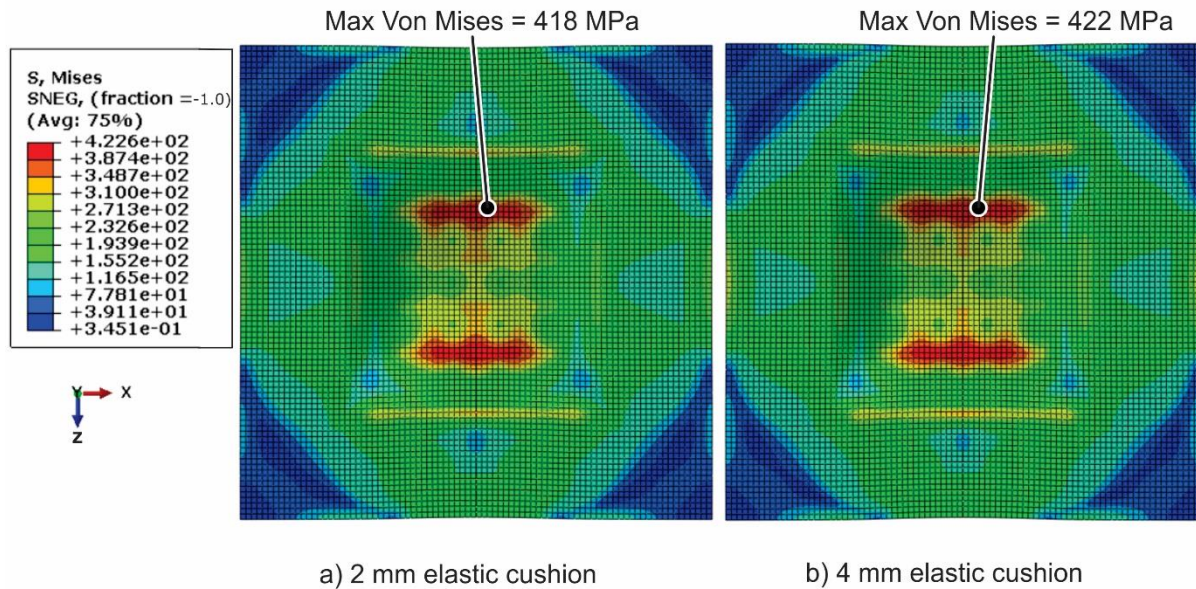


**Figure 5.9:** Stress (Mises) distribution on the surface of the sheet (without cushion)



### With 2 mm and 4 mm Elastic Cushion

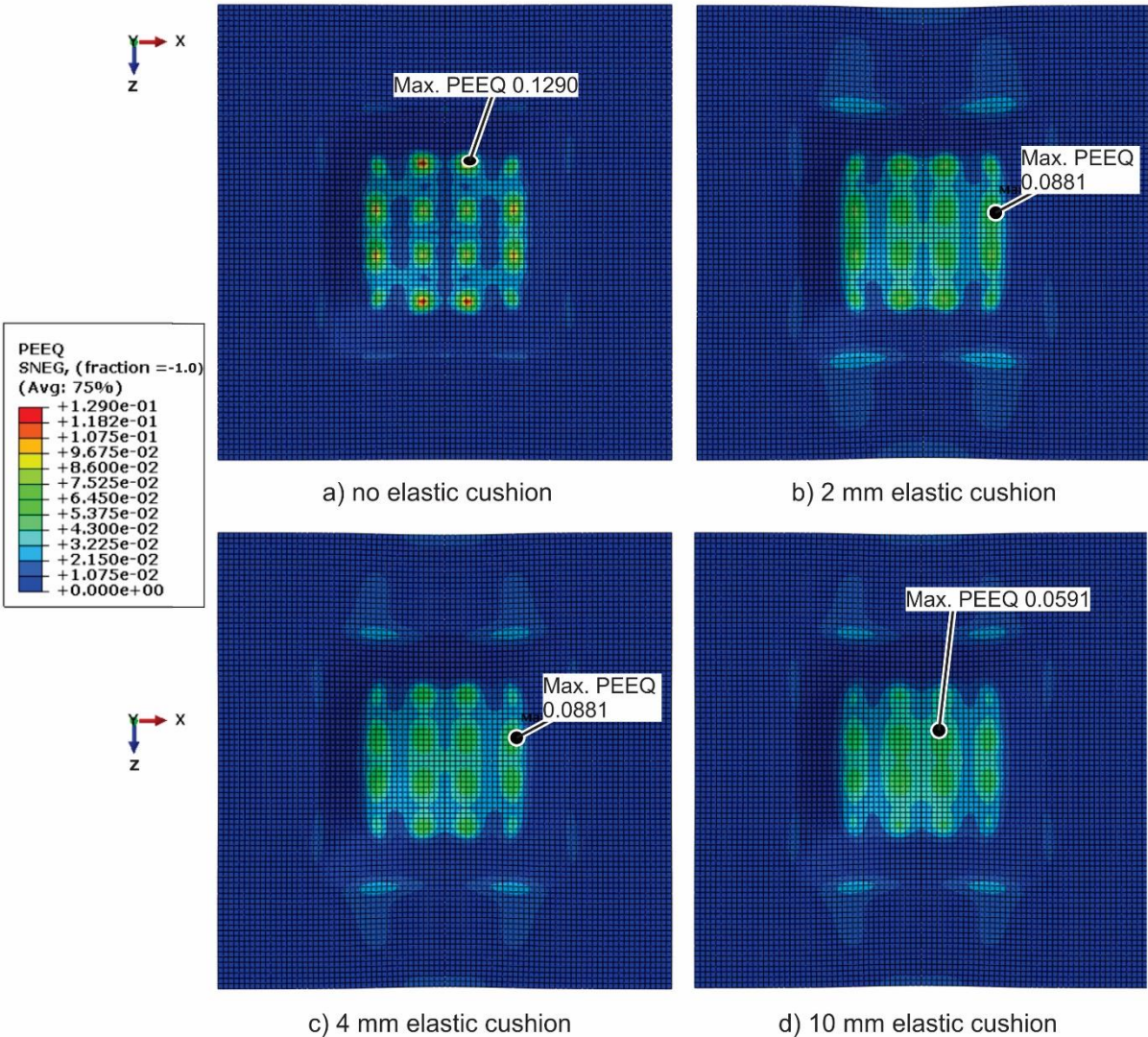
**Figure 5.10** shows that as the thickness of the elastic cushion increases the maximum von Mises stress increases while dimples are more suppressed (Wang et al. 2012).



**Figure 5.10:** Stress (Mises) distribution for **a)** 2 mm, **b)** for 4mm elastic cushion

### 5.4.3 Equivalent Plastic Strain Distribution

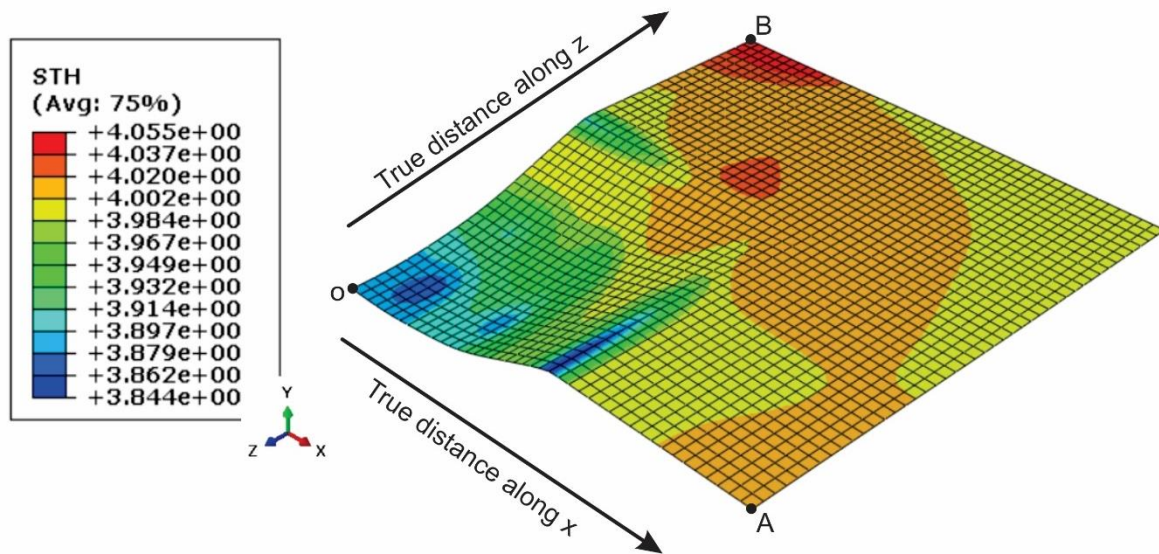
The maximum equivalent plastic strain of the formed part increases as the thickness of the elastic cushion decreases. The equivalent plastic strain is more uniformly distributed when the thickness of the elastic cushion is high (**Figure 5.11 d**). When no elastic cushion is used (**Figure 5.11 a**), the maximum equivalent plastic strain is at the contact point between the punch and the composite while the spaces in between the punch have almost minimum equivalent plastic strain.



**Figure 5.11:** Equivalent plastic strain distribution **a)** without elastic cushion, **b)** 2 mm elastic cushion **c)** 4 mm elastic cushion and **d)** 10 mm elastic cushion

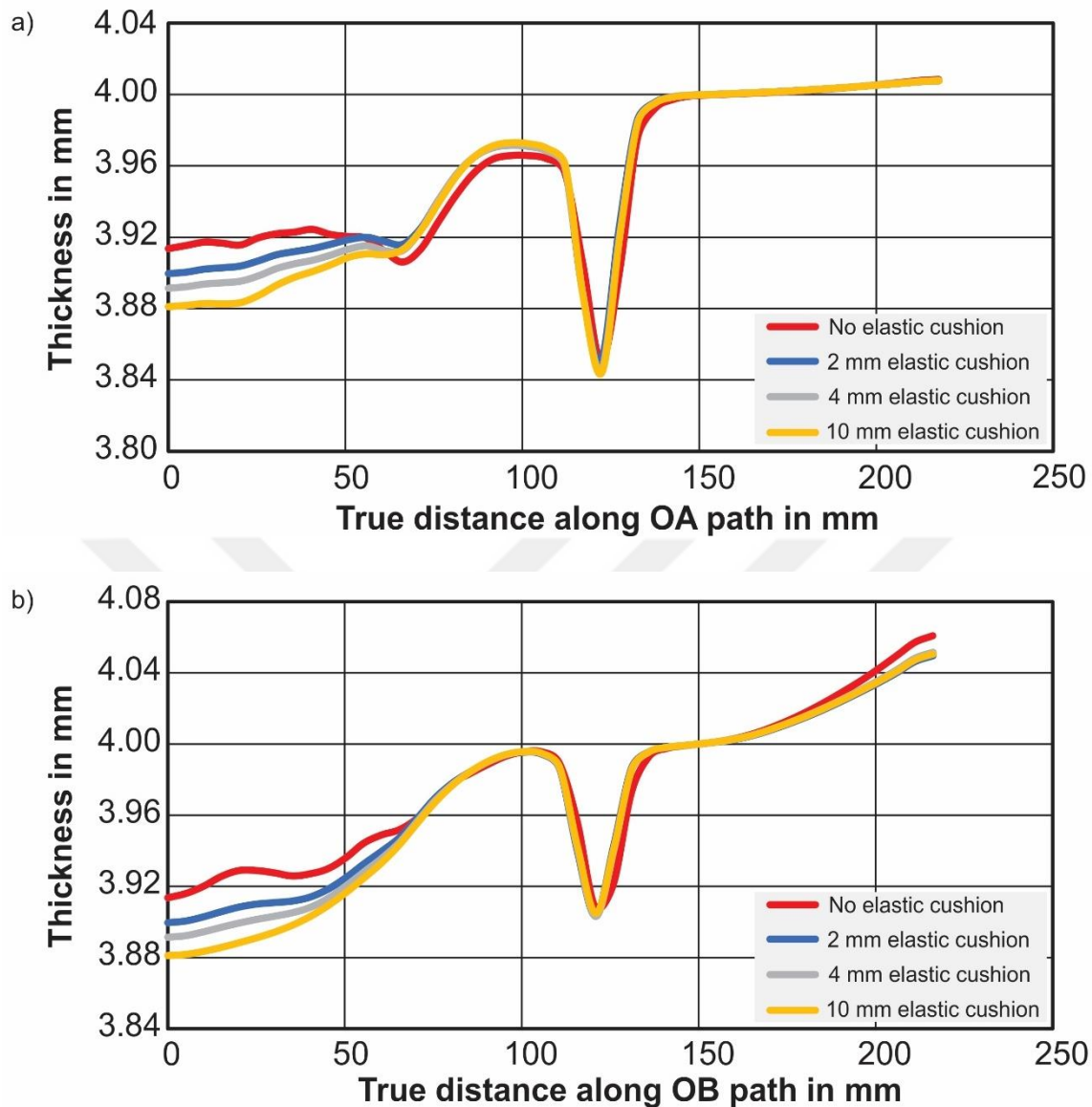
### 5.4.4 Thickness Distribution

Thickness variation on the formed part along X and Z axis from the centre of the formed part is also analysed. Two paths, namely OA and OB, are created from the centre of the formed part to the end of the part (215 mm from the centre) along the edges of the deformed geometry (**Figure 5.12**). Using this formed path, a graph of thickness variation against true distance along the created path can be computed.



**Figure 5.12:** Thickness variation on the surface of aluminium composite panel with 10 mm elastic cushion

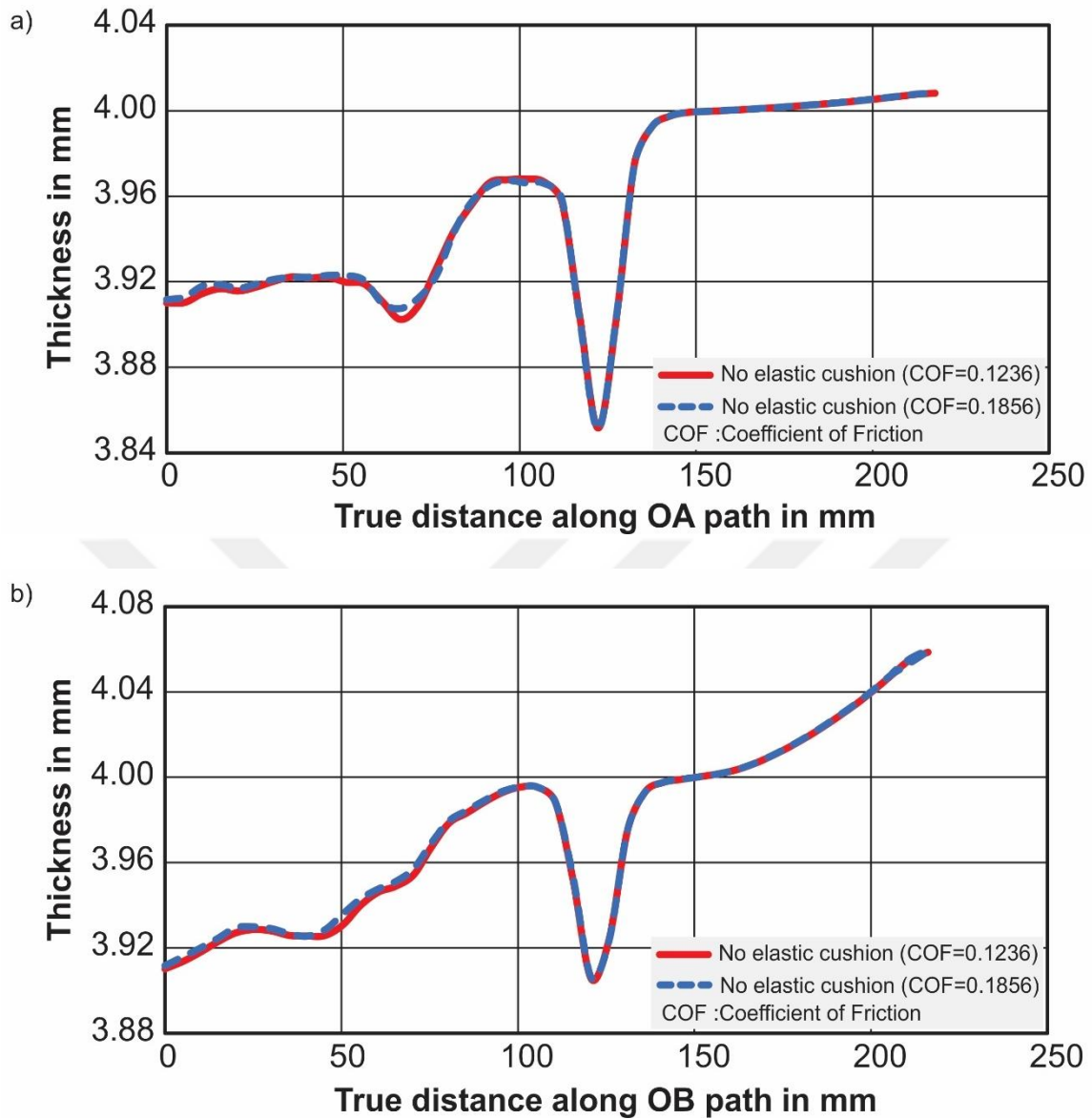
**Figure 5.13** shows the graphs of thickness variations along  $OA$  and  $OB$ , when different elastic cushions are used. From the graphs, it can be observed that the maximum thickness variation occurs at the centre of the formed part agreeing with the results obtained by Abosaf et al., (2017). The thickness variation along blank holder length (from 150 mm to 215 mm) on both  $OA$  and  $OB$  paths is almost the same for all four conditions. From the centre of the formed part to the blank holder, the fluctuation of thickness variations along both paths decrease as the thickness of elastic cushions increase, this indicates the disappearance of stress concentration (Wang et al., 2012). Along  $OA$  path, the thickness variation is maximum on the edge between the formed part and the blank holder because of the high deformation in the bending zone caused by complex loading conditions (Kadhim and Abbas, 2014). This explains why the 200 mm Nakajima test specimens (Figure 4.34) cracked on the bottom side of the specimen close the blank holder instead of cracking in the middle.



**Figure 5.13:** Thickness variation of the formed part from the centre to the end of the blank holder **a)** along OA path, **b)** along OB path

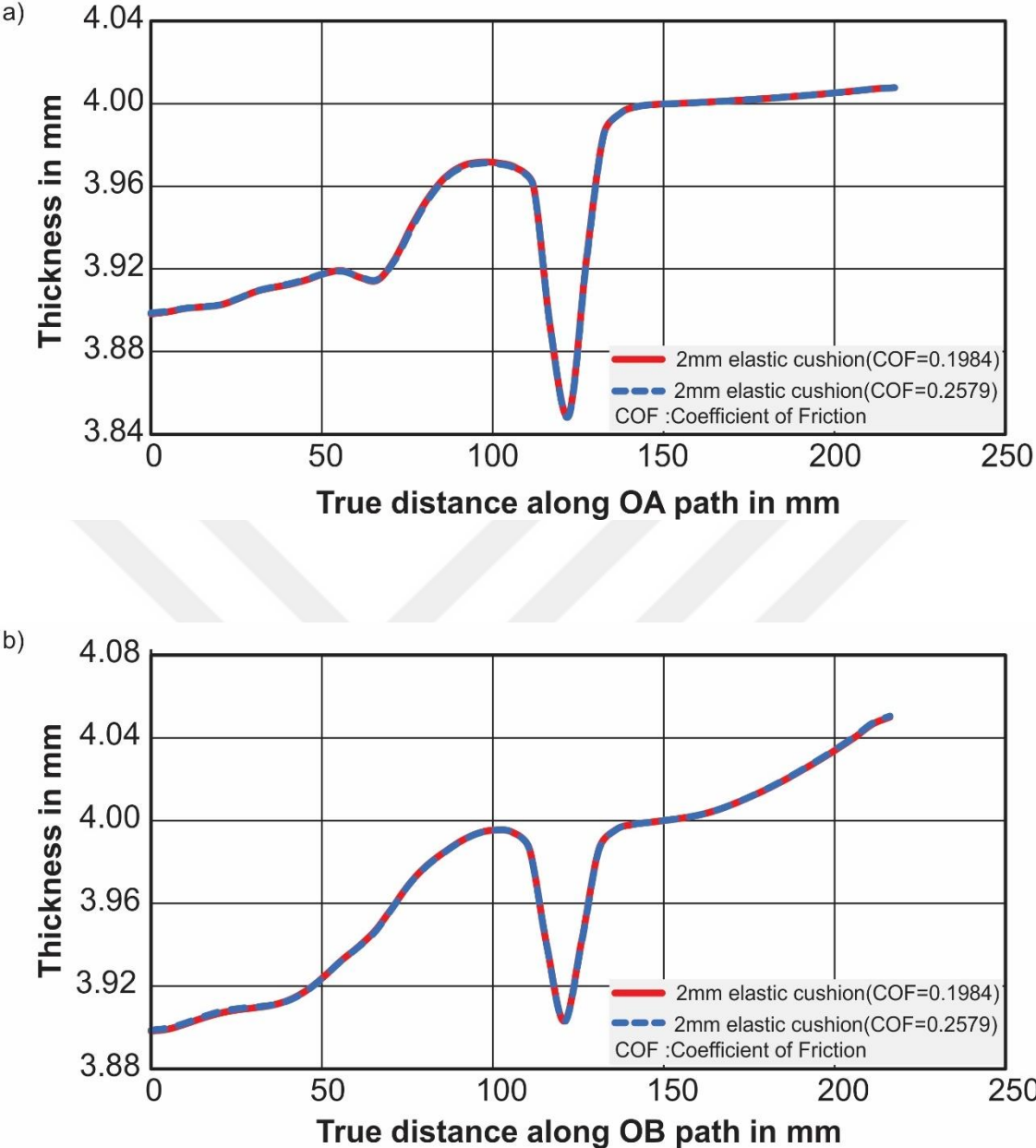
#### *Effect of Coefficient of Friction on Thickness Variation*

The effect of coefficient of friction on thickness variation when MPDF process without elastic cushion and with 2mm elastic cushion was analysed. For both cases (with elastic cushion and without elastic cushion), the forming process is simulated using different COF values found in Table 5.1 and all other conditions are kept constant. The graphs of thickness variation along OA and OB paths for different COF are drawn (**Figure 5.14** and **Figure 5.15**).



**Figure 5.14:** Thickness variation of the formed part without elastic cushion from the centre to the end of blank holder **a)** along OA path, **b)** along OB path

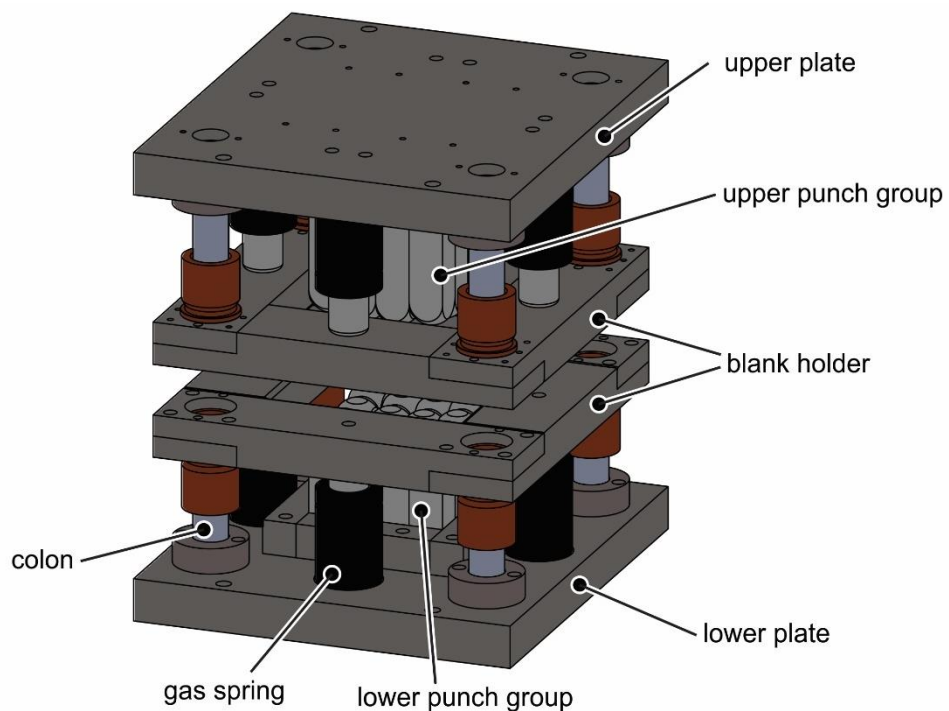
From Figure 5.14 and Figure 5.15 it can be seen that the coefficient of friction does not affect on the thickness variation of the formed part for both conditions analysed. Hence the effect of the coefficient of friction can be neglected.



**Figure 5.15:** Thickness variation of the formed part with 2mm elastic cushion from the centre to the end of blank holder **a)** along OA path, **b)** along OB path

## 6 Multi-Point Forming Die Design

The MPF die is made up of mainly seven components: colons, gas springs, lower plate, upper plate, blank holder, lower punch group and upper punch group. The upper MPF die group is designed similar to the lower die group to simplify production and assembly of the parts. When fully opened, the total height of the MPF die is 660 mm and 430 mm when fully closed. **Figure 6.1** shows the schematic of the designed multi-point forming die.



**Figure 6.1:** Schematic of designed Multi-Point Forming die.

### 6.1 Lower and Upper Plates

The lower and upper plates are identical with width, length and height dimensions of 450 mm, 500 mm and 50 mm respectively. The two plates are made from (DIN 1.0540) C50 steel. The upper plate is designed to be attached to the slide plate of the hydraulic press machine while the lower plate of the MPF tool sat on the bedplate. Four colons and four gas springs are connected to each plate using M8 screws.

## 6.2 Blank Holder

The outside dimensions of the blank holder are 430 mm x 430 mm while the inner dimensions are 330 mm x 330 mm. The inner edges of the blank holder have a radius of 5 mm designed to facilitate easy flow of the material during the forming process. The blank holder is connected to the lower and upper plates using four colons for each of the plates. Each blank holder is connected to four gas springs using M8 screws. A gas spring has a stroke of 80 mm, maximum working speed of 1.8 m/s, minimum and maximum pressure of 25 bar and 150 bar respectively. When closed, the gas spring provides the force of 10 kN. The pressure applied by the blank holder to the blank can then be calculated by dividing total force applied by gas springs when closed (40 kN) to the area of the blank holder in contact with the blank (132000 mm<sup>2</sup>). The calculated blank holder pressure ( $P_{BH}$ ) is 0.303 MPa.

## 6.3 Punches

Each side of the punch group contains 12 punches (Figure 5.1 b). The radius of the hemispherical top of the punch is 25 mm. Each punch has a dimension of 40 mm x 40 mm (Figure 5.1 a). The punches are arranged according to the pattern obtained from the calculation made in chapter 5.1. Punches are being held together to the upper and lower plates using 10 mm diameter pins passing through the lower bottom of each punch and are attached to the side bare of the plates.



## 7 Summary and Outlook

The aim of this work conducted at ASAS aluminium company in Turkey was to investigate on formability of 3105 aluminium composite panel which is mainly used as a building material. Multi-point forming process was used to form a symmetrically curved part using 3105 aluminium composite panel as a blank. Five different mechanical tests were conducted to examine different mechanical properties of AA3105 sheet, LDPE and aluminium composite panel under specific conditions.

The results of T-peel stripping test showed that the average peel strength of the bond between AA3105 sheet and LDPE is higher than the minimum values set by TS 13777 standard. The quality of the bond is good because the force is stable throughout the experimental path. Because of these reasons, 3105 aluminium composite specimens with the same angle of rolling direction taken from different area on a large composite panel are expected to have the same mechanical properties.

The tensile test results showed that 3105 aluminium composite panels have higher % elongation at fracture ( $A_t$ ) than AA3105 sheet due to the presence of the LDPE layer. The strain hardening exponent ( $n$ ) and strain rate sensitivity ( $m$ ) values of aluminium composite panel are higher than that of AA3105 sheet meaning that the forming limit curve (FLC) of aluminium composite panel has a higher height than that of AA3105 sheet (Marciniak et al., 2002).

The strain rate sensitivity ( $m$ ) of aluminium composite panel is very low that its effect can be neglected. The average plastic strain ratio ( $\bar{r}$ ) and planar anisotropy ( $\bar{\Delta r}$ ) of 3105 aluminium composite panel are 0.7711 and 0.5811 respectively. This means the anisotropic behaviour of the aluminium composite panel should be taken under consideration in FE simulation by using anisotropic yield criterion when modelling AA3105 sheet.

From the results of fracture analysis using scanning electron microscope (SEM), it is concluded that there is no slip between AA3105 sheet and LDPE before the fracture of the composite panel.

The in-plane torsion test results of AA3105 grooved specimen has an equivalent strain of almost 0.8 and it showed good agreements with the results of AA3105 tensile test specimens until almost 3% equivalent strain.

The Nakajima test results showed that there is inhomogeneous deformation of the aluminium composite panel causing multiple peaks on the strain-length curve of the section data taken by ARAMIS software before the fracture of the specimen. The section data had to be manually evaluated using best-fit parabola approximation method by using Excel software in order to compute the forming limit curve (FLC). The obtained FLC was not used in numerical simulation because in Abaqus/Explicit a forming limit curve cannot be assigned to a composite shell section.

The friction test results showed that the coefficient of friction (COF) value between aluminium composite panel and the elastic cushion is higher than the coefficient of friction value between aluminium composite panel and MPF die. Also, the sliding velocity has more effect on COF than forming force.

Numerical results showed that dimpling found on the surface of aluminium composite panel can be suppressed by using elastic cushion (for both maximum and minimum COF values). Also, it is observed that the effect of coefficient of friction on total punch (forming) force and on thickness variation of the formed part is insignificant and can be neglected. The total punch force when elastic cushion is used is higher than without an elastic cushion, this is in good agreement with results obtained by Kadhim and Abbas (2014). The thickness variation along *OA* and *OB* paths is very high close to the edge of the blank holders. This might cause fracture of the blank along this area and hinder the flow of material. The disappearance of stress concentration is indicated by a decrease of fluctuation of thickness variation along *OA* and *OB* paths as the thickness of elastic cushions increases. The outer regions of the formed part have more stress concentration caused by complex contact stresses due to blank holder force and forces between the punches.

Forming experiments are planned to be conducted when the parts of the multi-point forming die are produced and assembled. Then the results obtained from the forming experiments will be compared to the results obtained from the numerical analysis.

## 8 References

- Abosaf, M., Essa, K., Alghawail, A., Tolipov, A., Su, S., Pham, D., 2017. Optimisation of multi-point forming process parameters. *The International Journal of Advanced Manufacturing Technology*, vol. 92, 1849–1859.
- ASM International, 1990. *Properties and selection : Nonferrous alloys and special-purpose materials*, Volume 2, 10th ed., American Society for Metals, Metals Park, Ohio.
- ASTM D 1248-05. *Standard Specification for Polyethylene Plastics Extrusion Materials for Wire and Cable*, ASTM International.
- ASTM D 638-14. *Standard Test Method for Tensile Properties of Plastics*.
- ASTM D 903-98. *Standard Test Method for Peel or Stripping Strength of Adhesive Bonds*, ASTM International.
- Bagherzadeh, S., Mirnia, M.J, Mollaei Dariani, B., 2015. Numerical and experimental investigations of hydro-mechanical deep drawing process of laminated aluminum/steel sheets. *Journal of Manufacturing Processes*, vol. 18, 131–140.
- Banabic, D., Tekkaya, A.E, 2006. Numerical Simulation and Material Models of Aluminium Sheet Forming. In: Jürgen Hirsch (Ed.), *Virtual Fabrication of Aluminum Products : Microstructural Modeling in Industrial Aluminum Production*. Wiley-vch verlag GmbH, pp. 275–302.
- Barbero, E.J, 2011. *Introduction to Composite Materials Design*, second ed., CRC Press.
- Blau, P.J, 2001. Experimental aspects of friction research on the macroscale. In: Bharat Bhushan (Ed.), *Fundamentals of Tribology and Bridging the Gap Between the Macro- and Micro-Nanoscales*, pp. 261–278.
- Cai, Z.-Y., Li, M.-z., 2002. Multi-point forming of three-dimensional sheet metal and the control of the forming process. *International Journal of Pressure Vessels and Piping*, vol. 79, 289–296.

- Cai, Z.-Y., Li, M.-z., 2005. Finite element simulation of multi-point sheet forming process based on implicit scheme. *Journal of Materials Processing Technology*, vol. 161, 449–455.
- Cai, Z.-Y., Wang, S.-H., Xu, X.-D., Li, M.-z., 2009. Numerical simulation for the multi-point stretch forming process of sheet metal. *Journal of Materials Processing Technology*, vol. 209, 396–407.
- Daniel, I.M, Ishai, O., 2006. *Engineering Mechanics of Composite Materials*, second ed.
- Davoodi, B., Zareh-Desari, B., 2014. Assessment of forming parameters influencing spring-back in multi-point forming process. A comprehensive experimental and numerical study. *Materials & Design*, vol. 59, 103–114.
- DIN EN ISO 6892-1. *Metallic materials — Tensile testing — Part 1: Method of test at room temperature (ISO/DIS 6892-1:2014)*.
- DIN ISO 12004-2. *Part 2 :Determination of forming-limit curves in the laboratory, International Organization for Standardization (ISO)*.
- Doege, E., Behrens, B.-A., 2007. *Handbuch Umformtechnik. Grundlagen, Technologien, Maschinen*, Springer-Verlag Berlin Heidelberg, Berlin, Heidelberg.
- Emanuela, A., Marion, M., 2017. Metallographic Analysis of Nakajima Tests for the Evaluation of the Failure Developments. *Procedia Engineering*, vol. 183, 83–88.
- Fu, X.J, Li, J.J, Liu, Q., 2012. Friction Behavior under Different Forming Speed for Sheet Metal Forming. *AMR*, 472-475, 662–665.
- Fuxing, T., Mingzhe, L., Zhongyi, C., Xiangji, L., 2009. Formability analysis on the process of multi-point forming for titanium alloy retiare sheet. *Int J Adv Manuf Technol*, vol. 41, 1059–1065.
- Groover, M.P, 2012. *Fundamentals of Modern Manufacturing: Materials, Processes and Systems*, 5th ed., wiley.
- Hosford, W.F, Caddell, R.M, 2011. *Metal Forming Mechanics and metallurgy*, 4th ed., Cambridge University Press.

- Kadhim, A.J, Abbas, M.I, 2014. Three-Dimensional experimental and Numerical simulation of sheet metal forming process based on Flexible Multipoint Die. *International Journal of Mining, Metallurgy & Mechanical Engineering (IJMMME)*, Volume 2, 16–20.
- Lange, K. (Ed.), 1994. *Handbook of Metal Forming*, Society of Manufacturing Engineers.
- Li, M., Liu, Y., Su, S., Li, G., 1999. Multi-point forming. A flexible manufacturing method for a 3-d surface sheet. *Journal of Materials Processing Technology*, vol. 87, 277–280.
- Liu, C., Li, M., Fu, W., 2008. Principles and apparatus of multi-point forming for sheet metal. *Int J Adv Manuf Technol*, vol. 35, 1227–1233.
- Marciniak, Z., Duncan, J.L, Hu, S.J., 2002. *Mechanics of Sheet Metal Forming*, second ed., Butterworth-Heinemann.
- Mortensen, A. (Ed.), 2007. *Concise Encyclopedia of Composite Materials*, second ed., Elsevier.
- Najib, L.M, Alisibramulisi, A., Amin, N.M, Bakar I.A.A., Hasim S., 2015. The Effect of Rolling Direction to the Tensile Properties of AA5083 Specimen. In: Hassan R., Yusoff M., Alisibramulisi A., Mohd Amin N., Ismail Z. (eds). *InCIEC 2014*.
- Parsa, M.H., S. Nasher al ahkami, M. Ettehad, 2010. Experimental and finite element study on the spring back of double curved aluminum/polypropylene/aluminum sandwich sheet. *Materials & Design*, 4174–4183.
- Paunoiu, V., Teodor, V., Maier, C., Baroi, N., Bercu, G., 2011. Study of the tool geometry in reconfigurable multipoint forming, 139–144.
- Peng, H., Li, M., Liu, C., Cao, J., 2013. Study of multi-point forming for polycarbonate sheet. *Int J Adv Manuf Technol*, vol. 67, 2811–2817.
- Schuler, 1998. *Metal forming handbook*, Springer.
- Schwindt, C.D, Stout, M., Iurman, L., Signorelli, J.W, 2015. Forming Limit Curve Determination of a DP-780 Steel Sheet. *Procedia Materials Science*, vol. 8, 978–985.

- Semiatin, S.L. (Ed.), 2005. *Asm Handbook- Metalworking: Bulk Forming*, ASM International.
- Shen, W., Ren-jun Yan, Yue Lin, He-qi Fu, 2018. Residual stress analysis of hull plate in multi-point forming. *Journal of Constructional Steel Research*, 65–76.
- Tan, F.X., Li, M.Z., Cai, Z.Y., 2007. Research on the process of multi-point forming for the customized titanium alloy cranial prosthesis. *Journal of Materials Processing Technology*, 187–188, 453–457.
- Tekkaya, A.E, Pöhlandt, K., Lange, K., 1982. Determining Stress-Strain Curves of Sheet Metal in the Plane Torsion Test. *CIRP Annals*, vol. 31, 171–174.
- Traphöner, H., Heibel, S., Clausmeyer, T., Tekkaya, A.E, 2018. Influence of manufacturing processes on material characterization with the grooved in-plane torsion test. *International Journal of Mechanical Sciences*, 146-147, 544–555.
- Traphöner, H., Till Clausmeyer, A. Erman Tekkaya, 2017. Material characterization for plane and curved sheets using the in-plane torsion test – an overview.
- Wang, S., Cai, Z., Li, M., Lan, Y., 2012. Numerical simulation on the local stress and local deformation in multi-point stretch forming process. *Int J Adv Manuf Technol*, vol. 60, 901–911.
- Yin, Q., Soyarslan, C., Isik, K., Tekkaya, A.E, 2015a. A grooved in-plane torsion test for the investigation of shear fracture in sheet materials. *International Journal of Solids and Structures*, vol. 66, 121–132.
- Yin, Q., Tekkaya, A.E, Traphöner, H., 2015b. Determining cyclic flow curves using the in-plane torsion test. *CIRP Annals - Manufacturing Technology*, vol. 64, 261–264.
- Z. Hasan, R., Kinsey, B., Tsukrov, I., 2011. Effect of Element Types on Failure Prediction Using a Stress-Based Forming Limit Curve. *Journal of Manufacturing Science and Engineering*, vol. 133.

# Appendix A

## True Stress – Strain curves of AA3105, LDPE and Aluminium Composite Panel

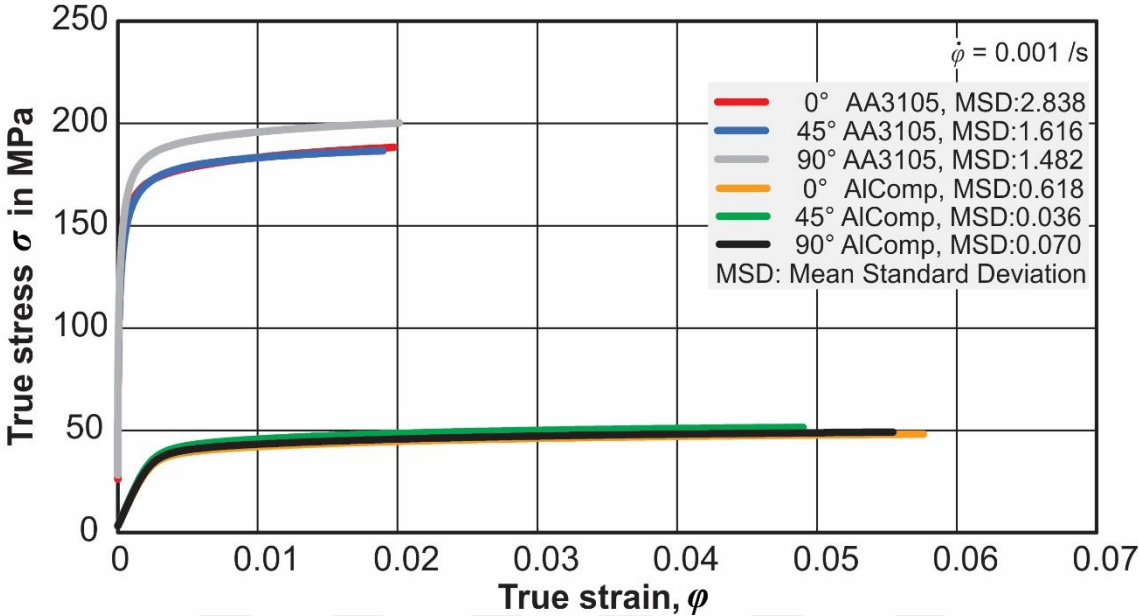


Figure A.1: True stress - strain graph of AA3015 and aluminium composite panel

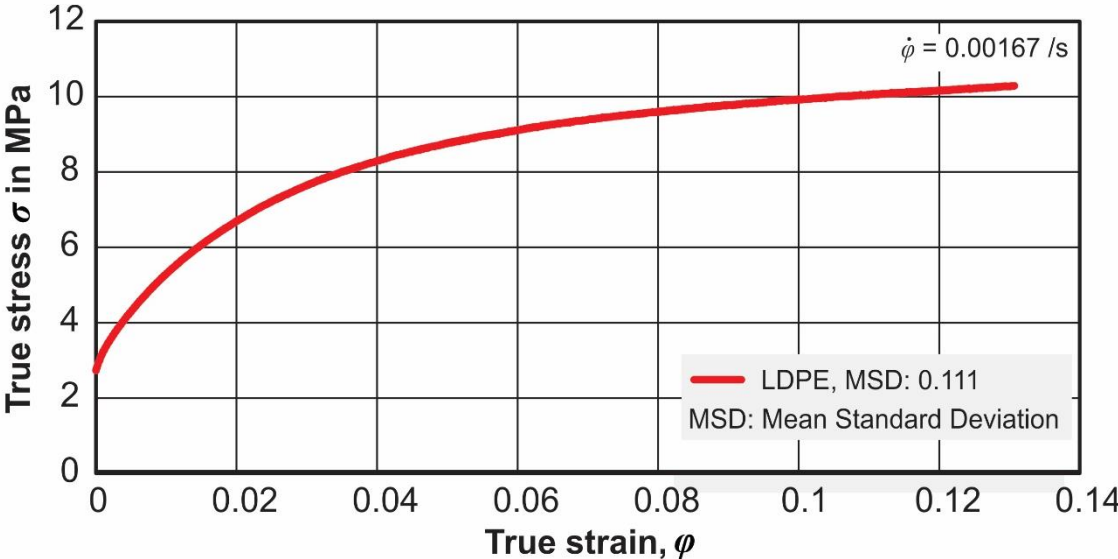
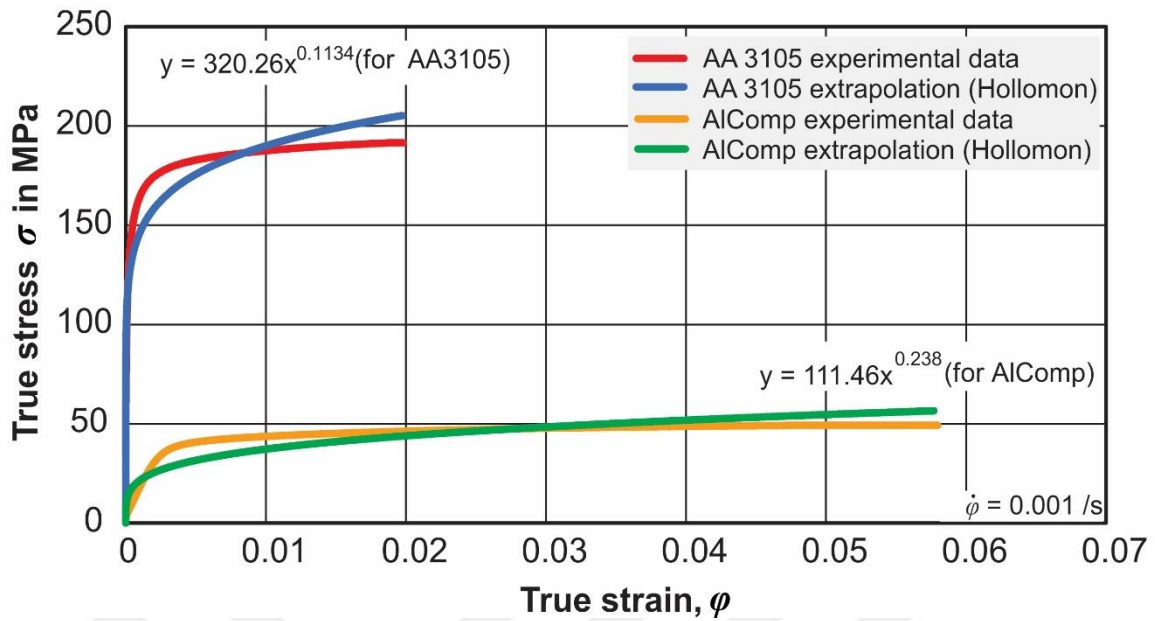
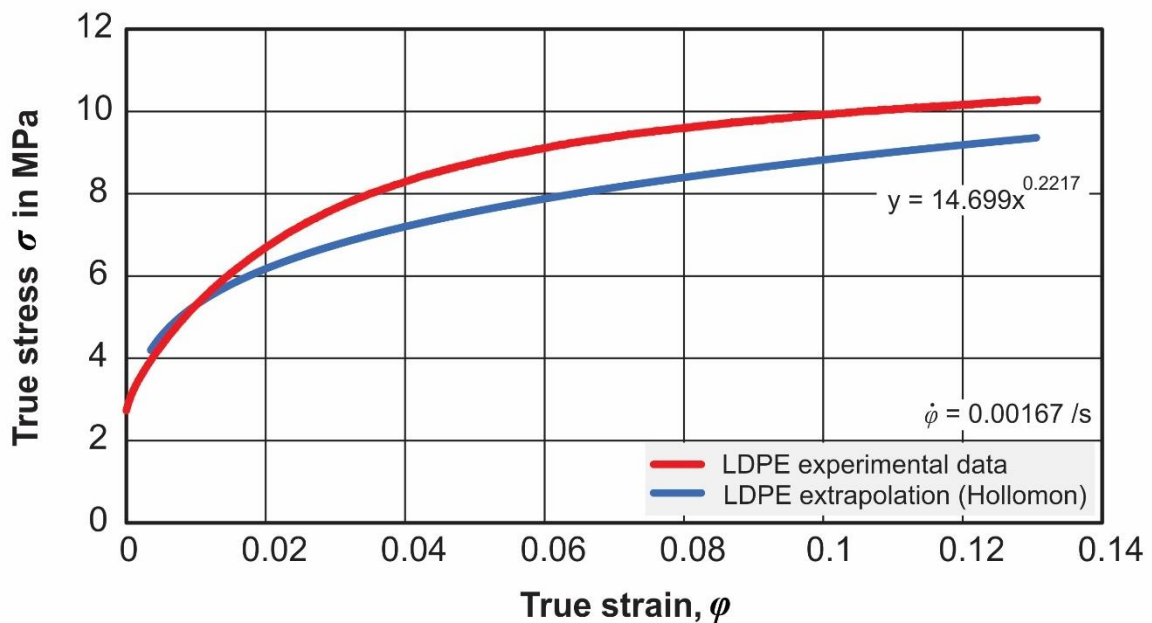


Figure A.2: True stress - strain graph of LDPE



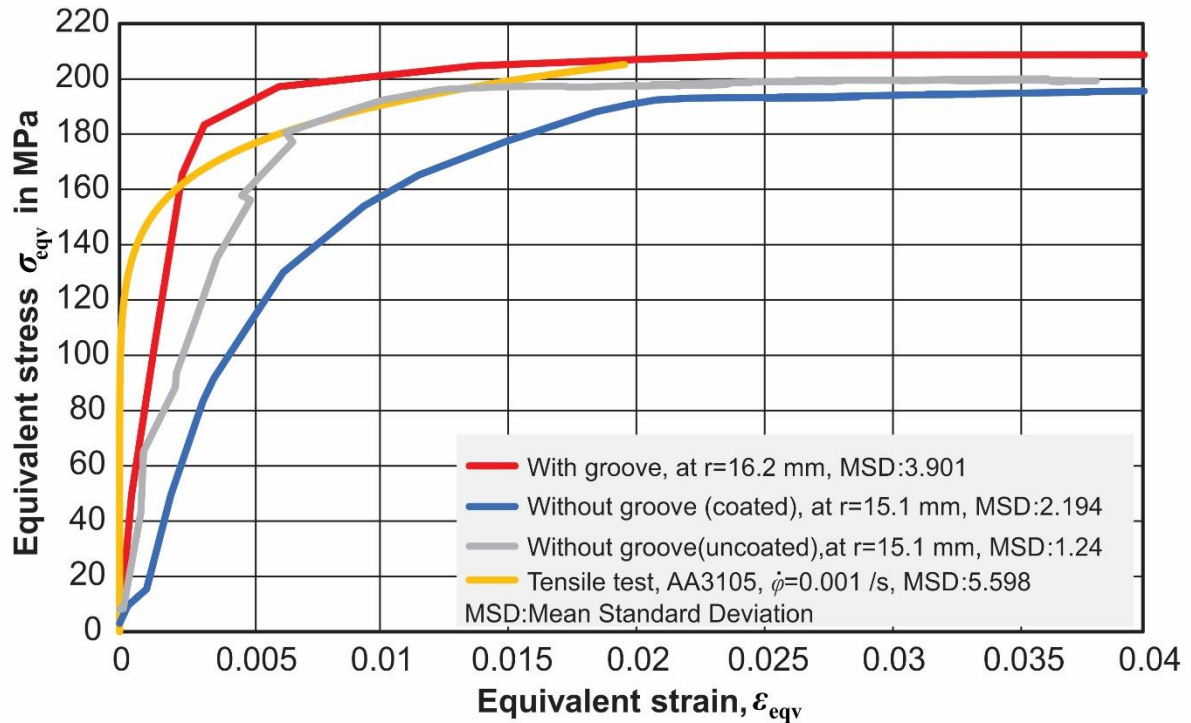
**Figure A.3:** Comparison of calculated strain-hardening behaviour and experimental strain-hardening behaviour of AA3105 and 3105 aluminium composite



**Figure A.4:** Comparison of calculated strain-hardening behaviour and experimental strain-hardening behaviour of LDPE



### Detailed Graph of the Results from In-Plane Torsion Test



**Figure A.3:** Equivalent stress – strain graph of the in-plane torsion test and tensile test results

## Appendix B

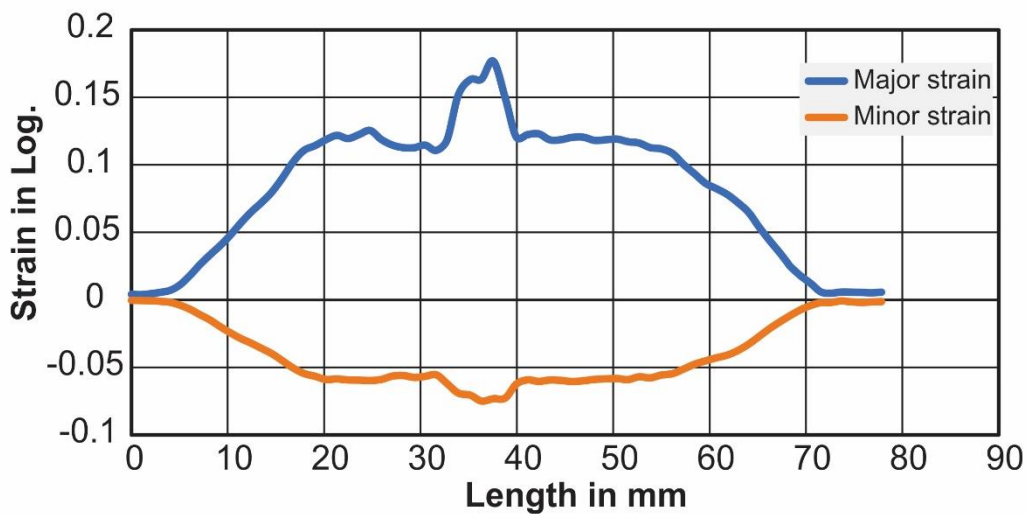
### Evaluation of Nakajima Test Results According to DIN ISO 12004:2008 standard

The strain-length curve with multiple peaks can be evaluated according to DIN ISO 12004:2008 standard using best-fit parabola approximation. The graph of major strain and minor strain against the length of the section in mm is drawn from section data obtained in ARAMIS software (**Figure B.1**). In this explanation, the strain – length curve of 20 mm specimen 2 - section 1 is used.

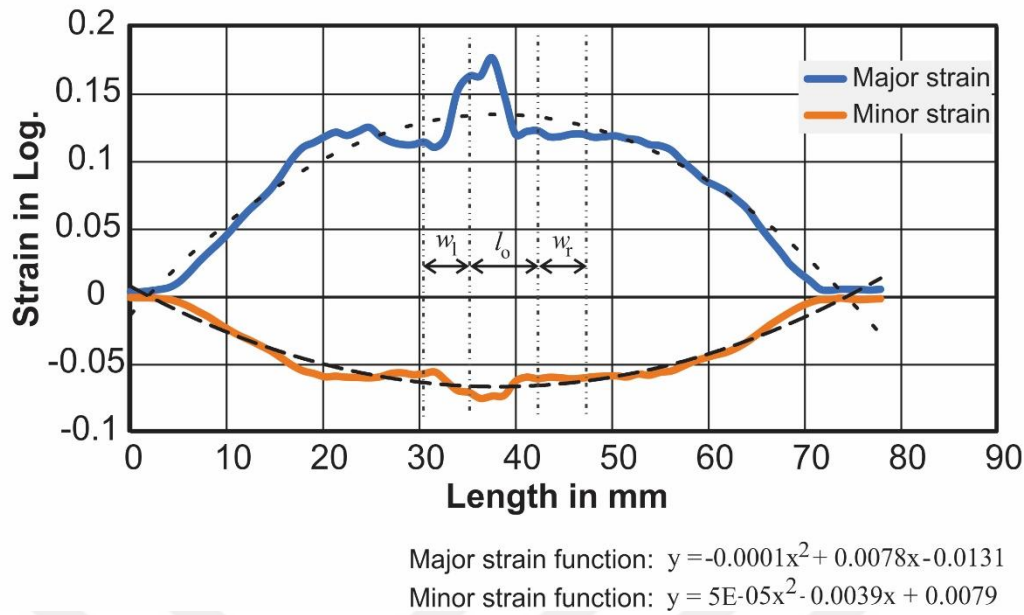
The parabola is inscribed to the graph using Trendline command and the functions of the major strain and minor strain parabola can be obtained. The inner border of the crack is placed 3mm away from the crack on both sides. The compensation window width,  $w$  is then calculated using **equation B.1** (DIN ISO 12004:2008).

$$w = 10 \cdot [1 + ((\varepsilon_{2,BL} + \varepsilon_{2,Br})/(\varepsilon_{1,BL} + \varepsilon_{1,Br}))] \quad (C.1)$$

Where  $\varepsilon_{2,BL}$  is the minor strain value of the left inner boundary,  $\varepsilon_{2,Br}$  is the minor strain value of the right inner boundary,  $\varepsilon_{1,BL}$  is the major strain value of the left inner boundary and  $\varepsilon_{1,Br}$  is the major strain value of the right inner boundary. The fit windows ( $w_l$  and  $w_r$ ) are then drawn on the left and right sides of omitted length between the inner fit limits ( $l_0$ ) (**Figure B.2**).



**Figure B.1:** Strain - length graph of 20 mm specimen 2 - section 1



**Figure C.2:** Determination of major and minor strain values using best-fit parabola approximation

Major strain and minor strain values (**Table B.1**) can then be calculated using functions obtained from the parabola by inputting values of x-positions (length).

**Table B.1:** Values of major and minor strains for 20 mm specimen 2 - section 1.

	Function	x-location of vertex	y-location of vertex (strain values)
Major strain	$y = -0.0001x^2 + 0.0078x - 0.0131$	38.9818	0.1390
Minor strain	$y = 0.00005x^2 - 0.0039x + 0.0079$	37.7880	-0.0681

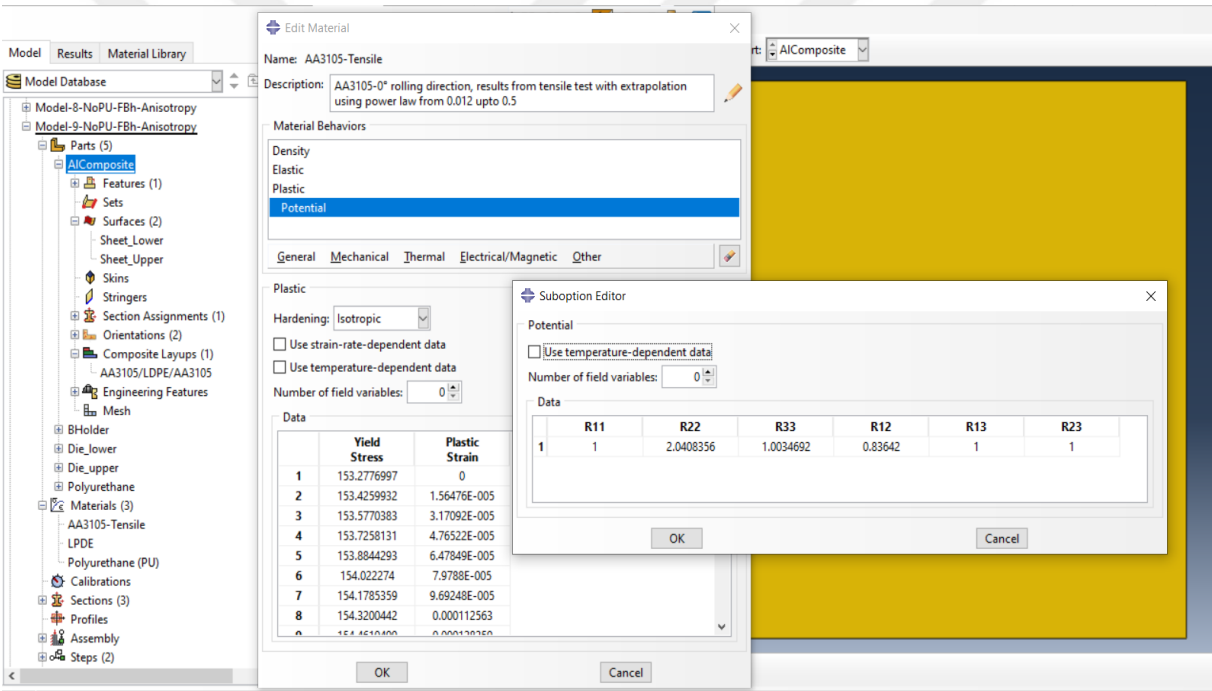
These procedures are repeated for every section data obtained from ARAMIS software. Then, the mean values of major strain and minor strain for every specimen are calculated and finally, the forming limit curve (FLC) of the aluminium composite panel is drawn from the mean values of the major strain and minor strain of the specimen (**Figure 4.36**).

# Appendix C

## Composite Material Modelling

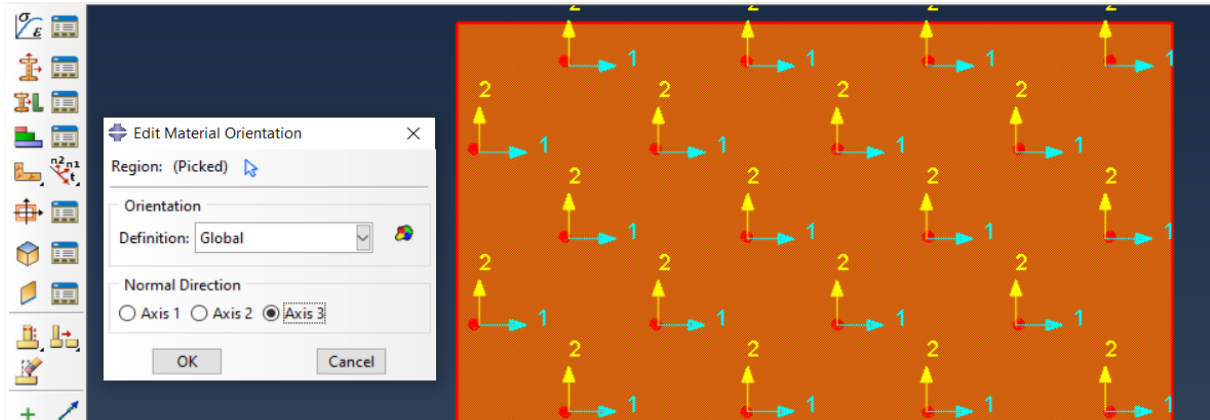
*Detailed Pictures on How to Model Composite Material in Abaqus/Explicit Software*

In Abaqus/Explicit software, AA3105 material data is created using Hill48 yield criterion. The Hill48 parameters are defined in **Sub-option** → **Potential**. The hill48 parameters are calculated in chapter 5.2.2. The Flow curve data (yield stress and plastic strain) is obtained from the tensile test (**Figure C.1**).



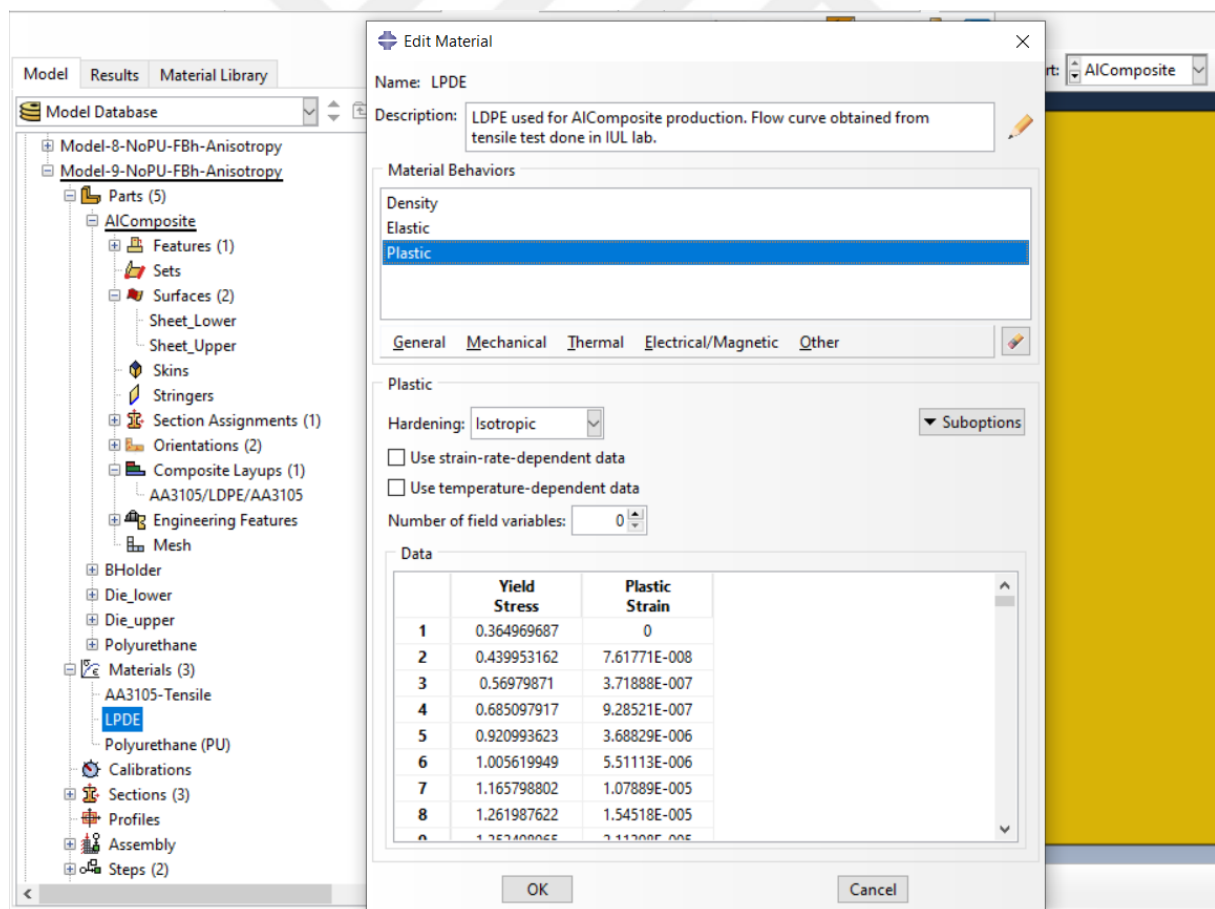
**Figure C.1:** Creation of AA3105 material data in Abaqus/CAE

Then the orientation of AA3105 is assigned to the composite part (**Figure C.2**).



**Figure C.2:** Assigning material orientation of AA3105

LDPE material is modelled using isotropic hardening and the yield stress and plastic strain data from the tensile test are added (**Figure C.3**).



**Figure C.3:** Material modelling of LDPE

Finally, the composite shell section is created with three-ply layers. Simpson thickness integration rule is used. The orientation angle of AA3105 is set to zero the same as how AA3105 is oriented during the production of the aluminium composite panel (Figure C.4). The created composite shell section is then assigned to the composite part (geometry).

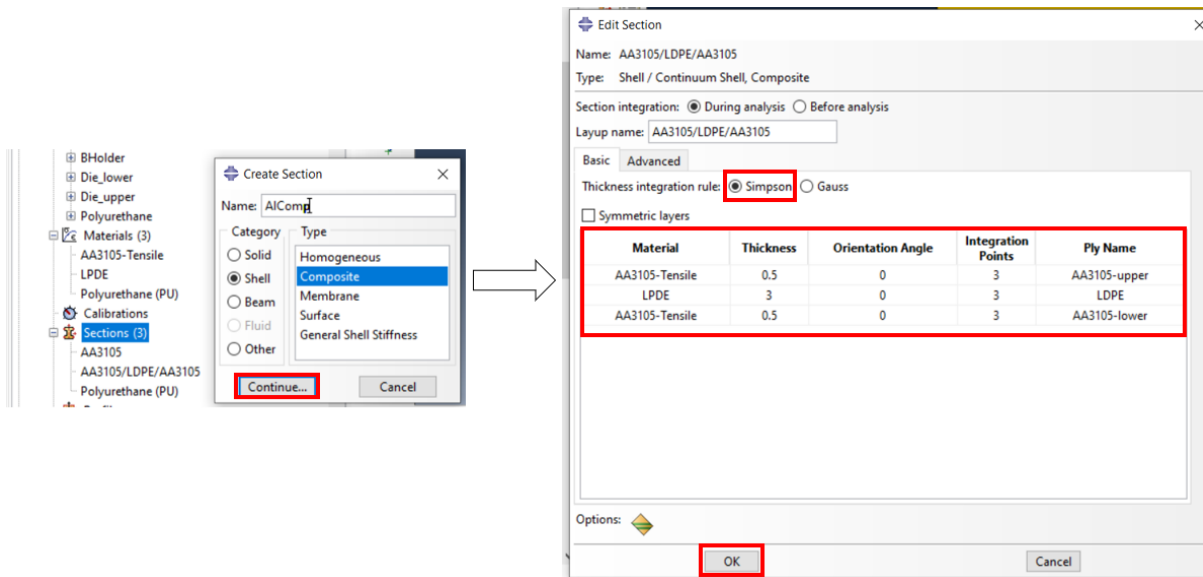


Figure C.4: Creation of composite shell section

The composite layup can be checked using Query->Ply stack plot

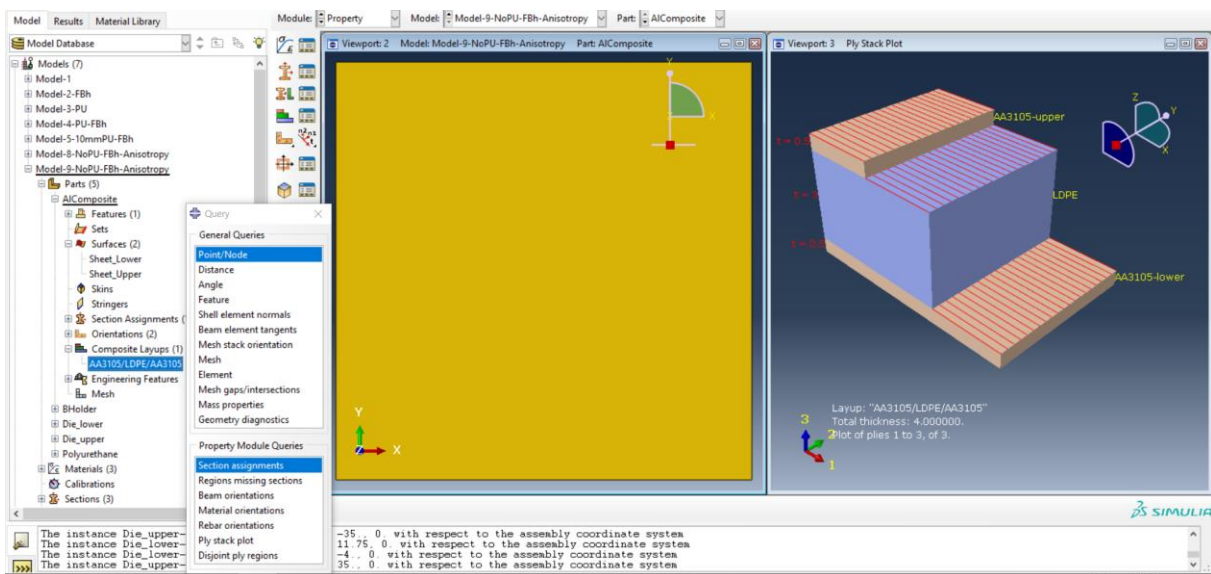


Figure C.5: Composite layup